Electron emission processes in cold cathode thermal arcs

Mollart, T.P.

ELECTRON EMISSION PROCESSES IN COLD CATHODE THERMAL ARCS

THESIS SUBMITTED IN CANDIDATURE FOR THE DEGREE
OF DOCTOR OF PHILOSOPHY

T. P. MOLLART
COLLEGE OF St. HILD AND St. BEDE.
DEPARTMENT OF PHYSICS
UNIVERSITY OF DURHAM

APRIL 1993.

This thesis is dedicated to my father.

DECLARATION

I declare that the work reported in this thesis, unless otherwise stated, was carried out by the candidate, that it has not previously been submitted for any degree and that it is not currently being submitted for any other degree.

Dr. A. W. Brinkman

Supervisor.

T.P. Mollart

Candidate.

ABSTRACT

In this Thesis the processes of electron emission from cathode electrodes are studied theoretically, and the applicability of these mechanisms to the non refractory cathodes that can be used to sustain thermal arcs was examined. Apparatus that was used to generate and manipulate thermal arcs along rail electrodes is described in this thesis. Techniques for driving arcs over polished sample electrodes with magnetic or aerodynamic forces are outlined.

Scanning electron microscopy was used to study emission site formation on highly polished electrodes with a natural 2.5 nm oxide layer. Theoretical maximum electron current densities that can be extracted by the arc were calculated and these were used, in conjunction with information from the experimental work, to make estimates of the lifetime of emission spots that are seen on the cathode electrodes of thermal arc devices. The lifetime was found to be dependent on the arc velocity over a range of velocity values from 3 to 80 ms^{-1}. The lifetime measured ranged from 2.4 μs to 0.024 μs. Experiments on arcs driven at a constant velocity using a combination of aerodynamic and magnetic forces showed that the formation of emission spots was independent of the applied external magnetic field. The presence of artificially grown copper (II) oxide layers, 50 nm and 100 nm thick, were found to influence the lifetime.

The effect of the oxide layer was predicted using a simple model accounting for the change of resistance that such an oxide layer would be expected to cause. Additional experiments showed that the resistance of the arc was independent of the oxide layer thickness, as predicted by the model.

ACKNOWLEDGEMENTS

This project was initiated and funded by Tioxide UK Ltd and I am grateful for the opportunity to complete a PhD that this has provide me with. I would like to thank Mr Alan Hare who initial ideas for the project provided a well planned beginning and for the invaluable insights that he has made through out the research programme. The help of Mr Robert Peeling at the beginning of the project and Mr. Paul Strefford during the latter part are appreciated.

I would like to thank Professor D.Bloor for the use of the facilities of the Applied Physics group. The supervision of Dr. A. W. Brinkman, Professor J.Woods and particularly Dr. J.S. Thorp made the project possible and their guidance in academic matters have been exemplary.

The technical support received through out the project has been of a very high standard, with helpful suggestions and improvements made though out the entire experimental programme. The laboratory support of Mr. Norman Thompson, Mr. Frank Spence, Mr John Gibson and Mr. Chris Pearson was appreciated and the help with sample polishing received from Mr. Davy Patterson was invaluable. The fabrication of the electrodes and holders was completed by Mr. Brian Blackburn and the staff of the mechanical workshop, with particular thanks to Mr. Roger Little for making the sample electrodes. Mr Jack Greensmith and Mr. Ian Garrette advice on the construction of the power supply also proved to be invaluable. The instrumentation apparatus was constructed by Mr. Peter Friend and the staff of the electronic workshop and their help was gratefully received.

Finally I would also like to acknowledge the considerable support that has been extended to me by my family throughout this project. Their help has made it possible for me to complete this thesis.

CONTENTS

CHAPTER 1 INTRODUCTION

1-1 INTRODUCTION

This project is a study of the emission of electrons from low temperature melting point, non refractory cathodes where the emitted electrons are used to provide the energy for a type of plasma known as a thermal arc. The term plasma encompasses a broad spectrum of different media, all with the common property of being a low density ionized gas. Plasmas occur naturally in nature, the Northern Lights is one example, where charged particles from the sun excite atoms and molecules in the upper atmosphere into a low temperature electrodeless plasma. A more common occurrence in nature is lightning where the negative charge built up in a cumulo-nimbus cloud formation is discharged to earth.

Plasmas have found domestic applications in the guise of electrical discharges. A plasma can be formed by applying a potential between electrodes, with the right conditions, the initial high resistance of the gas can be overcome and current will flow between the electrodes. Low power electric discharges are used in lighting, fluorescent tubes and high power arc discharges are used in electric arc welding.

Plasma processing is a term used to describe the techniques of harnessing the unusual properties of a plasma in industrial processes. It will play an ever increasing role in manufacturing, as in many cases the use of a plasma can provide a unique ability to make an industrial process possible. Arc electric furnaces are an example of a plasma process that has been successfully used in steel manufacturing for many years. There are many other applications where plasmas could be used to improve the efficiency of a manufacturing technique, but the lack of understanding of the physical processes of a plasma make it impossible. Adopting a plasma process often has an environmentally beneficial effect, when used for heating it produces less exhaust gases, when used for etching they make the process more efficient and produce less effluent and when used for incineration, it reduces the waste to a less harmful end product.

The devices and processes that have been developed have a tendency to have unpredictable behaviour, take lengthy development and are unusually inflexible in the uses to which they can be put, [1.1.] These characteristics are an anathema for production engineering and are preventing the more widespread adoption of plasma processing. Understanding why plasmas have such unpredictable behaviour is the reason that more basic research into plasma physics is necessary, as at the root of these problems lies the fundamental properties of the plasma, which are poorly understood.

Any experimental investigation is undertaken because the outcome of certain actions cannot be predicted and a desire to be able to influence the outcome exists. The ability to influence the behaviour of a plasma device and the knowledge of how and why this cannot be achieved, gained by a company with over twenty years experience of using a plasma process, was the basis from which this research was started. To obtain an insight into the problems involved it is first necessary to describe the specific process to which a plasma has found an application.

1-2 THE CHLORIDE PROCESS

Titanium dioxide is a pigment found in most inorganic white products from paint to plastic and paper. When used as a pigment it is necessary to refine naturally occurring titanium dioxide, rutile ore, into a high purity powder. This is a distillation process where the impurities are separated from the titanium dioxide. There are two industrial methods of purifying titanium dioxide, the sulphate process and the chloride process, the latter being a more modern development and more environmentally desirable. With this the rutile is fluidized with chlorine at a temperature of approximately 800 ^{o}C to 1000 ^{o}C which produces titanium tetrachloride and the other chlorinated impurities. The vapour stream is then cooled, resulting in many of the impurities being precipitated out. The remaining fluid is then fractionally distilled to achieve the desired purity.

The titanium tetrachloride is then converted back into titanium dioxide, oxidizing it, by burning it in oxygen at a temperature of 1500 ^{o}C. The high

temperature, needed for the reversible reaction to yield titanium dioxide, causes a problem for the producers of pigment. The titanium tetrachloride has to be heated cleanly without re-introducing impurities into the reaction. This is where a plasma can provide a convenient solution to the problem. If a plasma is created from one of the reactants it can be used to heat the reaction, because the plasma can be used to transfer electrical energy into thermal energy in the gas. The temperature of the reaction is achieved by heating a fraction of the oxygen to a temperature of 3500 ^{o}C with a device called a plasma torch.

The pure titanium dioxide is cooled and separated from the chlorine gas, which is recycled. The pigment is then subjected to various finishing stages to produce the final product. The main advantage of this system is that it produces fewer waste products than a comparable system, with the majority of the chlorine being recycled in a closed system. The direct waste from the process consists of the chlorinated impurities which have been separated from the titanium dioxide.

1-3 THE PLASMA TORCH

The oxygen is heated using a type of plasma torch known as a vortex stabilized thermal arc gas heater. A high power plasma known, i.e. a thermal arc, is struck between cylindrical electrodes and the gas is heated as it passes through the electrodes. A thermal arc has a high current density, greater than 1×10^{6} A cm^{-2}, with associated heat flux densities of 1×10^{6} to 1×10^{7} W cm^{-2}. The arc is distinguished from other electrical discharges by these electrical characteristics and other physical properties. The voltage needed to sustain a thermal arc is much lower than for other types of discharge and the arc column has a very high luminosity; when these characteristics apply to an electrical discharge it is usual to describe it as a thermal arc. It is the high heat flux densities that make this plasma suitable for heating gases; the high temperature and power mean that a large volume of gas can be passed through a torch and heated to a very high temperature, producing no combustion by-products and requiring no heat transfer as would be involved with other techniques.

Tioxide UK Ltd. plasma torches have been developed, in house, from technology bought from the Linde Corporation, a division of Union Carbide who, obtained original designs from Germany in 1945. These plasma torches could run at very high power outputs but the erosion rates of the electrodes meant that they had to be refurbished after a few minutes of operation. Tioxide UK Ltd. have developed plasma torches to run with pure oxygen in the arc gap with power outputs ranging from 250 kW to 2 MW. Increases in power are achieved by a scaling up of the physical size of the torch. The 2 MW torch is 1.7 metres long and when operating at 700 Amps, 1600 volts, continuously, produces a 1 MW power output, with an average electrode life of 600 hours. A schematic diagram of the plasma torch is shown in figure 1.1.

The torch consists of a cylindrical cathode and anode separated by a gap of between 2 mm to 4 mm. These are water cooled, to ensure the surface temperature of the electrode is approximately 300 ^{o}C. The plasma is initiated by passing helium through the torch lowering the threshold voltage to 600 volts and once it is running, oxygen replaces the helium. The plasma is prevented from fixing on to a point on the cathode or anode by a method known as vortex stabilization.

Vortex stabilized anode. When oxygen is pumped through the electrodes a vortex flow is induced. As the anode is cylindrical the plasma is driven down its length by aerodynamic forces until a point is reached when the electric field strength is insufficient to maintain the plasma. At this point the plasma will jump back to the beginning of the anode. This phenomena causes the plasma to oscillate along the length of the anode, with a velocity of approximately 50 metres per second. This ensures even degradation of the anode maximising the lifetime of the anode.

Vortex stabilized cathode. The cathode is a cylinder with one end blocked. Vortex flow occurs in the tube with gas travelling up the outside of the tube and gas pressure forcing it back down the centre of the tube. The plasma will then travel down the cathode and remain settled on a point at the end of the cathode,

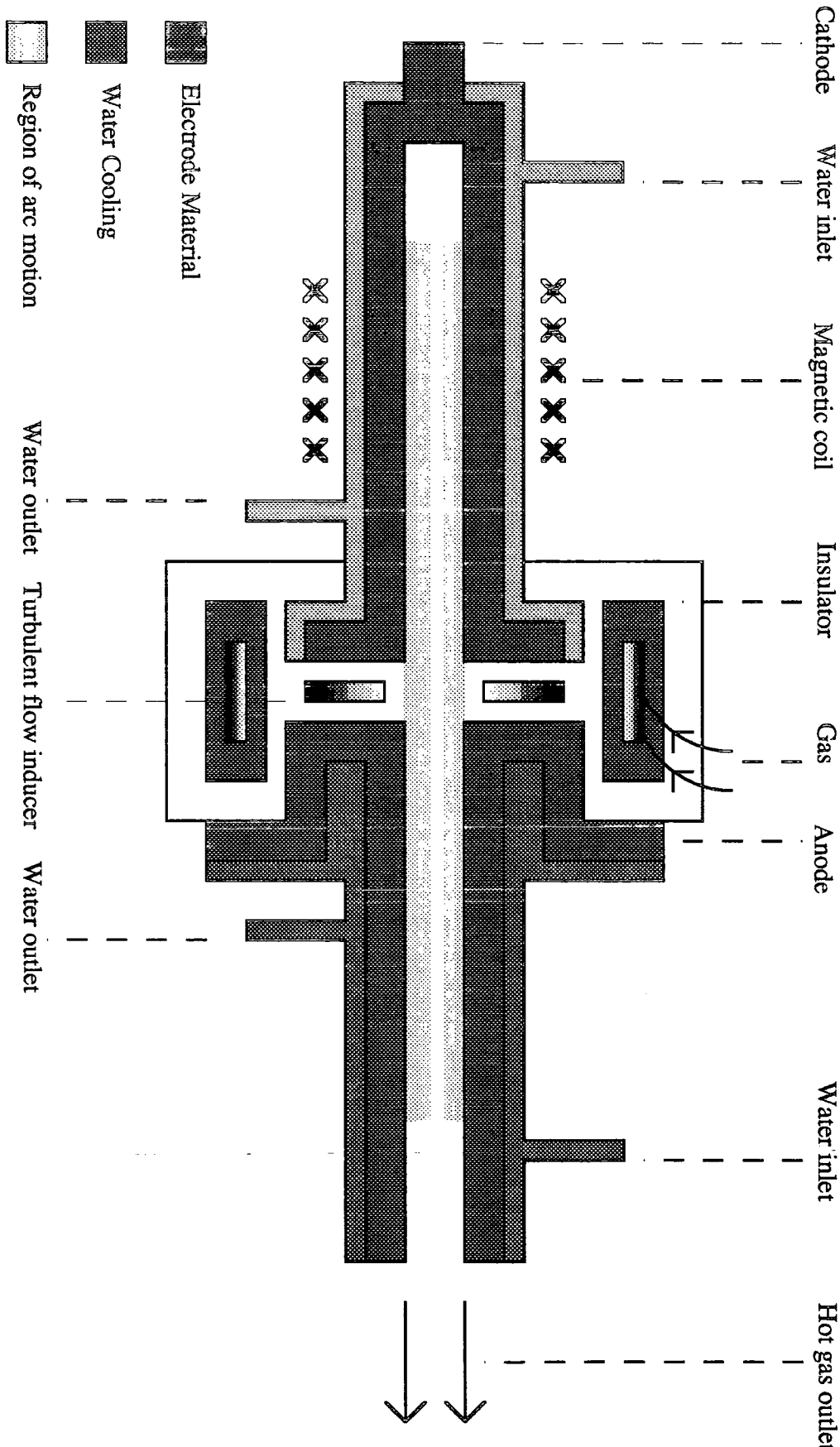

Figure 1.1 The plasma torch

resulting in rapid melting of the spot and breakdown of the cathode. To prevent this the plasma is made to oscillate along the length of the cathode by an axial magnetic field opposing the aerodynamic forces. The point where these two forces balance is the centre of oscillation, as the plasma is oscillated by varying the strength of the magnetic field. The movement induced is much less than in the anode and so degradation is much more rapid.

Electrode Construction. The material that the electrodes are fabricated from is a commercial secret, as achieving a long electrode life is what makes the use of a plasma gas heater viable in this process. The electrodes weigh 17 kg and have a mean life of 600 hours. After 600 hours they are replaced and examined. It is found that the standard deviation of electrode life is large. Degradation is measured in weight loss and after 600 hours the electrodes are visibly thinned out, with the cathode electrode being most eroded.

The electrode material was developed to enhance the life of the cathode, by trial and error using different materials in the actual plasma torch. The experimentation carried out by Tioxide UK Ltd. has not revealed the mechanism that makes the electrode material so successful. Generating and sustaining a thermal arc, in a high pressure gas flow, requires a large amount of power, which, in turn, requires a very high current to be flowing through the arc. This implies that the cathode of the torch has to emit a high flux of electrons. The current density of emitted electrons is higher than can be predicted by conventional electron emission mechanisms, such as thermionic and field emission, when applied to the voltage and temperature characteristics of the arc. This condition is called heavy current overload in this thesis, [1.2.] The development programme has indicated that the surface conditions of the electrode and the oxygen, of the plasma, form an oxide with the right properties to enhance heavy current overload emission. Developing a plasma torch is a trial and error process as the surface oxidation state of the material appears to be so critical for the performance of the device. Any change in the use of the device, such as different plasma gas or power output, will change the surface oxidation state of the electrodes and the performance

will be diminished. If plasma gas heaters are to be widely used in industrial processing the mechanisms allowing the Tioxide UK Ltd. plasma torch to have a long working life have to be understood. A clear picture of the process of efficient heavy current overload emission has to be made, to enable design of electrode materials that are efficient emitters for all types of gases and for different power levels.

Tioxide UK Ltd.'s development of a plasma torch has provided much experimental and background information, as well as the proof that such materials can be developed. The opportunity that Tioxide UK Ltd.'s expertise provides is to define clearly the areas in which research into heavy current overload emission should proceed while providing a vehicle on which to test the developing theories. Clearly this is not the first time that such an engaging topic has been investigated. Experiments with electric arcs have been conducted for almost 150 years and there have been many advances in the field of electron emission from electric arcs, notably by, von Engel in the late 1950's, [1.8,] Guile, [1.7,] Ecker and Daalder in the 1970's, [1.4, 1.6] and Jüttner in the 1980's, [1.5.]

1-4 THE RESEARCH PROGRAMME

Tioxide UK Ltd. initiated and funded this research in 1989. The need for basic research into plasma processing was highlighted at a recent conference on the subject and by a report by the Centre for Exploitation of Science and Technology, C.E.S.T., [1.3.] As a totally new research area to this department, the emphasis of this programme has been to develop an experimental apparatus to investigate the primary process of electron emission of an electrode in heavy current overload emission. This is achieved not by measuring erosion rates of plasma torches, but by examining the track of an arc over specially prepared electrodes. The purpose of this is to measure the parameters of the emission, such as the lifetime and the current density of the emission site and use these to build an emission mechanism model.

It was believed that the general background in solid state physics could be used to unravel the mysterious role of an oxide layer in the efficient emission of electrons

from the cathode. The research was to be centred on investigating the strange mechanisms of the the oxide layer. It is doubtful that the extraction of the electrons from the cathode is a totally undiscovered phenomenon, it is more likely that a conventional emission process is being affected in an unexpected manner by a unlikely operating parameter. The philosophy of this project has been to understand the conventional forms of electron emission and adapt the mechanisms to account for unusual experimental data. It was hoped that this approach would lead to a better understanding of the emission of electron in the regime of a plasma torch, enabling adaptation of existing technology to other applications.

1-5 REFERENCES

1.1 Gottscho R. *Plasmas make progress.* 1993 Physics World Vol 6 No. 3 p. 39 to 45.

1.2 Chapter 4

1.3 Campbell P. *Plasmas prepare to go beyond fusion.* 1992 Physics World Vol. 5 No. 9 p. 9 to 10.

1.4 Ecker G. *The vacuum arc cathode. A phenomenon of many aspects.* 1976 I.E.E.E. Trans. on Plasma Sci. Vol. PS-4 No. 4 p. 281 to 227.

1.5 Jüttner B. *Formation time and heating mechanism of arc cathode craters in a vacuum.* 1981 J. Phys D: Appl. Phys.Vol. 14 p. 1265 to 1275

1.6 Daalder J.E. *Erosion and the origin of charged and neutral species in a vacuum arc.* 1975 J. Phys D: Appl. Phys.Vol. 8 p. 1647 to 1659.

1.7 Guile A.E. *Arc electrode phenomena.* 1971 Proc. I.E.E., I.E.E. Reviews, Vol. 118, No. 9, p. 1131 to 1154.

1.8 Dickson D.J. Engel A. von *Resolving the electrode fall spaces of electric arcs* 1967 Proc. of the Roy. Soc. Series A Vol. 300 p. 316 to 325.

CHAPTER 2 PLASMA PHYSICS

2-1 INTRODUCTION

Plasma physics is the study of low density ionised gases. The term Plasma was first used in 1928, by Langmuir [2.1], to describe a collection of charged particles in an electric discharge. Langmuir used the word plasma as he believed there was a similarity in the function of impurity ions in a plasma and white corpuscles in blood plasma. The use of the word plasma is seen as the beginning of modern plasma physics, but the earlier work on electric discharges, by Thompson, Townsend, Debye and Tonks, heralds the true beginnings of the study of low density ionised gases.

During the inter war years plasma physics was a relatively small field of study as there were few earth bound occurrences and applications of plasmas. Work revolved around the use of high current electric discharges, arcs, for switching and high current rectification, and of low current , low pressure, discharges used in the design of the fluorescent lamp and for propagating radio waves in the ionosphere. The suggestion that high energy plasmas sustaining thermonuclear reactions were the source of solar energy fired the interest of astronomers in the occurrence of plasmas in space. Electric discharges were used as diagnostic tools to study atomic structure. As they are the easiest method of creating a laboratory plasma they were the most investigated and best understood type of plasma throughout the early years of plasma physics.

After the Second World War through the advances in nuclear science, a more fruitful application of plasma science became apparent. The conditions in a plasma could, in theory, be made extreme enough, in terms of particle energy, for a controlled nuclear fusion reaction between light elements to occur. The subsequent release of energy from this reaction could be utilised as a source of energy. It was believed that to harness fusion energy was a matter of development. A suitable device that could generate a sufficiently hot plasma, 5×10^7 K, and confine this, in a magnetic field, for long enough for a fusion nuclear reaction to occur (approximately 1 second), had to

be built. Research programmes were started in the, UK, USSR, and USA and the work was declared classified, in 1952. Plasma physics was then developing independently in these nations, until it was realised that a global effort was required before the goal of energy release from thermonuclear reactions could be achieved, as plasma physics had rapidly evolved into a highly complex field. Thermonuclear fusion work was declassified in 1958.This greatly advanced other aspects of plasma science as many theories that were being developed simultaneously in secret by the nations undertaking fusion research were published in 1958.

The first problem that the fusion experiments encountered was confinement of the plasma in a high enough density, of particles and energy, for long enough for a fusion reaction to occur within the plasma. The problem is known as instability and is a good illustration of the techniques needed to describe plasmas in a physical sense. Instability enables a plasma to escape from a configuration of magnetic and electric fields that would confine a single charged particle indefinitely. Langmuir showed that plasma waves can be sustained in a plasma when there are differences in the electron velocities. A wave propagating through the plasma, at a certain velocity, will take energy from faster moving electrons and give it to slower moving electrons, enabling the wave to grow in magnitude. This will cause a change in the electrical configuration of the plasma enabling it to escape from the confining fields. The goal of fusion research is to design a field configuration that confines the plasma for long enough to sustain a fusion reaction and to achieve this it is necessary to understand the formation of instabilities and describe the plasma. [2.4.]

The technological advantages of nuclear fusion power generation are so great that the drive to overcome the difficulties is the main reason that research into plasma physics takes place. Many of the modern advances in understanding have been the result of this research. However with the greater knowledge of plasmas has come the realisation that there are other possible uses. There is now a healthy interest in the non fusion applications of plasmas with much research and development into these more conventional plasma applications. [2.18.]

2-2 THE PLASMA STATE

A plasma is defined as an approximately electrically neutral assembly of unbound, but interacting, ions and electrons. The particles are collected in sufficient number for the long range Coulomb interactions to be significant and in a low enough density for the short range inter-atomic forces to be neglected. The number of systems that fall under this general definition is such that the plasma state is often referred to as the fourth state of matter lying between the gaseous state and the unnamed fifth state where the energy density is so high that matter anti-matter pair formation becomes important. Descriptions of such multi-bodied systems involve the physics of classical mechanics, electromagnetism and statistical mechanics as many of the properties of plasmas stem from long range Coulomb interaction of particles and are collective properties that involve many particles interacting simultaneously.

To use these areas of physics requires some basic parameters of the plasma system to be defined. Some, such as the distribution function of the particles in the plasmas, the interaction length of particles, can be found from other branches of physics. Other parameters such as the plasma approximation (the number of ionised particles within the interaction sphere) plasma frequency and transport mechanisms have to be derived specially for plasma physics. [2.17]

Plasma equilibrium and meta-equilibrium. Plasmas are often described as being in thermodynamic equilibrium. This is when the electrons and ions are each described by a Maxwellian distribution characterised by the same parameter, the temperature. In this situation the plasma is in equilibrium with the surroundings absorbing and radiating energy at the same rate. Clearly this situation does not exist in a plasma as it would be destroyed when two particles collide, but many theoretical studies are made by studying perturbations from such a meta-equilibrium state.

Debye Shielding and the Plasma Approximation. If a charged particle in a plasma is separated from another particle by more than the Debye length, λ_D, it behaves as if the other particle is not present. The plasma, within the volume defined by λ_D (the Debye sphere), 'screens out' the electrostatic potential that would otherwise arise between them. This is known as Debye shielding. The plasma is able to behave in this manner only if there are enough charged particles within the Debye sphere to be attracted to oppositely charged particles and shield its electrostatic charge from other charged particles. The Debye length was originally derived for electrolytes defining their sphere of influence in a solution, but is found to be valid for plasmas and is given by

$$\lambda_D = \left[\frac{kT}{8\pi ne^2}\right]^{1/2}$$

equation 2.1,

where k is the Boltzmann's constant, n is the density of electrons or ions (cm^{-3}), T is the absolute temperature and e is the charge on an electron.

The plasma approximation stems from assuming that the number of plasma particles in the Debye sphere, the plasma parameter (g), is large enough for Debye shielding to occur in the plasma itself. The value of g is given by

$$g = \frac{1}{n\lambda_D^3}$$

equation 2.2

The approximation that Debye shielding occurs in a laboratory plasma enables the solution of the equations of motion for the plasma particles. The plasma parameter is a measure of the ratio of the particle's kinetic and potential energies and can be equated to the energies of the particle,

$$g = \frac{1}{n\lambda_D^3} \approx \frac{n^{1/2}}{T^{3/2}}$$

equation 2.3

For the particles to be treated as a plasma then g tends to zero, as this is the requirement for Debye shielding to occur. The approximation that g tends to zero is known as the plasma approximation. [2.15]

Plasma quasi-neutrality and plasma oscillations. A fundamental property of a plasma is its tendency to remain overall almost electrically neutral, the number density of electrons and ions remaining almost equal to one another. This is known as quasi-neutrality and is caused by the outcome of two conflicting tendencies. The faster moving electrons (due to their lighter mass) escape more readily from any confinement regime. A charge imbalance is created by the remaining ions, which generates a large electrostatic restoring force. The net result is the plasma remains quasi-neutral, as shown in figure 2.1.

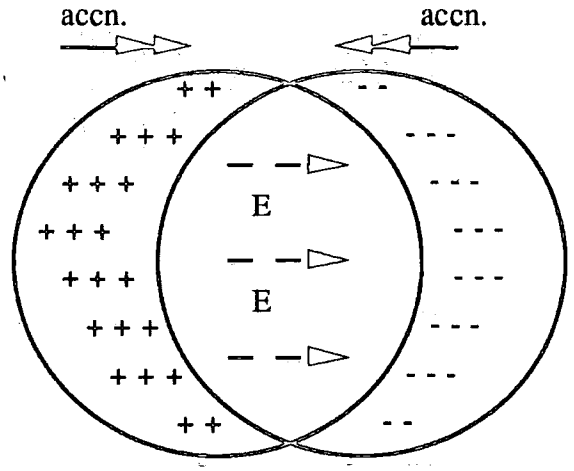

Figure 2.1. The origin of quasi-neutrality and plasma oscillations. The electric field, E, produced by charge separation accelerates positive ions towards each other.

Suppose there is a uniform initial number density, n_o, of electrons neutralised by an equal number of ions. The electron density, n, is disturbed to $n = n_o + n'$. To describe the subsequent behaviour of the plasma some approximations have to be made. The electrons are assumed to be the only particles moving, the ions' large inertia causing them to remain stationary. The number density of electrons, n', is taken as being large enough to enable the electrons to be described as a fluid and the hydrodynamic equation of motion used. This equates the the rate of change of momentum of an element or fluid to the force acting on it,

$$nm\left[\frac{\partial v}{\partial t} + (v.\nabla)v\right] = -neE$$

equation 2.4

where v is the velocity of the fluid, e is the electric charge, m is the mass of the particle, $\mathbb{E}$ is the electric field strength and ne$\mathbb{E}$ is the force acting on the particle. If the rate of increase of density of a small volume is described by the continuity equation,

$$\frac{\partial n}{\partial t} + \text{div}(n\mathbf{v}) = 0$$

equation 2.5

the electric field is related to the net charge density. If Poisson's equation,

$$\text{div } \mathbb{E} = 4e\pi(n_+ - n_-)$$

equation 2.6.

is used in conjunction with equation 2.4 then the equation of motion for the electron in the plasma can be solved. These three equations are simplified further by assuming the products of small changes can be neglected and equations 2.4, 2.5, and 2.6 become,

$$\frac{\partial v}{\partial t} = -\frac{e}{m}\mathbb{E}$$

equation 2.7,

$$\frac{\partial n'}{\partial t} + n_o \text{div } v = 0$$

equation 2.8

and

$$\text{div } \mathbb{E} = 4e\pi v n'$$

equation 2.9.

respectively.

It is then possible to obtain an equation for the time development of $n'(\bar{x})$ by taking the time derivative of equation 2.8, the divergence of the second and making the substitution for div $(\partial v/\partial t) = -(e/m)$ div $\mathbf{E} = 4\pi(e^2/m)n'$ to obtain a wave equation,

$$\frac{\partial^2 n'}{\partial t^2} + \frac{4\pi n_o e^2}{m} n' = 0$$

equation 2.10

The characteristic frequency of this wave equation, ω_p can be found and is given by equation 2.11,

$$\omega_p^2 = \frac{4\pi ne^2}{m}$$

equation 2.11

This shows that that a disturbance from equilibrium n'(x) will oscillate with a characteristic frequency, ω_p. This was first discovered by Langmuir [2.1] and is known as the plasma oscillation, and ω_p is known as the plasma frequency. This was one of the first characteristics to be predicted by a theoretical analysis of the plasma and was later confirmed experimentally by, Merrill and Webb [2.2].

Creating a laboratory plasma in which these phenomena can be studied is very difficult as it has to achieve a high degree of ionisation to approach the plasma state and ionisation is an energy intensive process. Generating plasmas in the laboratory requires the transfer of large amounts energy to ionise the gas and create the plasma. Fortunately electric discharges present a relatively simple method of transferring the energy to the gas. Electric discharges are generated by applying a potential between two electrodes in such a way as to overcome the ionization threshold of the gas in which the discharge is struck. Electrons are generated at the cathode and are shot into the gas, as primary electrons. When the excited electrons collide with the gas atoms, some of the atoms are ionised which produces more electrons and secondary electrons and by these processes the high degree of ionisation needed to generate a plasma is achieved. As an electric discharge is a relatively easy way to achieve a laboratory plasma it was one of the first types of plasma to be studied experimentally and theoretically, with the D.C. arc being one of the best understood, [2.3].

Magnetohydrodynamics. The description of a conducting fluid interacting with electric and magnetic fields is called magnetohydrodynamic. The magnetohydrodynamic equations are derived by accounting for the magnetic force in the normal hydrodynamic equations and using Maxwells' equations and Ohms' law as

equations of state to determine the resultant forces. The magnetohydrodynamic equations are;

$$\frac{\partial \rho}{\partial t} + \rho(\nabla . v) = 0$$

equation 2.12

$$\rho \frac{dv}{dt} = - \nabla P - \frac{1}{8\pi\mu}\nabla(\mathbb{B}^2) + \frac{1}{4\pi\mu}(\mathbb{B}.\nabla)\mathbb{B}$$

equation 2.13

$$\frac{d\mathbb{B}}{dt} + - (\mathbb{B}.\nabla)v = \frac{c^2}{4\pi\mu\sigma}\nabla^2\mathbb{B}$$

equation 2.14

$$\nabla . \mathbb{B} = 0$$

equation 2.15

$$\nabla . v = 0$$

equation 2.16

where P is the induced gas pressure, ρ is the density of the gas, μ is the permeability, v is the mean fluid velocity, $\mathbb{B}$ is the induced magnetic field, c is the velocity of light and t is the time. The equations cannot be solved analytically and solutions are obtained by either making further approximations for some of the parameters or finding numerical solutions. Despite the complexity of the equations they enable the prediction of the behaviour of the plasma to be determined when subjected to various stabilizing forces.

The external stabilizing force counters the internal forces, generated by the current flow and presence of an electric field, enabling the arc to reach equilibrium, in terms of its position in a confinement regime. Much can be learnt of the magnetohydrodynamic characteristics of a plasma by stabilizing it to be stationary by applying a magnetic field against the presence of a gas stream. When this technique is applied to an electric arc it is found that the magnetic field needed to stabilize into a stationary arc is proportional to the square of the gas velocity. This can be predicted from the MHD equations. If a transverse magnetic field is applied then the driving magnetic pressure, P_{mag}, can be found from equation 2.12 to be

$$P_{mag} = \frac{1}{8\pi\mu}\nabla\mathbb{B}^2$$

equation 2.17

This square law relationship between magnetic field and gas flow shows that an arc behaves as a solid body and is subject to aerodynamic drag. The arc is moved as a solid body along the electrodes when an external driving force is applied.

2-3 THE PHYSICS OF AN ELECTRIC ARC

Many of the properties of the electric discharge can be deduced by considering the conditions in which a conducting channel in a gas carrying a large current can be maintained, as shown in figure 2.2.[2.6.] A typical example of an electric arc might have the characteristics described as follows. The channel is assumed to be uniform throughout its length and cross section, with a radius, a, of 0.1 cm and electric field gradient, $\mathbb{E}$, of 6 Vcm^{-1} carrying a current, I, of 50 A.

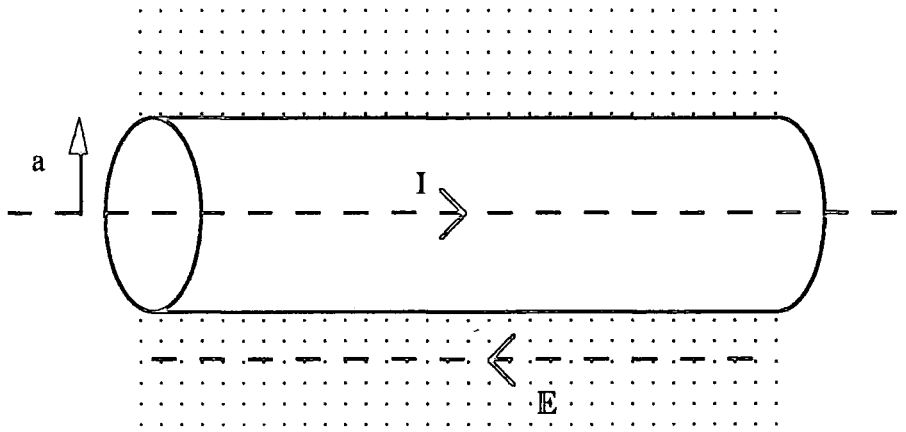

Figure 2.2. A conducting channel within a gas, with a radius, a, field gradient, $\mathbb{E}$, and carrying a current I.

With this simple model many of the properties of the electric arc can be demonstrated, the first being to show that quasi-neutrality must be maintained. If the current was maintained by the electrons only then the electron current density would be given by equation 2.18

$$j_a = n_e e v_e = \frac{I}{\pi a^2}$$

equation 2.18

where j_a is the electron current density of 1591 A cm^{-2}, n_e is the number density of electrons, e is the charge on an electron and v_e is the drift velocity. It is possible to calculate n_e if the drift velocity can be evaluated. The drift velocity can be calculated from an expression derived by Townsend,

$$v_e = 0.815 \times 10^7 \frac{\mathbb{E} e \lambda}{mu}$$

equation 2.19

where λ is the mean free path of the electron, u is the root mean square velocity of random electron motion and m is the mass of an electron. If the temperature of the gas is known then u and λ can be calculated. The gas is assumed to be at a temperature of 7000 K. The value of λ is found to be approximately 8.36×10^{-5} cm with u equal to 5.18×10^7 cm sec^{-1}, then v_e is calculated to be 1.39×10^4 cm sec^{-1}. Substituting this value into equation 2.12. gives n_e as 7.15×10^{17} electrons cm^{-3}. If this number of electrons existed in the channel, without other oppositely particles present, then there would be an electric field gradient of 5.5×10^{11} V cm^{-1}. The forces acting on each electron in the presence of such a field strength would be enormous and this shows that any departure from quasi-neutrality, where positive ions are present in almost exactly the same number, is not possible.

The electron drift velocity, v_e, is much larger than the ion drift velocity, v_i, as the mass of an ion is much greater than that of an electron and although the current density should be expressed as,

$$j_e = ne(v_e + v_i)$$

equation 2.20

it is still valid to assume that n approximately equals n_e as the majority of the current will be carried by electrons and the ions serving chiefly to neutralize the space charge of the electrons. The ions play a secondary role by helping to keep the fast moving electrons in the plasma column and not allowing them to diffuse out of the channel. The

high velocity of the electrons causes them to rush out from the centre of the plasma to the walls of the plasma, leaving the walls of the plasma column negatively charged and the central region positively charged. The negatively charged edge of the plasma is known as the column sheath.

The column sheath. At the wall of the plasma for quasi-neutrality to hold the ion and electron fluxes should remain equal. For this to occur the ions must acquire the mean thermal speed of the electrons, which would require them to attain very high energy levels. It is not possible for the walls to remain quasi-neutral and they acquire a negative charge. The negative charge on the walls of the plasma generates a large electric field which repels electrons and attracts ions known as the plasma sheath, as shown in Figure 2.3. The thickness of the plasma sheath is found to be approximately twice the Debye length.

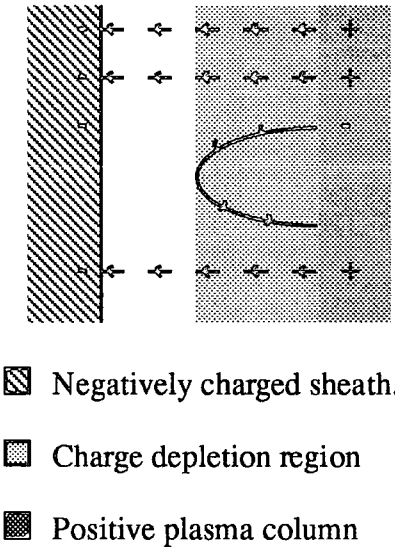

Figure 2.3. The formation of the plasma sheath. The positive ions are attracted from the plasma column, while the electrons are repelled from the negatively charged sheath.

The condition for the plasma remaining quasi-neutral is that the kinetic energy of the particles in the plasma remains less than the thermal energy of the particles. If this is met then any disturbance in the charge distribution will not grow. If this is not met then the disturbance in the plasma will grow rapidly exponentially over a distance of the order of the Debye length, λ_D, and a large charge separation will appear.

As the velocity of the ions is much slower than that of the electrons the effect of the plasma sheath is to hold back the faster diffusing particles to a diffusion rate that is close to the ion diffusion rate. The overall diffusion of particles out of the plasma is said to be ambipolar. This leaves the central region of the arc positively charged and it is known as the positive column.

The positive column. A simple model of the positive column can be found in [2.4] and was originally developed by Schottky, [2.5]. The plasma particles are considered as inter-diffusing gases and the temperature is assumed to be uniform throughout the plasma. The drift of the ions and electrons is then represented by mobility equations,

$$(nv)_- = -q_-\left[kT_-\nabla n_- + n_-e\mathbb{E}\right]$$

equation 2.21,

$$(nv)_+ = -q_+\left[kT_+\nabla n_+ - n_+e\mathbb{E}\right]$$

equation 2.22,

where the sum of the forces due to the partial pressure gradient, grad p = $kT\nabla n$, and the electric field force, $ne\mathbb{E}$, are equated to the retardation $q^{-1}(nv)$, due to friction between the charged and neutral component gases. If the number of electrons and ions is assumed to be equal, $n_- = n_+$ (quasi-neutrality), then the electric field can be eliminated from a mobility equation, which results in equation 2.23,

$$nv = -k(T_+ + T_-)\frac{q_+q_-}{q_+ + q_-}\nabla n$$

equation 2.23,

which has the form of a diffusion equation, equation 2.24

$$n\mathbf{v} = - D_a \nabla n$$

equation 2.24.

where D_a is the ambipolar diffusion coefficient. The diffusion coefficient is related to the mobility q by D = qkT. So

$$D_a = \frac{D_+ D_-}{T_+ D_- + T_- D_+}(T_+ + T_-)$$

equation 2.25

As the mobility and temperature of the electrons are much greater than those of the ions it is possible to approximate equation 2.25 by,

$$D_a \approx D_+ \frac{T_-}{T_+}$$

equation 2.26

The ions diffuse to the wall of the plasma column under the pressure caused by the electrons, with a mobility determined by the rate of loss of momentum from ions to neutrals. This equation can now be used to determine the spatial distribution of ionized components in the plasma. The approximation that the ions and electrons are produced at a rate that is proportional to the electron density is necessary to allow a solution of equation 2.24 to be found. The equation of continuity for the ions becomes

$$\mathrm{div}(n\mathbf{v}) = \kappa n$$

equation 2.27

where κ is the ionization rate per electron. The ambipolar diffusion equation for the distribution of the ionized gas is found from

$$\nabla^2 n + \frac{\kappa}{D_a} n = 0$$

equation 2.28

This equation can be solved to give the spatial distribution of the ions and electrons in the plasma. The boundary conditions are that the gradient should vanish on the axis of symmetry of the containing vessel and the density must fall to approximately zero at the walls of the vessel. Any solution to this is dependent on the geometry of the confinement vessel and a solution is not attempted in this section. The positive column

model describes the centre section of the plasma, but at the edge of the plasma the assumption that the density is approximately zero does not hold and quasi-neutrality of the plasma is no longer a valid assumption.

Charged particles will be escaping from the plasma column in a radial direction. The ions slow the faster particles' diffusion rate to a sustainable rate where the lost charged particles can be replaced by ionization of particles within the plasma column. The energy for this ionization is most likely to come from the electric field that is present along the arc column. The mechanism of ionization will be from atoms in collision with electrons and other particles within the plasma. At atmospheric pressure it is possible to prove that the ions and electrons must be in thermal equilibrium . The electrons gain energy when they move parallel to the electric field and if the electric field is 6 Vcm^{-1} then an electron moving 1 cm parallel to it will gain 6 eV of energy. The velocity of the electron can be assumed to be at least the root mean square velocity, u, of the gas (5.18×10^7 cm sec^{-1},) because the electrons gain their energy from the electric field and transfer it to the plasma particles. In drifting 1 cm parallel to the electric field the electron will zigzag a path at least 3700 cm long and will make (3700 / λ) 4.5×10^7 collisions with the plasma atoms. For the ions and electrons to be in thermal equilibrium the electrons must transfer at least (6 /4.5×10^7) = 1.35×10^{-7} eV per collision. If the collisions are all assuming to be elastic the amount of energy that is transferred per electron particle collision can be calculated. If this amount of energy is greater than the minimum energy transfer to maintain a thermal equilibrium then the electrons and ions can be assumed to be in thermal equilibrium. Calculations done by J.M. Somerville [2.6] show that at least 1.35×10^{-7} eV of energy is transferred per elastic collision and the arc must be in thermal equilibrium.

Thermal equilibrium will only occur if the mean free path, λ, is relatively short and there are a relatively large number of collisions. If the plasma were at a low pressure the electrons would gain a large amount of energy between collisions and their temperature would rise much higher than the other molecules in the plasma. Thermal equilibrium can only be assumed for electric discharges at relatively high pressures. In

vacuum discharges λ is much longer and the subsequent electron energy much higher than the ions.

The ionization processes in the plasma are referred to as *thermal ionization,* a general term for the ionizing action of molecular collisions, radiation and electron collisions occurring in gases at high temperatures. The degree of ionization, x, is defined as the number density of ionized particles divided by the total number of particles and for a known gas can be predicted by Saha's equation,

$$\left(\frac{x^2}{1 - x^2}\right)p = 3.16 \times 10^{-7}\, T^{2.5}\, \mathrm{Exp}\left[\frac{-eV}{kT}\right]$$

equation 2.29

where p is the pressure of the gas, T is the absolute temperature, e is the charge on an electron, V is the ionization potential and k is Boltzmann's constant, [2.6, 2.7]. For a temperature of 7000 K at atmospheric pressure the ionization potential of an air burning electric arc is approximately 9.5 volts, [2.7,] the degree of ionization, x, is 9.96×10^{-4}. This corresponds to a ion density, n_i, of 1.21×10^{17} ions per cm^3. This is of the same order of magnitude as the number density of electrons, n_e, that were calculated as needed to sustain the current flow through the arc column, showing that the initial assumption of a column temperature 7000 K is a reasonable one.

2-4 PLASMA TYPES

There are several different types of plasma that exist which are characterized by the amount of energy that is used to create and sustain the plasma. The types of plasmas can be sub-divided into two groups thermal equilibrium (hot) plasmas, where the electrons and ions are in thermal equilibrium and non equilibrium plasma, where the electrons are much hotter than the ions. A non equilibrium plasma is called a cold plasma as the discharge gas temperature is usually close to room temperature. Figure 2.4. shows some of the plasma types that are encountered in nature defining them by their electron temperature.

The ionosphere. The ionosphere may be regarded as a plasma although the number density of ionized particles and their temperature are low. The ionization processes that occur in the ionosphere are not dominated by thermal ionization as the energy of the particles is not high enough. Solar radiation will cause ionization and this is an important factor in the number density of ions in the plasma. Other contributory factors in the degree of ionisation in the ionosphere include atmospheric conditions, polluting gases which cause changes in the ionization energy of the gas making the ionosphere an ever changing terrestrial natural occurrence of a plasma.

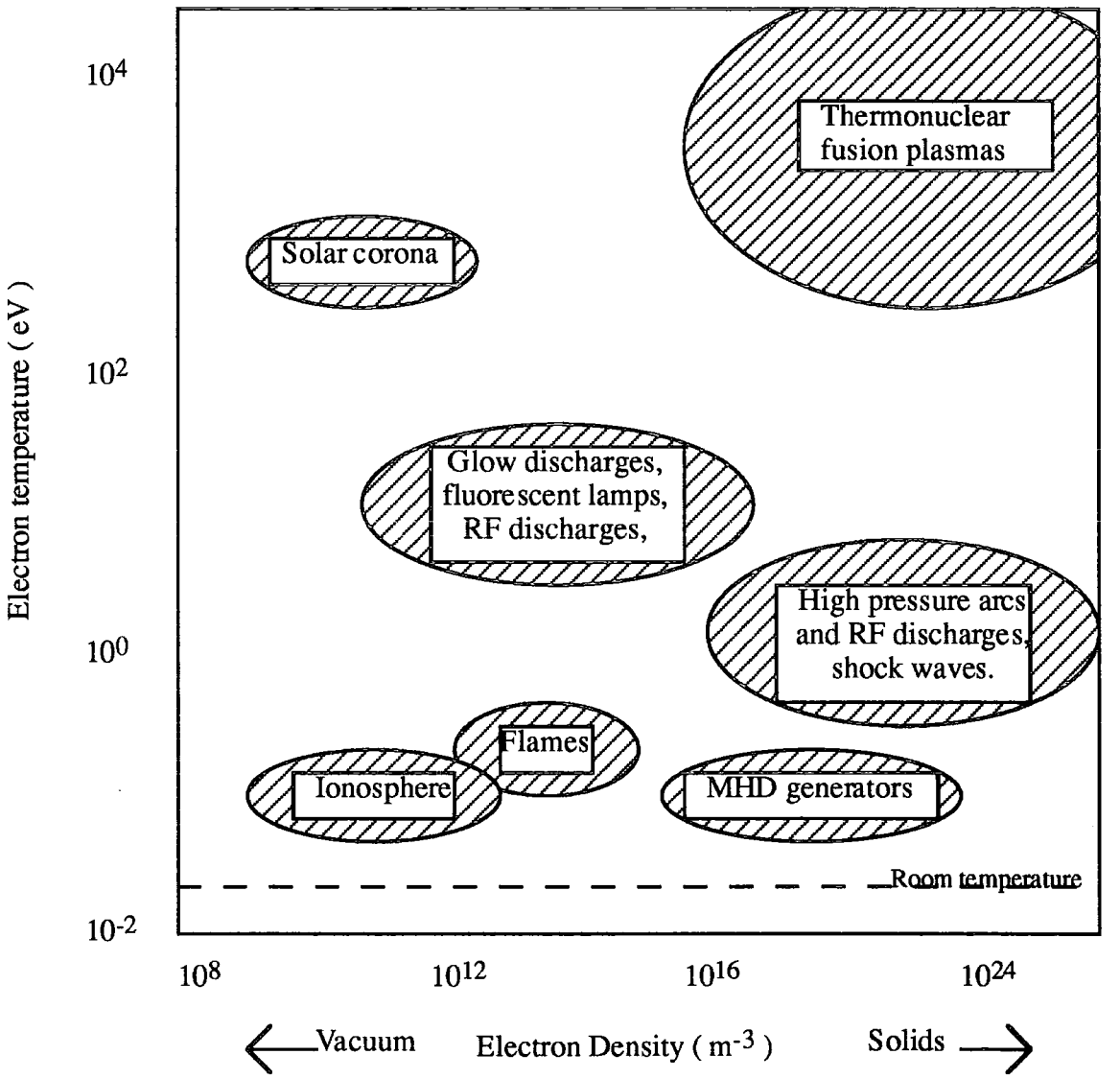

Figure 2.4. Electron densities and electron temperatures for various plasmas.

Flames. A flame is the term used to describe very hot gases where thermal ionization processes will take place. In most hot gases the degree of ionization is small as predicted by Saha's equation, equation 2.29 and the number of charged particles relatively low. The energy of the free particles in the gas will be small as the temperature is not sufficient to turn the gas into a true thermal equilibrium plasma. In some cases where the temperature of the gas is heated to a sufficient temperature the gas does display plasma properties. An example of this is the nose cone of a re-entry vehicle where the frictional heating to the area around the nose cone will cause a sufficiently large increase in temperature for a *flame* type plasma to be created.

MHD. Generators. Magnetohydrodynamic generators are designed to convert the energy flowing in a plasma into electricity. A heat source is used to create a low density plasma which is forced to expand into a channel with speed u_x. A magnetic field B_z is set up perpendicular to the flow direction and this causes an electric field to be induced, perpendicular to the flow direction and the magnetic field, E_y. This electric field can be coupled into a load, generating electricity from a heat source. The efficiency of the MHD generator depends on the conductivity of the plasma. This is dependent on the degree of ionization of the plasma and for efficient operation an unusual type of plasma, in terms of energy components, has to be generated. The plasma is achieved by burning common gases, such as oxygen, nitrogen and carbon dioxide, which have high ionization values, with varying trace amounts of low ionization gases, usually alkali metal vapour, to achieve the optimum plasma conductivity, see [2.17.]

Fusion plasmas. Fusion plasmas are formed when the thermal energy and particle density are sufficiently large enough to allow nuclear fusion reactions to occur. They do not occur naturally terrestrially, but are the mechanism through which energy is released in the universe. Fusion plasmas are fully ionized, high density, $n \approx 1 \times 10^{15}$ cm^{-3} plasmas where the particle energy exceeds 5 KeV. This corresponds to a temperature of approximately 5×10^7 Kelvin. Such intense plasmas are difficult to generate artificially, but they can be generated and confined long enough for the

reaction to occur using an explosion to compress the plasma, which releases fusion energy in an explosive manner. More controlled fusion plasmas are difficult to generate and require highly complex experimental apparatus. Despite 40 years of experimental investigation it is only within the last 2 years that fusion plasmas have actually been generated in a controlled manner in a laboratory.

2-5 ELECTRIC DISCHARGES

The type of discharge that is formed when spark breakdown occurs between two electrodes depends on the pressure of the gas, the discharge length, geometry of electrodes and the parameters of the external circuit. Figure 2.5. shows the current voltage characteristics of a discharge at a gas pressure of 1 mm Hg. The boundaries between transition from one type of plasma to another are only approximate as the actual transition is dependent on many factors unique to each experiment. Townsend discharges are low current, non self sustaining discharges that depend on an external ionizing source, but the energy of the electrons in the discharge is sufficient to ionize by collision other particles in the plasma.

Glow discharges. Glow discharges are those where the positive column of the plasma can be seen to radiate light from a diffuse source, are self sustaining, with a high discharge voltage carrying a low current. The potential of the discharge is found to follow a similarity law where an increase in gas pressure will not alter the discharge voltage provided the dimensions of the gap are decreased correspondingly. The glow discharge has a distinct electrical structure, as shown in figure 2.6., with the voltage discharge being distributed in three regions, the cathode region, the anode region and the positive column.

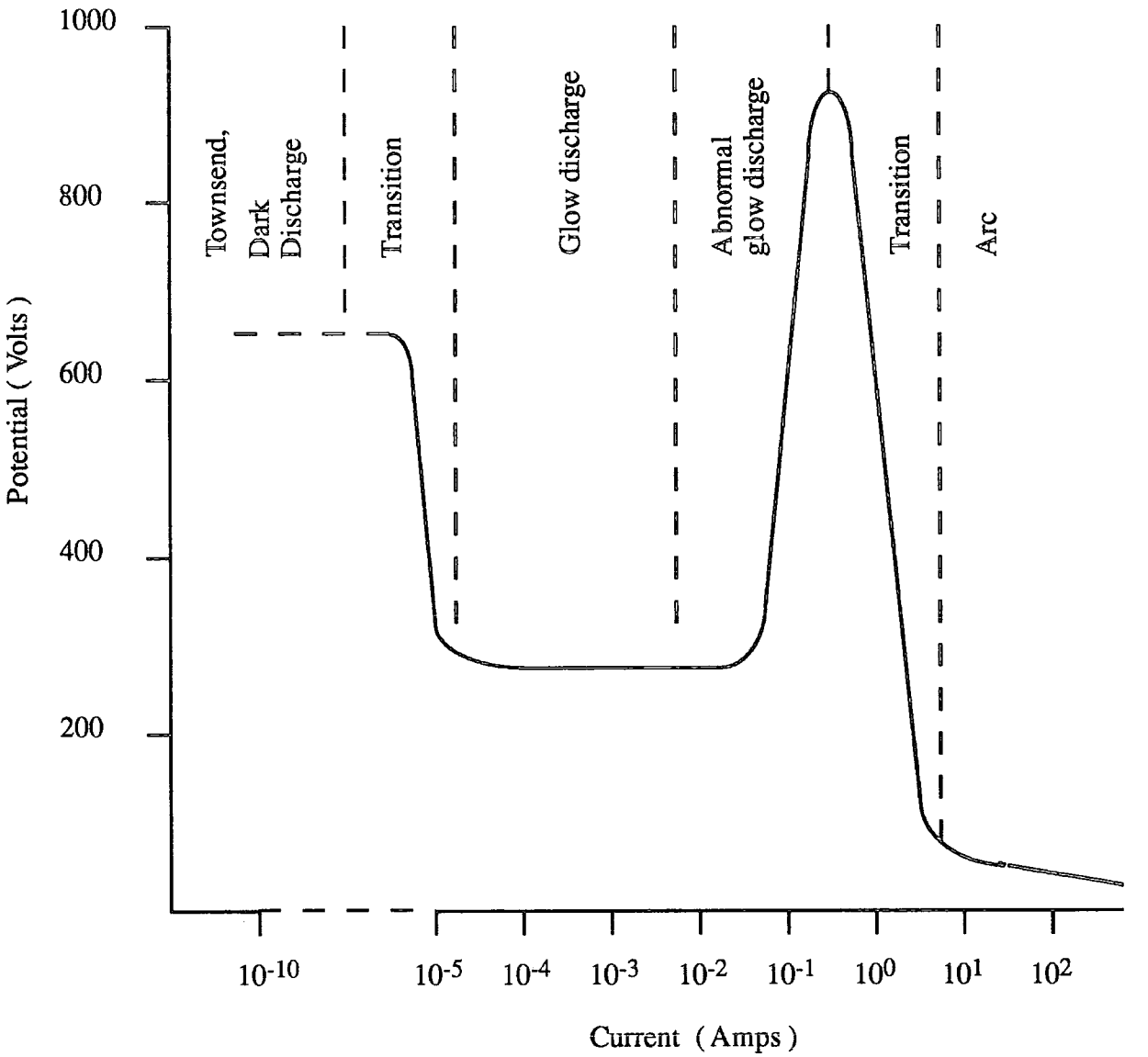

Figure 2.5. Static voltage diagram of a discharge at low pressure, showing the transitions between different types of discharge as the current is increased, see [2.7.]

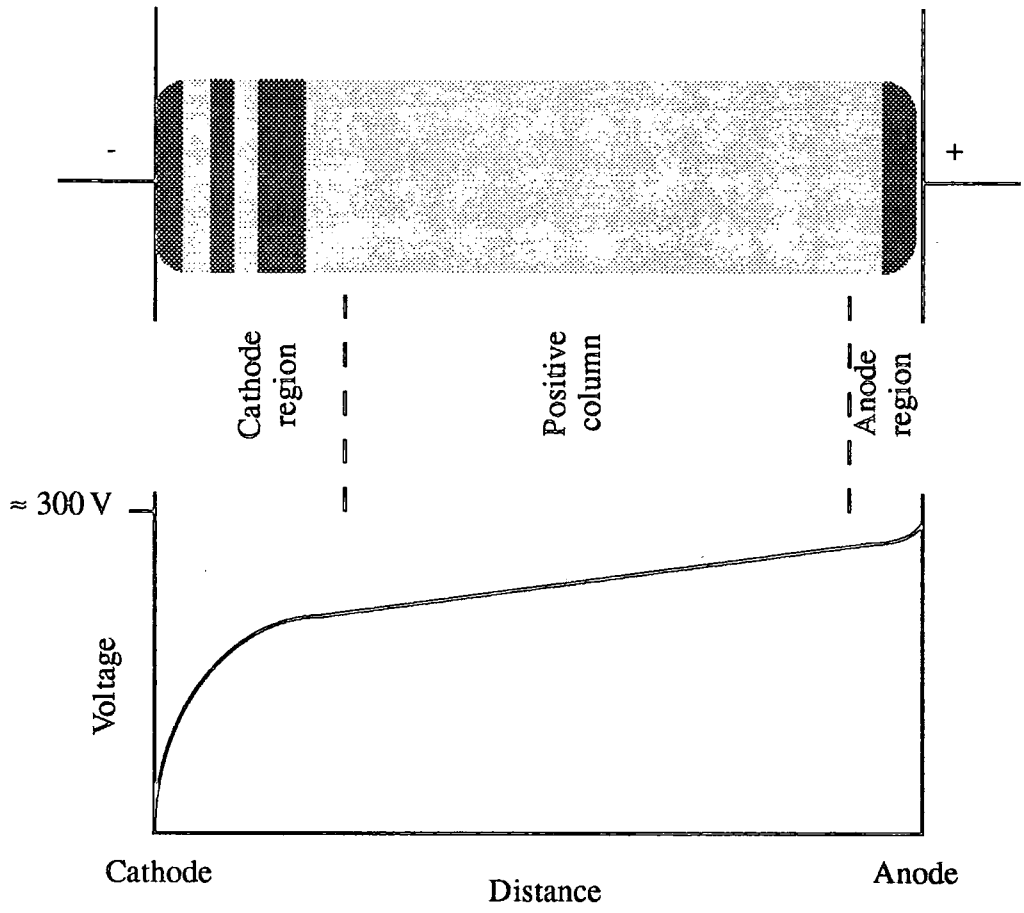

Figure 2.6. The voltage distribution of a glow discharge, showing the distinctive glow regions.

The majority of the discharge voltage is distributed in the cathode region, where the energy is used to liberate electrons from the cathode. The cathode voltage fall is material and gas dependent, but is usually approximately 100 V. The cathode region has alternate bright and dark regions which are characteristic of the glow discharge. Immediately in front of the cathode is the *Aston dark space*, followed by a bright region called the *cathode glow*. The length of the cathode glow depends on the type and pressure of the gas, but it often obscures the Aston dark space. The *cathode dark space* separates the cathode glow from the brightest region of the discharge the *negative glow*. The positive column is divided from the negative glow by the *Faraday dark space*. These light and dark regions vary in length and brightness with the conditions of the glow discharge and they are caused by differing levels of ionization and excitation within these regions.

The positive column of the discharge exhibits a glow which are the lines of the arc spectrum for the discharge gas. The colour of the discharge is therefore linked to the ambient gas and can be varied over a wide range of colours. This makes glow discharges particularly useful for illumination. Glow discharges exhibit quasi-neutrality, but the ions and electrons are not in thermal equilibrium. The temperature of the gas in the column is usually less than 100 °C and therefore the electrons are much hotter than the ions in the plasma. Energy is lost from the column by raising the gas temperature, interaction with the walls of the discharge and the emission of light which only accounts for a very small percentage of the total losses. The high temperature of the electrons causes the formation of a negatively charged sheath at the discharge walls and this enables a positive column to form. The formation of both these phenomena are described in section 2.3. and the equations that describe the glow discharge are similar to those which describe an electric arc.

At the anode there may be a bright glow called the *anode glow* followed by the *anode dark space*. An electric space charge exists immediately in front of the anode, no positive ions are created, or exist, at the anode and the charge is supported entirely by electrons. The positive ions formed in the gas are accelerated away from the anode surface. The resulting space charge region causes a potential drop at the anode. The potential drop is measured to be approximately equal to the ionization potential of the gas and is dissipated over such a small area that it is difficult to measure experimentally.

2-6 THE ARC DISCHARGE.

The transition from the low current, high voltage regime of a glow discharge to the high current, low voltage characteristics of an electric arc requires a change in the electron emission processes. This is because the mechanism that extracts electrons from the cathode, in a glow discharge, is responsible for the majority of the voltage that is dropped across the discharge. In an arc discharge the mechanisms change dramatically as the voltage dropped across an arc discharge is much less yet the current, carried by

the arc, can be much higher. Figure 2.5. shows how the characteristics of the discharge change as the current density is increased. The glow discharge first becomes an abnormal glow discharge, where the column glow is obscured by the brighter negative glow region. As the current density is increased the cathode region decreases in thickness, which in turn increases the electric field strength in the cathode region. The energy dissipated in the cathode region is increased and this causes changes in the electron emission mechanisms, in the cathode region, which do not require such a large voltage drop. Figure 2.7 shows the electrical structure of an arc discharge, which is similar to the structure of a glow discharge, having three regions where the total voltage of the arc is not dropped uniformly across the length of the arc. In this section the properties of the high pressure arc are described, rather than the low pressure arc which is more commonly depicted in descriptions of electric arcs. High pressure arcs are those where the pressure of the discharge gas is of the order of atmospheres whereas low pressure arcs describe discharges in gas pressures of a few mm of mercury. There are few differences in the electrical characteristic, but, as described in section 2.3, the ions and electrons are in thermal equilibrium in a high pressure arc whereas in low pressure arc the discharge gas is at a much lower temperature than the electrons.

The anode region. The anode region provides an electrical connection between the high temperature plasma of the arc and the low temperature anode. Charge carrier generation occurs by two methods, field ionization and thermal ionization. Field ionization is where the energy for ionization is obtained from an electric field generated across the anode region, and for ionization to occur the anode voltage fall must be relatively high. In low pressure arcs field ionization is the dominant process as the temperature of the gas atoms is relatively low. Subsequently the anode voltage fall is found to be relatively high, usually of the order of the ionization potential of the gas.

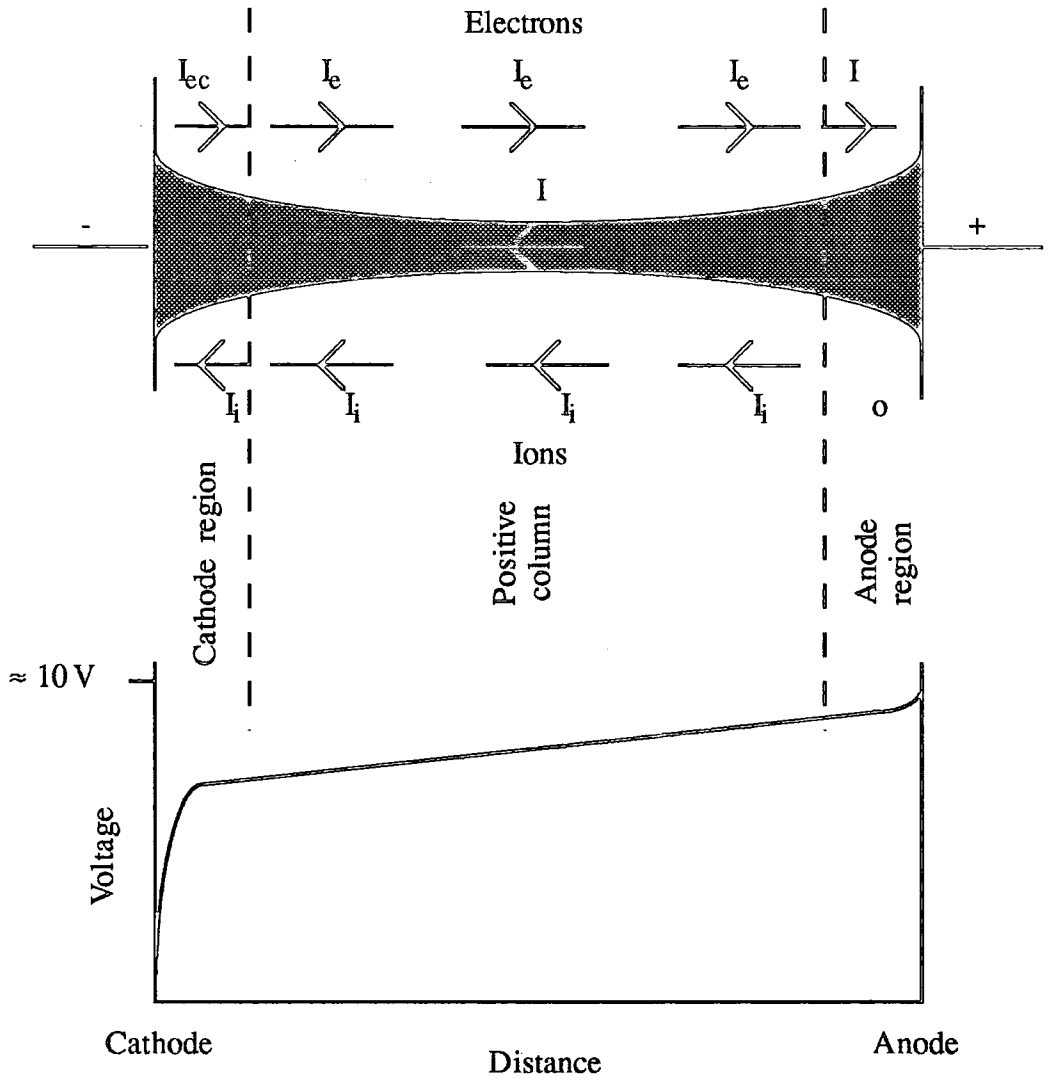

Figure 2.7. The voltage distribution of a high pressure arc discharge, showing the distinct regions. The arrows indicate the direction of motion of the charge carriers.

Thermal ionization processes are dominant in high pressure arc discharges where the particles have a much higher thermal energy and are more likely to ionize by collision processes. The potential drop across the anode region of high pressure arcs is found to be only a few volts and in some cases it is found to be negative.

There have been few investigations of phenomena associated with the anode region as it is of less engineering interest than the cathode electrode. This is because the performance of the anode region, in terms of charged particle emission per second, is much less than in the cathode region. Figure 2.7 shows the motion of the charged carriers in the arc, with the total arc current, I, being carried by both electrons, I_e, and

ions, I_i, where $I = I_e + I_i$. The higher mobility of the electrons results in $I_e >> I_i$. At the anode the current is entirely electronic, therefore I_e / e, where e is the charge of an electron, carriers enter and I_i / e electrons leave the anode region per second. Within the anode region I_i / e carriers must be created per second. In the cathode region I_{ec} / e electrons are extracted from the cathode electrode, where I_{ec} is the extracted electron current, and $(I_e - I_{ec})$ / e electrons are created in the cathode region. The total number of electrons that are extracted or created in the cathode region is therefore I_e / e per second. Extraction and ionization of electrons are both energy intensive processes and as $I_e >> I_i$ the energy input or the performance of the cathode has to be much greater than the anode.

The arc column. The anode and cathode regions are very small regions of the arc within close proximity of the electrodes themselves; these two electrode regions are connected by the positive column. Why the column of the arc is positively charged, because of the higher diffusion coefficients of the electrons and how this is utilized to confine the plasma and maintain quasi-neutrality is described in section 2.3. One of the distinguishing features of a high pressure electric discharge is the very high temperatures of the gas in the plasma column. The temperature can be accurately measured by spectroscopic techniques and is found to be dependent on many factors as shown in tables 2.1. and 2.2.

Electrode material	Temperature (Kelvin)
Copper	4050
Copper (Oxidized)	> 4050
Tungsten	5950
Iron	6020
Carbon	5500

Table 2.1. Temperature of the positive column of the atmospheric pressure air arc. [2.8]

The connection between column temperature and arc current arises because the total energy distributed in the arc column, Q, is proportional to the current flowing in the arc, I, and the electric field gradient of the column, $\mathbb{E}$,

$$Q = I \times \mathbb{E}$$

equation 2.30

However the energy distributed in the column does not increase linearly with the arc current as is suggested equation 2.31 as $\mathbb{E}$, the electric field strength is related to the electric current by

$$\mathbb{E} = \frac{B}{I^n}$$

equation 2.31

where B and n are constants which are heavily dependent on the operating conditions of the arc. [2.9] Substituting equation 2.32 into equation 2.31 gives the energy that is distributed as the current is increased and this can be plotted graphically as shown in figure 2.8.. This is calculated for an atmospheric pressure nitrogen arc burning on copper electrodes and this shows that the energy distributed will increase as the arc current is increased. As shown in section 2.3 the higher temperature is also required to increase the degree of ionization of the gas, to sustain quasi-neutrality, when the current density is increased.

Table 2.2. shows how the temperature of the column depends on factors other than the arc current. The pressure of the discharge gas, the discharge gas and the electrode material all determine the characteristics of the column. The voltage gradient along the arc column is one of the parameters that is altered by the above factors. It can be measured by oscillating the electrode spacing by Δx and measuring the difference in voltage ΔV, with the voltage gradient being $\Delta V / \Delta x$. [2.9, 2.10] Measuring the voltage distribution with Langmuir probes does not give an accurate recording of the voltage distribution of an electric arc. The insertion of the probe introduces cooling around the probe which alters the voltage distribution of the discharge surrounding it and does not give a true representation of the voltage of the arc. [2.11]

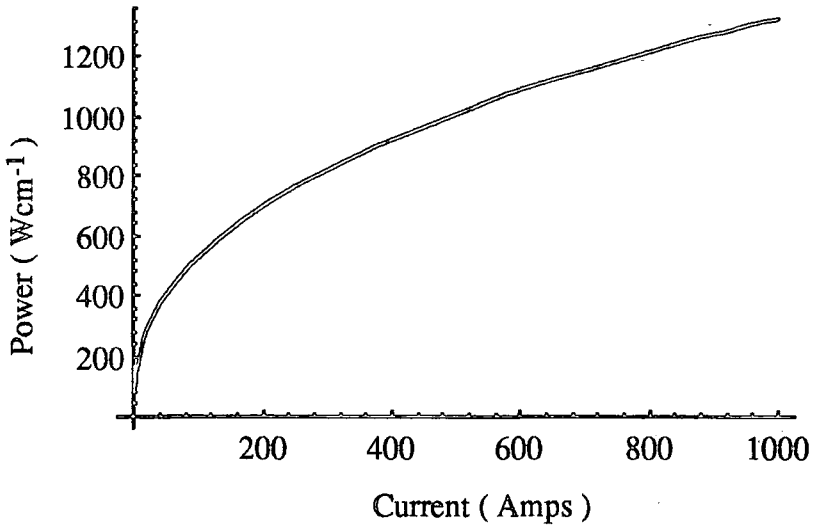

Figure 2.8. Power distributed in an arc column as a function of arc current density.

The discharge gas has an understandable effect on the plasma column as the difference in ionization potential will affect the energy needed to sustain the required number of carriers in the column and therefore the voltage gradient of the arc column. The pressure will have a similar effect due to the increased energy required to ionize particles the higher the gas pressure.

The electrode material will also have a similar effect on the ionization potential of the gas. In any arc discharge, electrode material will be introduced into the arc. This will create a situation where trace elements of metals will be present in the ionized gas. The introduction of trace elements into a gas is usually a reliable method of altering its ionization potential and the amount that it is altered depends on, the element type and the amount found in the gas. An electric discharge is an unusual system where the amount of electrode material in the gas will depend on the current of the discharge and the type electrode material, [2.12, 2.13]. This will result in a discharge gas in which the ionization potential will be difficult to predict theoretically and measure consistently, as few discharge systems produce exactly the same arc characteristics.

Gas	Pressure (atm)	Arc current (Amps.)			
		1	2	5	10
		Column temperature (Kelvin)			
Nitrogen	1	5950	6020	6250	6400
	5	6400	6450	6770	7050
	10	6680	6780	7160	7470
	20	7030	7150	7620	7980
	30	7230	7400	7920	8320
	100	-	-	-	8800
	1000	-	-	-	10200
Hydrogen	1	6500	6600	7000	7400
Air	1	4050	-	-	-
Argon	1	-	-	-	12000

Table 2.2. Dependence of arc column temperature on arc current, discharge gas and pressure.

There is a further complication in that , the cathode electrode material can have a profound effect on the electrical distribution of the electrode regions, particularly the cathode region where the effect is so acute it can determine the characteristics of the discharge as a whole. The behaviour of the cathode region determines the performance of most arc plasma devices and will be discussed in Chapters 3 and 4.

2-7 REFERENCES

2.1.Tonks. L. Langmuir I. 1929 *Oscillations in ionised gases*, Phys. Rev. Vol. 33 p. 195.

2.2. Merrill H.S. Webb H.W. *Electron scattering and plasma oscillations*. 1939, Phys. Rev. Vol 55, p. 1191. .

2.3. Langmuir I. Kingdom K.H. *Thermionic effects caused by vapours of alkali metals*. 1925 Proc. Roy. Soc. A 107, p. 61.

2.4. Thompson W.B. *An Introduction to Plasma Physics*. 1962 London: Pergamon Press.

2.5. Schottky w. 1925 Z.F. Phys. Vol. 31, page 163.

2.6. Somerville J.M. *The Electric Arc* . London: Methuen 1957

2.7 Cobine J.D. *Gaseous Conductors, theory and engineering applications*. 1958 New York: Dover Publications Inc.

2.8 Suits C.G. Physics Vol. 6. p. 315 1935.

2.9.Suits C.G. *High pressure arcs in common gases in free convection*. Phys Rev. Vol. 55. p. 561 1939.

2.10 Dickson D.J. Engel A. von *Resolving the electrode fall spaces of electric arcs* 1967 Proc. of the Roy. Soc. Series A Vol. 300 p. 316 to 325.

2.11 Mason R.C. *Probe measurements on high pressure arcs*. 1937 Phys. Rev. Vol. 51. p.28

2.12 Chapter 3 section 3.8.

2.13 Chapter 4 section 4.4.

2.14 Chapter 5 section 5.3

2.15 Keen B.E. (Ed.). *Plasma Physics* London Inst. of Physics.1974

2.17. Krall A. Trivelpiece A.W. *Principles of plasma physics* New York McGrall - Hill. 1976.

2.18. Feinman J. (Ed.). *Plasma technology in Metallurgical Processing*. Warrendale Iron and Steel Society inc. 1987.

CHAPTER 3 EMISSION MECHANISMS

3-1 INTRODUCTION

The process of sustaining a D.C. thermal arc depends on the performance of the cathode electrode as this is the source of the majority of the electrical current. The energy required to sustain a D.C. thermal arc places demands on the cathode electrode that are not encountered in any other physical situation. The low voltage, high current regime of an arc requires the performance of the cathode, in terms of particle emission per unit energy input and particle emission per second, to be very high. The electron emission current density for a thermal arc is estimated to be approximately 10^{12} Am^{-2}. These enormous current densities require the cathode to employ unusual electron emission processes for which there is no complete physical description. [see Chapter 4]

An accurate physical description will result from gradually modifying existing theories of electron emission to the known experimental evidence of the cathode region. In this Chapter the known physical emission processes will be described and their applicability to the conditions encountered in a thermal arc will be discussed. This will result in a picture of what can be described by already known electron emission mechanisms and which characteristics cannot.

3-2 THE THEORY OF ELECTRON EMISSION FROM METALS

Theories of electron emission from a metal are traditionally solved separately for different mechanisms of electron emission depending on how the electrons overcome the work function of the metal. All the different theories for electron emission can be derived from solving the integral, given in equation 3.1., [3.1] by applying statistical distribution theory and the quantum mechanical solution of electron tunnelling. Equation 3.1. states that the current density of emission, j_e, is given by

$$j_e = e \int_{-E_a}^{\infty} D(E,\mathbb{F})N(E)\,\partial(E)$$

equation 3.1

where e is the charge on an electron, E_a is the average potential energy of a free electron inside the metal, D(E,F) is the probability that an electron with energy E with an applied external electric field strength $\mathbb{F}$ will emerge from the metal and N(E) is the distribution function.

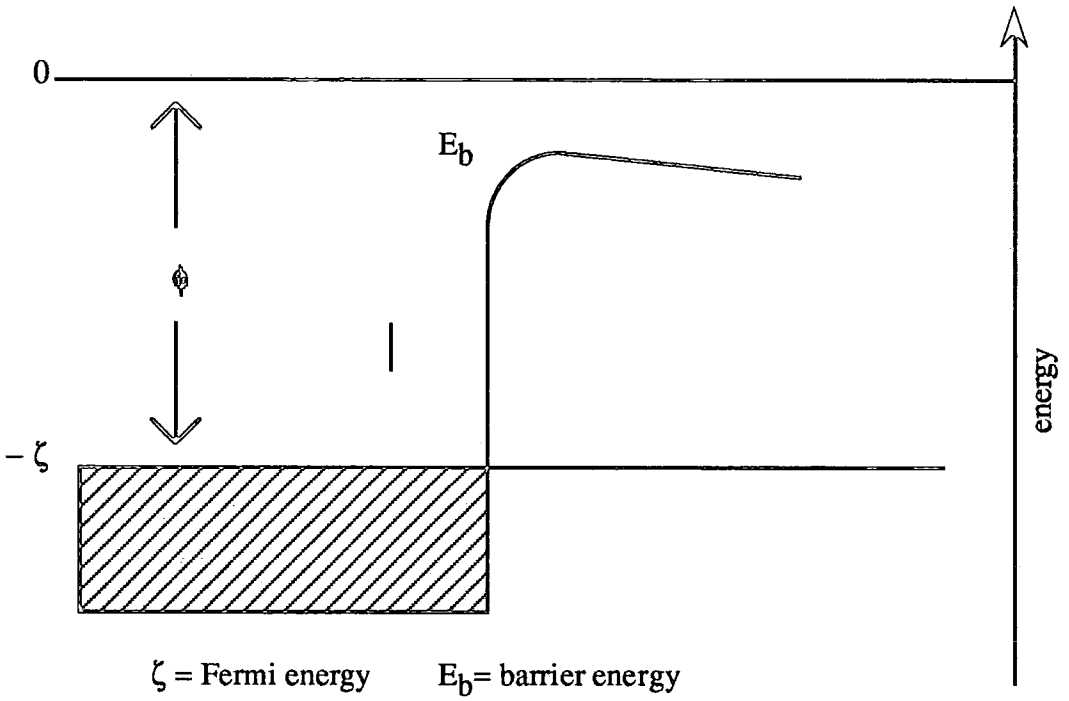

Figure 3.1. The workfunction.

The starting point to any solution of equation 3.1. is a description of the energy barrier which the electron has to overcome and a graphical description of the energy barrier is shown in Figure 3.1. The energy barrier is assumed to be continuous enabling mathematical description. All energies are measured from zero for a free electron outside the metal, so the work function, ϕ, is $-\zeta$, the Fermi energy. E is only the part of the energy for the motion normal to the surface. A mathematical expression for the supply function is taken from the Fermi Dirac distribution and is described by

$$N(T,\zeta,E)\partial E = 4\pi mkTh^{-3} \times \ln\left[1+\mathrm{Exp}\left[\frac{-(E-\zeta)}{kT}\right]\right]\partial E$$

equation 3.2

where T is the absolute temperature, m is the mass of an electron, k is Boltzmann's constant and h is Planck's constant. The energy of the electron normal to the surface is

$$E = \left[\frac{\mathbb{p}^2(x)}{2m}\right] + \mathbb{V}(x)$$

equation 3.3

where $\mathbb{p}(x)$ is the electron momentum normal to the surface and $\mathbb{V}(x)$ is the effective electron potential energy. The potential energy of the electron is taken to be given by

$$\mathbb{V}(x) = \frac{-e^2}{4x} - e\mathbb{F}x, \qquad \text{when } x > 0$$

equation 3.4

$$\mathbb{V}(x) = -E_a \qquad \text{when } x < 0$$

equation 3.5

where $-e^2(4x)^{-1}$ is the image force and $e\mathbb{F}x$ is the contribution from an externally applied electric field. The barrier is assumed to be continuous as shown in figure 3.1 and the potential energy of the particles does not differ from equations 3.4 and 3.5 and the image force is taken to be approximated by the classical image force resulting from the coulombic attraction of the charged particles.

To obtain an expression for $D(E,\mathbb{F})$, the penetration coefficient, the most common solution is to use the Wentzel, Kramers, Brillouin (W.K.B.) approximation. [3.2] The approximate probability that an electron incident on a barrier, will tunnel through the barrier, is given by

$$D(E,\mathbb{F}) = \left[1 + \mathrm{Exp}\left[-2i\hbar\right]^{-1} \int_{x_1}^{x_2} P(\zeta)\partial\zeta\right]^{-1}$$

equation 3.6

where x_1 and x_2 are points where $\mathbb{p}^2(x)$ becomes zero and $\hbar$ is Planck's constant divided by 2π. From equations 3.3, 3.4 and 3.5 it can be shown that the momentum of an electron $\mathbb{p}(x)$ is

$$p(x) = \left[2m\left(E + e^2(4x)^{-1} + e\mathbb{F}x\right)\right]^{1/2}$$

equation 3.7

Equation 3.7 is only valid over a limited range of electron energies as there are singularities above a limiting value, because of the assumption made to describe the energy barrier, and the limiting value, E_l, is given by equation 3.8

$$E_l = -\frac{1}{2}\sqrt{2}(e^3\mathbb{F})^{1/2}$$

equation 3.8

When calculating the emission current it found that the penetration coefficient, D(E,𝔽), is given by combining equations 3.6 and 3.7 below the limiting energy value E_l which above E_l it can be taken as [3.3] Murphy and Good

$$D(E,\mathbb{F}) \approx 1$$

equation 3.9.

according to Murphy and Good [3.3.] The integral in equation 3.6 can be solved using elliptical functions to produce a standard integral. This in turn can be solved to give a solution for the penetration coefficient for energies below E_l which is

$$D(E,\mathbb{F}) = \left[1 + \mathrm{Exp}\left[\frac{4}{3}\sqrt{2}\left[\frac{\mathbb{F}\hbar^4}{m^2e^5}\right]^{-1/4} y^{-2/3}v(y)\right]\right]^{-1}$$

equation 3.10

Here the resulting integrals have been turned into an easier form to solve. Using elliptical integrals by substituting in the Nordheim function v(y) where y is a material dependent constant [3.4,] the emission current density is then given by substituting equations 3.2, 3.9 and 3.10 into equation 3.1. The general expression for the current density of emitted electrons when overcoming a potential barrier, of the form shown in figure 3.1, then becomes

$$j_e(F,T,\zeta) = \frac{kT}{2\pi^2}\int_{-Ea}^{E_l} \frac{\ln\left[1 + \mathrm{Exp}\left[-(E-\zeta)/kT\right]\right]}{1 + \mathrm{Exp}\left[\frac{4}{3}\sqrt{2}\mathbb{F}^{-1/4}y^{-2/3}v(y)\right]}\partial E + \frac{kT}{2\pi^2}\int_{E_l}^{\infty}\ln\left[1 + \mathrm{Exp}\left[-(E-\zeta)/kT\right]\right]\partial E$$

equation 3.11

where j_e is the current density expressed in units of A cm^{-2} / $m^3e^9\hbar^{-7}$, $\mathbb{F}$ is the electric field strength Vcm^{-1} / $m^2e^5\hbar^{-4}$ and ζ, kT, E, E_a and E_l are the corresponding energies divided by $me^4\hbar^{-2}$. This notation is in what is known as Hartree units and they are used throughout this chapter. This expression for the current density is in a format from which it is possible to solve for various conditions of applied electric fields, field emission, applied temperature, thermionic emission and combinations of applied temperature and electric field.

3-3 THERMIONIC EMISSION

Thermal emission of electrons from metals or thermionic emission describes the process where free electrons in the Fermi surface are given enough thermal energy to overcome the work-function potential barrier and become free from the metal. There are two methods of approaching this problem, a thermodynamic approach, as used in the original derivation of the thermionic emission equation by Richardson. [3.5] and a statistical approach. This was the approach used by Schottky [3.6] and is the most useful as it uses the thermal distribution of the electrons in the metal (the Fermi Dirac distribution) [3.7] which gives more information on the behaviour of the electrons. A statistical approach is the one outlined in section 3.2 and the general equation for current density (3.11) can be applied to thermionic emission. In a thermionic emitter where the electric field is found to be small it is possible to replace the distribution term in equation 3.11 by a first order logarithmic expansion

$$\ln\left[1 + \mathrm{Exp}\left[-(E-\zeta)/kT\right]\right] = \mathrm{Exp}\left[-(E-\zeta)/kT\right] - \frac{1}{2}\mathrm{Exp}\left[-2(E-\zeta)/kT\right]$$

equation 3.12

By using a similar expansion for the penetration coefficient

$$\frac{4}{3}\sqrt{2}\mathbb{F}^{-1/4}y^{-2/3}v(y) = -\pi\mathbb{F}^{-1/4}\varepsilon + \frac{3}{16}\pi\mathbb{F}^{-2/3}\varepsilon^2$$

equation 3.13

where $\varepsilon = 1 + E\mathbb{F}^{-1/4}$. Substitution in equation 3.11 results in a simplification of the integral. The expression for the current when these two expansions are inserted into 3.11 becomes

$$j_e(F,T,\zeta) = \frac{kT}{2\pi^2}\int_{-Ea}^{E_1}\frac{\mathrm{Exp}\left[-(E-\zeta)/kT\right]}{1 + \mathrm{Exp}\left[-\pi\mathbb{F}^{-1/4}(1+E\mathbb{F}^{-1/2})\right]}\partial E + \frac{kT}{2\pi^2}\int_{E_1}^{\infty}\mathrm{Exp}\left[-(E-\zeta)/kT\right]\partial E$$

equation 3.14.

Equation 3.14 can be simplified still further if the conditions in which it will be applied are considered. If an extra factor of

$$\left[1 + \mathrm{Exp}\left[-\pi\mathbb{F}^{-1/4}(1+E\mathbb{F}^{-1/2})\right]\right]^{-1}$$

is inserted into the second integrand of equation 3.14, then it can be combined with the first integrand further simplifying equation 3.14. into one integral. This factor rapidly tends to unity with increasing energy and at the lower limit will be

$$\left[1 + \mathrm{Exp}\left(-0.92\mathbb{F}^{-1/4}\right)\right]^{-1}$$

equation 3.15.

In defining the region of thermionic emission it is necessary to limit the applied electric field strength to a sufficiently small level to allow equation 3.15. to be approximately equal to unity. If this is the case equation 3.14. can be simplified to

$$j_e(\mathbb{F},T,\zeta) = \frac{kT}{2\pi^2}\int_{-Ea}^{\infty}\frac{Exp\left[-(E-\zeta)/kT\right]}{1 + Exp\left[-\pi\mathbb{F}^{-1/4}(1+E\mathbb{F}^{-1/2})\right]}\partial E$$

equation 3.16.

These substitutions are only applicable under certain conditions. The limits of when these substitutions are valid are the boundaries of the temperature and electric field strength within which the thermionic equation applies. The boundary is defined as the region in which the approximations made should be valid in the range of energy E that equation 3.16. is appreciable. If d is defined to be

$$d = \frac{\mathbb{F}^{3/4}}{\pi kT}$$

equation 3.17

then the limits within which the thermionic emission equation is valid can be shown to be

$$\ln\left[\frac{(1-d)}{d}\right] - \frac{1}{d(1-d)} > -\pi\mathbb{F}^{-3/4}(\phi - \mathbb{F}^{1/2})$$

equation 3.18

and

$$\ln\left[\frac{(1-d)}{d}\right] - \frac{1}{d(1-d)} > -\pi\mathbb{F}^{-1/8}$$

equation 3.19

where z has been replaced by - ϕ. As the energy $-E_a$ is below the Fermi level, for a metal, the integral in equation 3.16 can be approximated by the integral,

$$j_e(F,T,\zeta) = \frac{kT}{2\pi^2}\int_{0}^{\infty}\frac{Exp\left[-(E-\zeta)/kT\right]}{1 + Exp\left[-\pi\mathbb{F}^{-1/4}(1+E\mathbb{F}^{-1/2})\right]}\partial E$$

equation 3.20.

which is a standard integral which has the solution given in equation 3.21

$$j_e = \frac{1}{2\pi^2}(kT)^2\left[\frac{\pi d}{\sin\pi d}\right]\mathrm{Exp}\left[-\frac{\phi - \sqrt{\mathbb{F}}}{kT}\right]$$

equation 3.21.

where j_e is the current density expressed in Hartree units. When d is taken to be very small $\pi d / \sin\pi d$ tends to 1 and equation 3.21 becomes the thermionic emission equation, incorporating the Schottky effect.

This derivation provides the boundary conditions for the thermionic emission equation to be valid. The region is always bounded by the d = 1 line and equations 3.18. and 3.19. and these arguments can be used to define when thermionic emission is the valid emission mechanism for arcing conditions.

Figure 3.2, i, ii and iii illustrate the thermionic function with an electric field of 1000 V cm^{-1} the function is primarily dependent on the temperature with little emission below the threshold temperature. The emission current becomes significant when appreciable numbers of electrons gain enough thermal energy to overcome the workfunction. At this low electric field strength the function is only weakly dependent on this parameter and only becomes significant at field strengths of 1×10^5 V cm-1 as shown in figure 3.3, when electron tunnelling becomes significant.

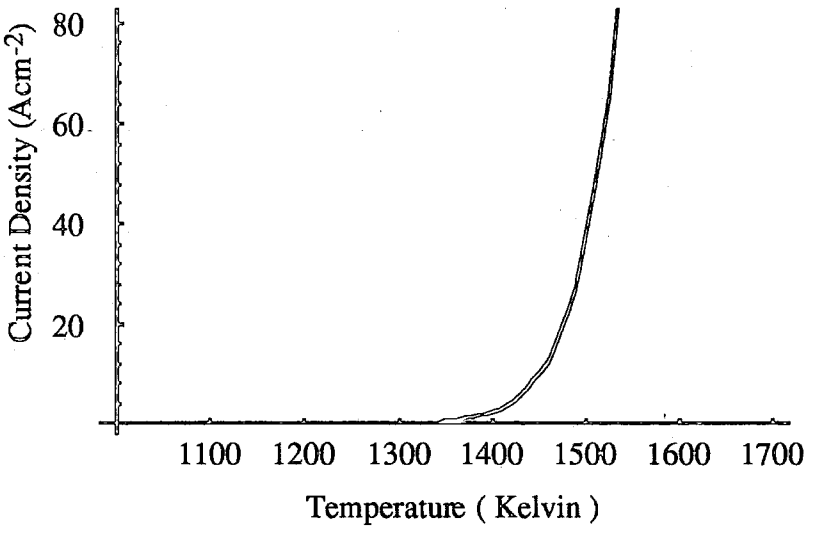

i

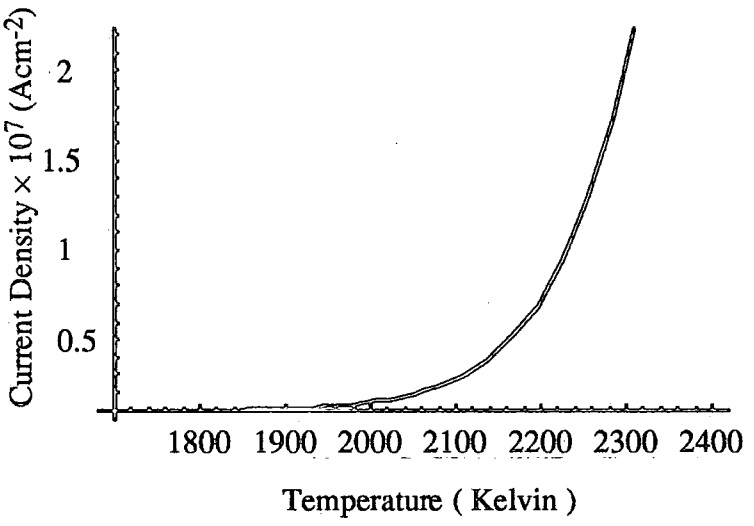

ii

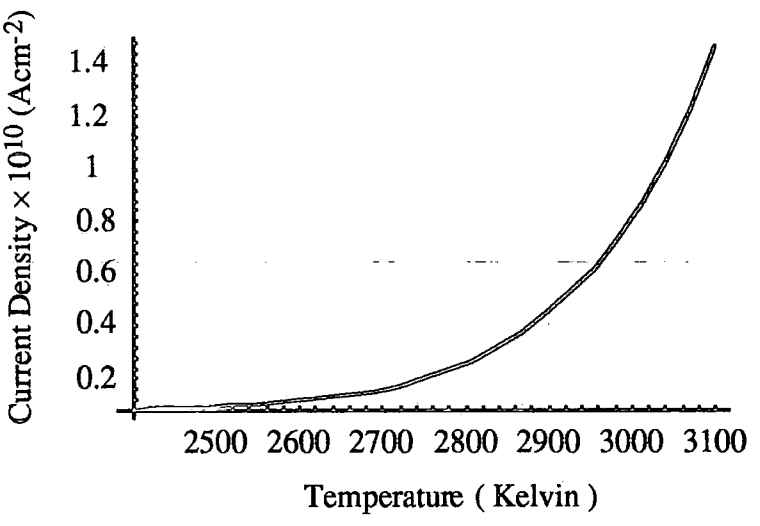

iii

Figure 3.2 i, ii and iii. The thermionic emission equation, equation 3.21, plotted with current density versus temperature, with an electric field of 1000 V cm^{-1}.

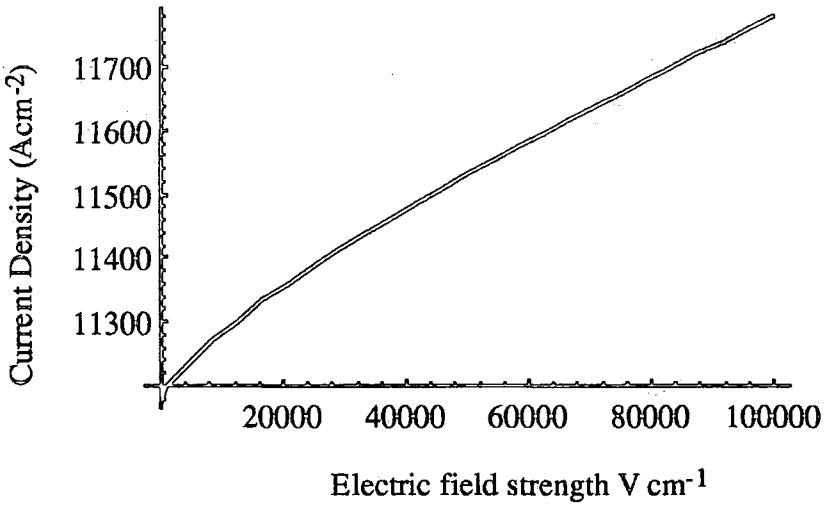

Figure 3.3 The electric field dependency of the thermionic emission equation, at a temperature of 1400 K.

3-4 THE FIELD EMISSION REGION

The low temperature high electric field strength condition of electron emission is called the field emission region as the current density is heavily dependent on the electric field strength. The equation that describes the process of electron emission by the application of a high electric field is the Fowler Nordheim equation [3.8]. The field emission equation was first derived by calculating the emission or reflection coefficient of an electron at the surface of a metal and integrating over all incident electrons according to the electron conductivity model of Sommerfeld [3.9]. The field emission equation derived in this section accounts for the electron having some thermal energy and uses the Fermi Dirac distribution rather than the Sommerfeld model, however the Fowler Nordheim equation can be defined when emitters at room temperature are considered.

The field emission equation can be derived from the general emission equation 3.11. A substitution of the penetration coefficient is made and careful analysis of the region of field emission enables a suitable solution of the resulting integral to be made. As with thermionic emission this results in an equation which is valid over a set of

defined conditions of temperature and applied electric field strength. The substitutions are for the penetration coefficient term in equation 3.11 which are first and second order expansions,

$$1 + \mathrm{Exp}\left[\frac{4}{3}\sqrt{2}\mathbb{F}^{-1/4}y^{-2/3}v(y)\right]^{-1} = \mathrm{Exp}\left[\frac{4}{3}\sqrt{2}\mathbb{F}^{-1/4}y^{-2/3}v(y)\right] \times \left[1 - \mathrm{Exp}\left(\frac{4}{3}\sqrt{2}\mathbb{F}^{-1/4}y^{-2/3}v(y)\right)\ldots\right]$$

equation 3.22

and

$$\frac{4}{3}\sqrt{2}\mathbb{F}^{-1/4}y^{-2/3}v(y) = - b + c(E-\zeta) - f(E-\zeta)^2 \ldots$$

equation 3.23

where

$$b = \frac{4}{3}\sqrt{2}\mathbb{F}^{-1}\phi^{2/3}v(\sqrt{\mathbb{F}}/\phi)$$

equation 3.24,

$$c = 2\sqrt{2}\mathbb{F}^{-1}\sqrt{\phi}t(\sqrt{\mathbb{F}}/\phi)$$

equation 3.25,

and when

$$f = \frac{1}{2}\sqrt{2}\mathbb{F}^{-1}\phi^{2/3}(\phi^2 - \mathbb{F})^{-1}v(\sqrt{\mathbb{F}}/\phi)$$

equation 3.26.

The function t(y) is a derivative of the elliptical functions which was evaluated by Nordheim [3.10] and evaluated numerically by Burgess, Kroemer and Houston [3.11]. When the first term of equation 3.22. and the first term of equation 3.23. are substituted into equation 3.11 the equation becomes,

$$j_e = \frac{kT}{2\pi^2}\int_{-Ea}^{E_1} \mathrm{Exp}\left[-b + c(E-\zeta)\right]\ln\left[1 + \mathrm{Exp}\left[-(E-\zeta)/kT\right]\right]\partial E + \frac{kT}{2\pi^2}\int_{E_1}^{\infty} \ln\left[1 + \mathrm{Exp}\left[-(E-\zeta)/kT\right]\right]\partial E$$

equation 3.27

The second part of this integrand makes a negligible contribution to the current in the field emission region and is neglected in the solution for the field emission equation. This forms part of the limit in conditions for which the solution is valid. As the second integrand is neglected the limits of the first integral are assumed to be zero, (as the emitter is a metal) and infinity, and as only the first integral is significant it is possible to extend the upper limit to make the integral a standard integral,

$$j_e = \frac{kT}{2\pi^2}\mathrm{Exp}[-b]\int_0^{\infty} \mathrm{Exp}\left[c(E-\zeta)\right]\ln\left[1 + \mathrm{Exp}\left[-(E-\zeta)/kT\right]\right]\partial E$$

equation 3.28.

The solution to this integral gives an expression for the current emitted when an electric field is applied with a relatively low temperature,

$$j_e = \frac{\mathbb{F}^2}{16\pi^2\phi t^2}\left[\frac{\pi ckT}{\sin\pi ckT}\right]\mathrm{Exp}\left[-\frac{4\sqrt{2}\phi^{2/3}v}{3\mathbb{F}}\right]$$

equation 3.29

This expression becomes the field emission equation when the temperature is low as the expression $\pi ckT / \sin \pi ckT$ tends to 1. The boundaries within in which this equation are valid are defined by the assumption that the second integrand in equation 3.27. does not contribute significantly to the current density as the temperature is not high enough. The energy at which the integral is a maximum, at energy E_{max}, is given by ,

$$ckT\left[1 + \mathrm{Exp}\left[(E_{max} - \zeta)/kT\right]\right]\ln\left[1 + \mathrm{Exp}\left[(E_{max} - \zeta)/kT\right]\right] = 1$$

equation 3.30.

which gives conditions for temperature and electric field as the two maxima occur when $E_{max} = \zeta - c\text{-}1$ and $E_{max} = \zeta + kT\ln[ckT/(2 - 2ckT)]$. This results in the energy range where the current contribution from the second integrand is significant when the energy is in the range

$$\zeta + kT(1\text{-}ckT)^{-1} > E > \zeta - 2c^{-1}$$

equation 3.31

The other approximation made to solve the first integrand was to use only the first order of the expansion, in equation 3.22, in substituting into equation 3.11. This is valid when

$$\mathrm{Exp}\left[\frac{4}{3}\sqrt{2}\mathbb{F}^{-1/4}y^{-2/3}v(y)\right] < \mathrm{Exp}[-1]$$

equation 3.32

In terms of the electron energy this is satisfied when

$$E < -\sqrt{\mathbb{F}} - \pi^{-1}\mathbb{F}^{3/4}$$

Equation 3.33

The approximation of the expansion 3.23 is linear over the integration range is only valid when

$$f(E - \zeta)^2 < \frac{1}{2}$$

equation 3.34

and this leads to another range of conditions outside which equation 3.29 is no longer valid. These two inequalities, 3.31 and 3.33 can be combined to give in terms of temperature and electric field the expression,

$$\zeta + kT(1-ckT)^{-1} < -\sqrt{\mathbb{F}} - \pi^{-1}\mathbb{F}^{3/4}$$

equation 3.35.

Replacing the energy term ζ by $-\phi$, rearranging the inequality 3.35 and combining it with 3.34 gives the range of conditions over which the field emission equation is valid, namely

$$f - \sqrt{F} > \pi^{-1}\mathbb{F}^{0.75} + \frac{kT}{1 - ckT}$$

equation 3.36,

and

$$1 - ckT > \sqrt{2}fkT$$

equation 3.37.

These inequalities demonstrate that there is a large range of external conditions of temperature and electric field strength in which neither thermionic emission, equation 3.21 or field emission equation, equation 3.29 is applicable. There is an intermediate

region in which the general equation for the current density, equation 3.11, has to be solved resulting in a third relation.

Figure 3.4 shows the relation of equation 3.29 with electric field and is similar to the Fowler Nordheim emission equation as shown in Chapter 1. This equation has a slight dependency on the temperature that is not accounted for by the Fowler Nordheim emission equation. The effect of temperature is not readily apparent in these calculations because of the initial high temperature that is used. The initial temperature of 1000 K is used as the cathode will emit from a molten spot which will be at a minimum temperature of 1000 K.

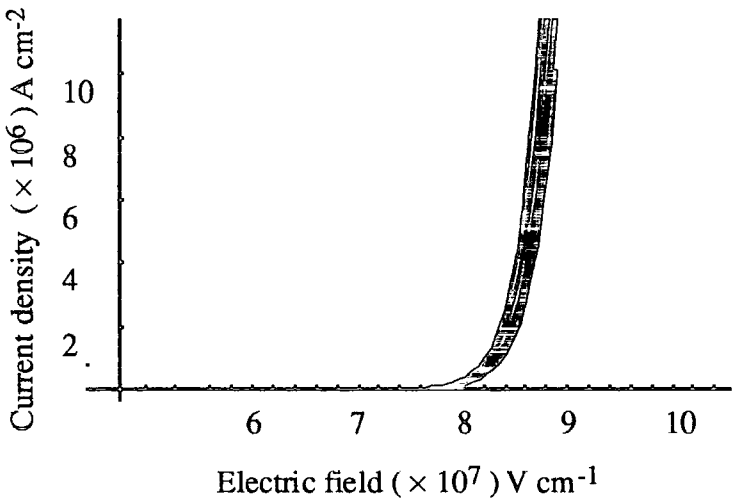

Figure 3.4 The field emission equation, equation 3.29, showing the slight temperature dependency, from 1000 K to 2000 K.

3-5 THE INTERMEDIATE REGION EMISSION

The solution to this problem is to combine the expansions in equations 3.13, 3.22 and 3.23 and substitute into the general emission equation, 3.11, to give the following expression of current density

$$j_e = \frac{kT}{2\pi^2}\int_{-Ea}^{E_1} Exp\left[-\frac{E - z}{kT} - \frac{4\sqrt{2}v(y)}{3F^{1/4}y^{2/3}}\right]\partial E$$

$$+\frac{kT}{2\pi^2}\int_{E_1}^{\infty} \ln\left[1 + Exp\left[-\frac{E-\zeta}{kT}\right]\right]\partial E$$

equation 3.38.

This particular approximation of equation 3.11 can be solved analytically to a high degree of accuracy. The solution is similar to the one used to solve the field emission equation, 3.27, in that the second integral is assumed not to make a significant contribution to the overall current.[3.3] The result is an intermediate emission equation,

$$j_e = \frac{\mathbb{F}}{2\pi}\left[\frac{kTt}{2\pi}\right]^{1/2} Exp\left[-\frac{\phi}{kT} + \frac{\mathbb{F}^2\Theta}{24(kT)^3}\right]$$

equation 3.39.

in which Θ is the function, $\Theta = 3t^{-2} - 2vt^{-3}$ where the arguments of v and t are $\sqrt{\mathbb{F}}$ and η where η is

$$\eta = -\frac{\mathbb{F}^2}{8(kT)^2t^2(1)}$$

equation 3.40.

The boundary conditions of the intermediate region are defined by the approximations that are used when assuming the expansions for the terms in equation 3.11. When these are valid then the solution is valid as the solution to the integral is sufficiently accurate over the whole range of temperature and electric field. The boundary conditions are determined by

$$\left[\frac{\sqrt{\mathbb{F}}}{-\eta}\right]^{-1} > 1 + \frac{\mathbb{F}^{1/4}d}{\pi(d - 1)}$$

equation 3.41.

where

$$d = \frac{2\sqrt{2}}{\pi}\left[\frac{\sqrt{\mathbb{F}}}{-\eta}\right]^{-1/2} t_\eta)$$

equation 3.42.

and $t_\eta = \sqrt{\mathbb{F}} / -\eta$ and

$$-\frac{\mathbb{F}^2}{8(kT)^2t_\eta^2} > -\phi + kT\frac{1}{1 - \mathbb{F}\left[2\sqrt{2\phi}\, kTt_\phi\right]^{-1}}$$

equation 3.43

where $t_\phi = t(\sqrt{2} / \phi)$.

Equations 3.42 and 3.43 can be used to determine when the current density equation, 3.39, should be used.

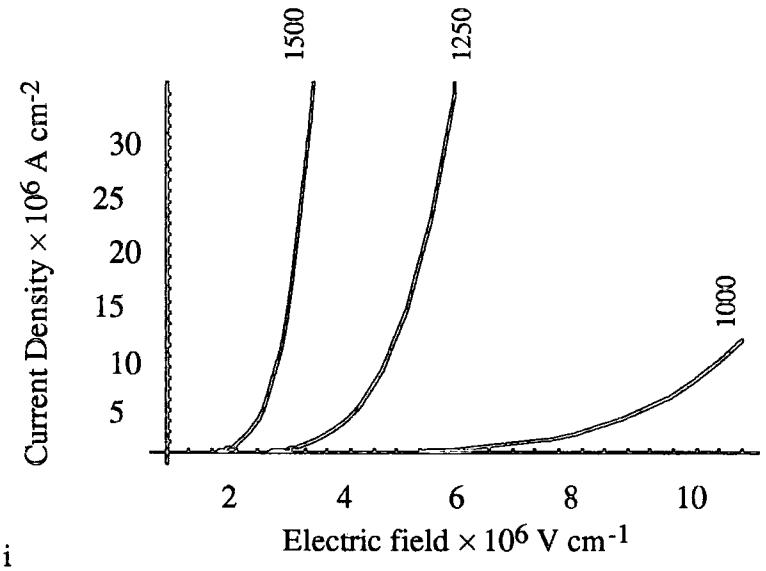

i

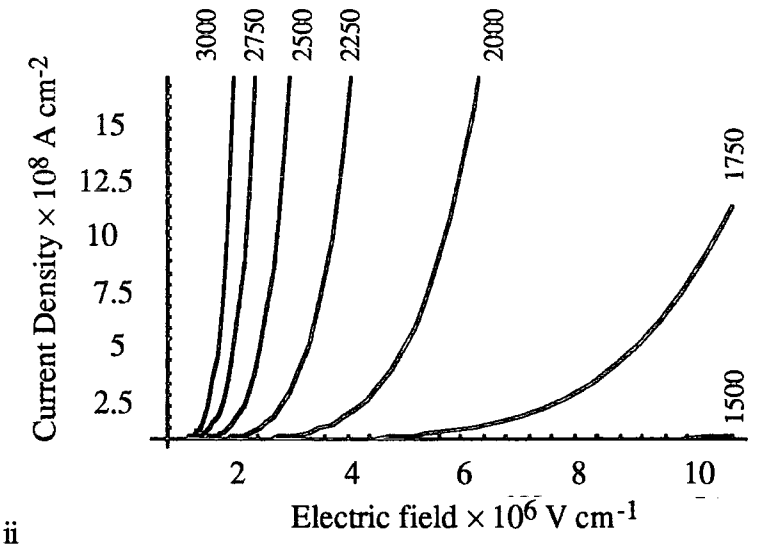

ii

Figure 3.5, i and ii. The electric field dependency of the intermediate region emission equation, equation 3.39 for various temperatures (Kelvin.)

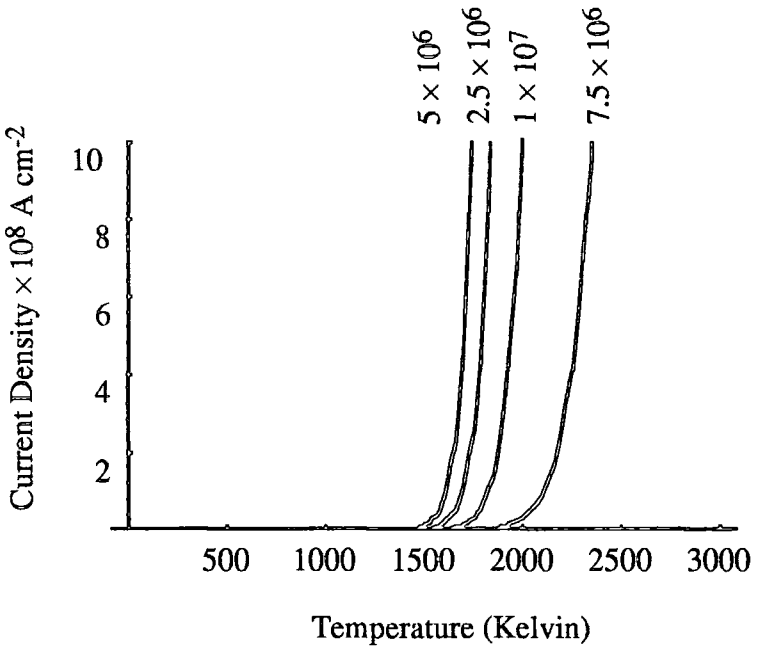

Figure 3.6. The intermediate region emission equation, equation 3.39, plotted with current density versus temperature for various electric field strengths (V cm^{-1}.)

3-6 THE EMISSION REGIONS

Sections 3.3, 3.4 and 3.5 have described what can be termed the emission equations for extraction of electrons by energy transfer from the electric field and thermal processes. With each different derivation there arises a set of inequalities for which the emission equation is valid in terms of the temperature and field strength. The appropriate emission equation has to be used and determination of this requires solutions to the various inequalities. It is possible to find individual solutions for specific values of temperature and electric field strength and determine exactly which equation gives the best approximate solution of the general emission equation, equation 3.11. However the emission equations 3.21 and 3.29 are valid for a wide range of temperature and electric field strengths and it is possible to determine quickly when these equations are obviously appropriate and when more care should be taken over the determination of which equation should be used. Holmes [3.21] gives two simple inequalities that indicate when the thermal and electric field energy transfer processes are dominant and which equation is applicable. These inequalities have been used to

construct figure 3.7 which is intended to be a guide to which equation is appropriate for an electric field and temperature combination. Figure 3.7 is only an approximate guide and when the parameters combine to be in the shaded region more careful consultation of the inequalities given in sections 3.3, 3.4 and 3.5 should be made.

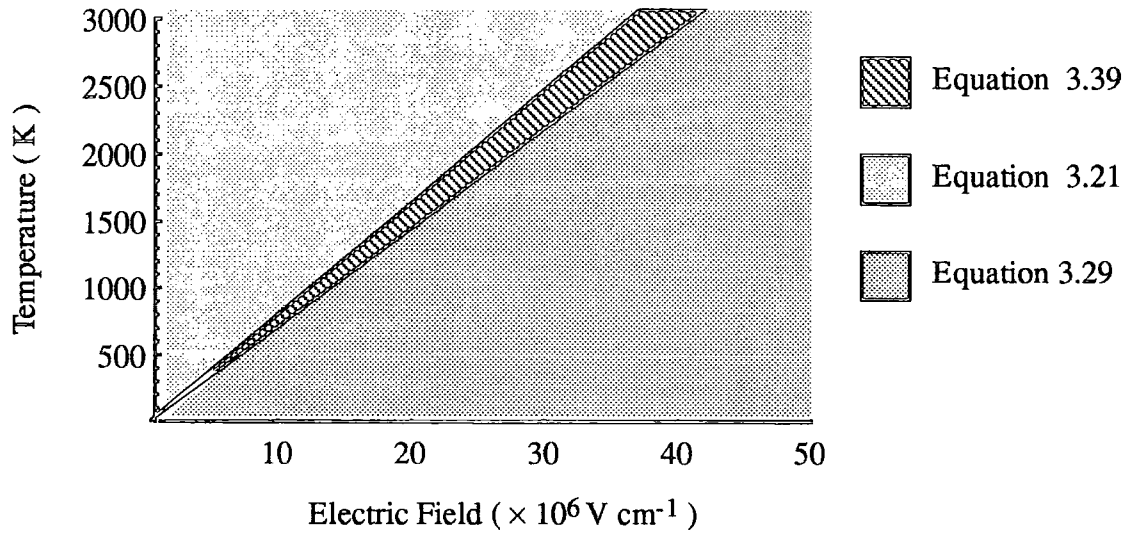

Figure 3.7 An approximate graphical representation of the electric field strength and temperature values for which each of the three emission equations is valid.

3-7 THE PHOTOELECTRIC EFFECT.

In this chapter so far, mechanisms for overcoming the work function by energy transfer mechanisms other than thermal and electric field energy transfer, have been ignored. It would be expected that the photoelectric effect, where an electron absorbs a photon to acquire the energy to overcome the work function, would be significant in an arc regime, as the arc is a very luminous body.

The photoelectric effect was first discovered by Hertz, in 1886, who noticed that electric discharges could be struck more readily when U.V. light was shining on the cathode. [3.12] Lenard investigated the effect experimentally in 1900, [3.13] and observed that an increase in the intensity of light did not increase the kinetic energy of the emitted electrons, but did increase the photoelectric current, which was contrary to the classical theory of light. Einstein proposed the mechanism of the photoelectric effect

in 1905, which explains the classical contradiction by representing the light in terms of a stream of particles, photons. The photons are absorbed singularly by an escaping electron. The energy of the photon, E, is

$$E = h\upsilon$$

equation 3.44

where h is Planck's constant and υ is the frequency of the light. The kinetic energy of the escaping electron is given by

$$\frac{mv^2}{2} = h\upsilon - \phi_o.$$

equation 3.45

where ϕ_o is the photoelectric workfunction. Equation 3.45. shows that there is a threshold frequency below which there will be no electron emission. The threshold frequency, υ_o, given by,

$$\upsilon_o = \frac{\phi_o}{h}$$

equation 3.46.

Above the threshold frequency the current density of emission will depend on the intensity of the light impinging on the cathode, and the quantum efficiency of the emission process. If the intensity of light with frequency υ_o, incident on the cathode is P_L Wm^{-2} the current density will be given by

$$j_p = \beta P_L$$

equation 3.47.

where β is the quantum efficiency of the photoelectric effect in the material and j_p is the photoelectric current density in A cm^{-2}. The number of electrons emitted per photon absorbed, β, depends on the material and the surface state of that material. Specially developed photoemitters have quantum efficiencies close to one tenth. For the purposes of discussing the relevance of the photoelectric emission to the cathode region of a thermal arc it will be taken as one to provide the upper limit on j_p. In practice most metals have β values of approximately 1×10^{-3}. It is more difficult to evaluate P_L and a large number of simplifications have to be made. The light is emitted from the arc

column and, to estimate the power density, the shape of the column is assumed to be cylindrical as shown in Figure 3.8 with a radius, a, taken to be 1 mm [3.14] and the light emitted uniformly in all directions

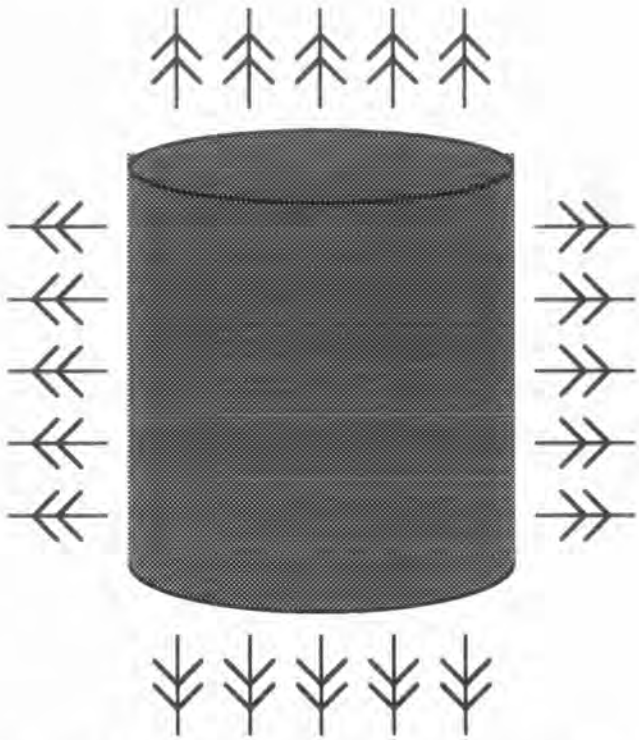

Figure 3.8 The arc column and light emitted from it.

The arc is highly luminous and has found many applications in illumination applications and an estimate of the power density that is emitted from the column is possible. One of the simplest procedures is to assume that the arc column is a blackbody emitter and then calculate the power emitted from such a body at the temperature of the arc column, assumed to be 7000 K. [3.15] In the general context of the relevance of photoelectric emission to thermal arcs blackbody radiation gives a sufficiently accurate representation of the emission spectrum of a thermal arc. [3.16] The energy per unit volume radiated from a blackbody source, $P(\lambda)$, at a temperature T is

$$P(\lambda)\,\partial\lambda = \frac{8\pi hc}{\lambda^5}\left[\mathrm{Exp}\left[\frac{hc}{\lambda kT}\right] - 1\right]^{-1}\partial\lambda$$

equation 3.48.

where c is the velocity of light, k is Boltzmann's constant and λ is the wavelength of the light. The energy density as a function of wavelength and temperature is shown in Figure 3.9

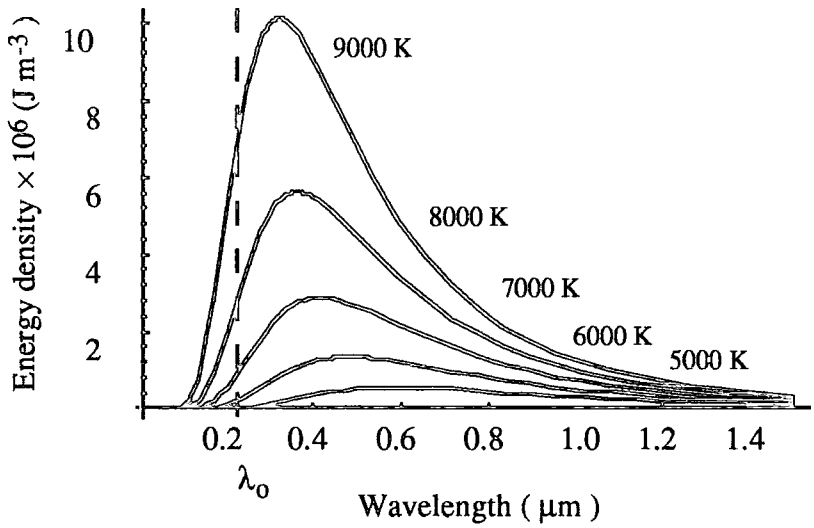

Figure 3.9. The energy density of at various temperatures as a function of wavelength, showing the upper cut off wavelength, λ_o, for emission of electrons from copper.

The energy that is emitted above the threshold frequency and below the cut off wavelength can be found by integrating the area under the curve in Figure 3.9 to the left of λ_o. Figure 3.9 also shows how critical the estimation of the temperature of the arc column is. The wavelength at which the curve is a maximum decreases as the temperature increases and the energy distributed above the threshold frequency will increase. The power distributed above the critical frequency can be found by solving the integral

$$R_C(\lambda) = \int_0^{\lambda_o} \frac{8\pi hc}{\lambda^5} \left[Exp\left[\frac{hc}{\lambda kT}\right] - 1 \right]^{-1} \partial\lambda$$

equation 3.49.

The solution of the integral over all wavelengths results in Stefan's law ,

$$R_T = \sigma T^4$$

equation 3.50.

where $R_{T\,is}$ the total power radiated by the source and σ is the Stefan-Boltzmann constant. (5.67×10^{-8} W m^{-2} K^{-4}) The integral in equation 3.49 was solved numerically, using an iteration routine to give the power density of radiation above the critical frequency υ_0, and for a temperature of 7000 K was found to be $R_C = 1.556 \times 10^6$ W m^{-2}. Substituting this intensity value into equation 3.47 and assuming a quantum efficiency, β, of one gives a current density of 1.556×10^6 A m^{-2}. This is the maximum current density that could be obtained from photoelectric emission, at a temperature of 7000 K. The estimates of the current density at the cathode are of the order of 10^{12} A m^{-2} and this shows that the intensity of light that is generated by the arc cannot account for the total emission.

Figure 3.9 shows how the proportion of light that is emitted above the cutoff frequency increases as the temperature of the arc column increases. This would increase the photoelectric current significantly. However to increase the temperature of the arc column to a level which would make the photoelectric current significant would require a large amount of energy to be diverted from more energy efficient emission mechanisms. To emit the required current density the radiative energy would have to be so intense that destruction of the cathode would result.

3-8 EXPLOSIVE EMISSION

Explosive emission is a term used to describe the mechanism of electron emission where the electrons are ejected from the cathode as part of the material that is vaporized from the cathode. As the atoms are vaporized from the cathode they will be drawn into the arc column and thermally ionized, either in the cathode region or the arc column. The current density that is drawn from the cathode in this way depends on the amount of material that is vaporized and the degree of ionization that occurs in the process. The mechanism is difficult to represent in mathematical terms as there are many operations involved, vaporization of the cathode material, passage through the

cathode region and ionization of the vaporized atoms. One model has been proposed by Bugaev et al, [3.17] that does fit the experimental evidence.

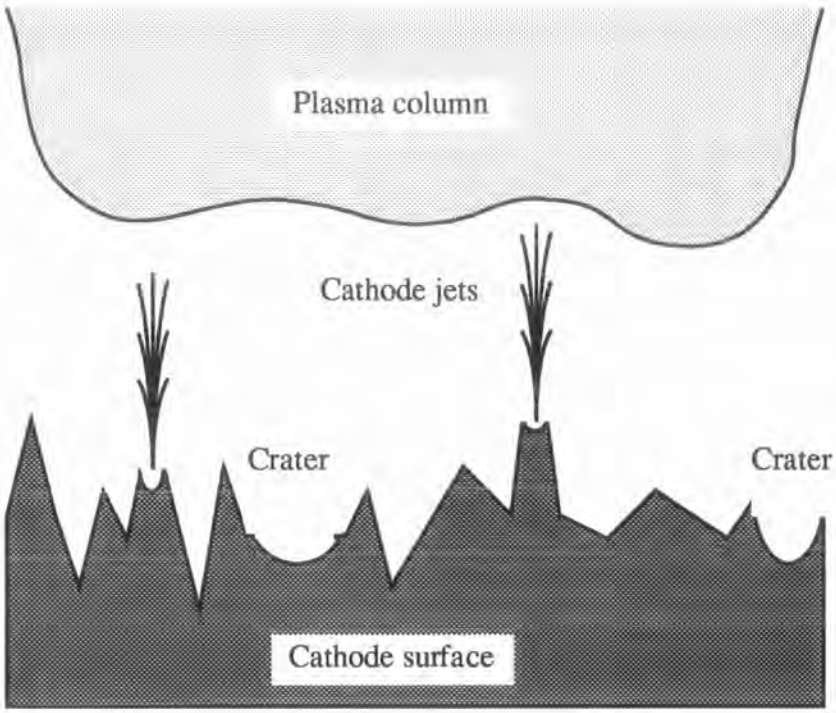

Figure 3.10 Explosive emission. The macro-points on the cathode surface intensify the electric field causing electron emission from these points. The current flow will heat the point causing the formation of a cathode jet.

The surface of the cathode will not be smooth even when polished optically flat, there will be undulations in the surface as shown in Figure 3.10. The cathode region electric field will be accentuated at these points. The higher electric field strength will make the point a preferential site for thermally enhanced field emission. The current that flows through this point and the positive ions that impact onto the site, will cause heating, which vaporizes the point. Some of the atomized material will be ionized due to the high temperature and the electrons attracted into the arc by the intense electric field, with the positive ions being drawn onto the surface of the cathode. The particles that remain unionized will be pulled into the column by the high pressure that is created around the jet. [3.18] To calculate the contribution to the total electron current density

that explosive emission makes it is necessary to estimate the amount of material that is lost from the cathode.

There have been many experiments that have attempted to measure the amount lost from the cathode in terms of erosion rates and direct extrapolation from photographs of the craters. [3.19] Bugaev et al devised an equation that predicted the mass lost by an electrode, M, from a macro-point with a curvature θ, when a current pulse , i is passed for a duration, t_p, between two electrodes, i.e

$$M=\left[6\sqrt{\pi}\sin\theta/4\right]^{-1}\left[\frac{3\sqrt{\rho\kappa}}{c\ln(T_{CR}/T_o)}\int_o^{t_p} i^2\ \partial t\right]^{3/4}$$

equation 3.51.

where r is the conductivity, k is the thermal conductivity, c is the specific heat capacity, T_{CR} is the melting point and T_o is the initial temperature. If this equation can be extended to the conditions of a continuous arc where craters exist for a lifetime τ and pass a current i_c then the mass lost from such a crater predicted by equation 3.51 is approximately 4×10^{-8} g. Expressing this mass in terms of the number of moles it represents and multiplying by Avogadro's number will give the number of atoms present, approximately 3.79×10^{10}. If each atom is singularly ionized then this releases 3.79×10^{10} electrons into the arc. Over the duration of the emission spot, τ, this will correspond to a current of 6 amps. If the macro-point is taken to have a diameter of 2 μm then the current density will be approximately 1.9×10^{12} A m^{-2}.

This calculated current density is of the same order of magnitude as that calculated, by many, to be the current density that occurs from such an emission site. [3.19] Explosive emission could be the mechanism that sustains an arc on a cold cathode. The expression above contains a large number of assumptions namely; the calculated mass of lost material, the degree of ionization that occurs and that the vaporized material flows into the arc column. The calculated mass of material is in quite close agreement with that measured in erosion rate and crater measurement experiments, [3.19, 3.20], but the assumption that this vaporized material has entered the arc system is conjecture and cannot be confirmed by experimental work.

The degree of ionization of the vaporized atoms was assumed to be 100 %. Studies of the arc column show that the degree of ionization in the column is dependent on the temperature, but for the 50 amp model arc that is used in this work the temperature of the column is calculated to be 7000 K and the degree of ionization is 9.96×10^{-4}. If the vaporized material is only ionized to this extent then there will be a severe reduction in the current density. Unfortunately the degree of ionization that occurs in the cathode region is unknown, but as conditions are extreme, in terms of electric field strength, it has been assumed that a high degree of ionization occurs in this region.

The number of electrons that are removed from the atoms is also unknown and has been assumed to be the most readily removed (valence) electrons in the outer shell. It has been shown, however, that explosive emission does contribute a significant number of carriers into the arc from an electrode in crater form of emission. This probably is the mechanism that makes up the shortfall between the current density calculated from the classical emission mechanisms to the experimentally measured current density.

3-10 REFERENCES

3.1 Lee T.H. *T-F theory of electron emission in high current arcs.* 1959 J. Appl. Phys. Vol.30 no. 2 p. 166 to 171.

3.2 Busch G. Schade H. *Lectures on solid state physics.* 1980 Oxford: Pergerman Press. p. 186

3.3 Murphy E.L. Good R.H. *Thermionic emission, field emission and the transition region.* Phys. Rev. vol. 102 No. 6 p. 1464 to 1473.

3.4 Dolan W.W. Dyke W.P. *Temperature and field emission of electrons from metals* 1954 Phys. Rev. 95 p. 327 to 332

3.5 Richardson. 0.W. *The Emission of electricity from hot bodies.* 1921 London: Longmans.

3.6 Schottky W. 1925 Z.F. Phys. Vol. 31, page 163

3.7 Herrmann G. Wagener S. *The oxide coated cathode.* 1951 London: Chapman and Hall.

3.8 Fowler R.H. Nordheim L.W. *Electron emission in intense electric fields.* 1928 Proc. Roy. Soc. (London) Series A Vol. 119 p 173 to 181

3.9 Busch G. Schade H. *Lectures on solid state physics.* 1980 Oxford: Pergerman Press. p. 159

3.10 Nordheim L.W. *The effect of the image force on the emission and reflection of electrons by metals.* 1928 Proc. Roy. Soc. (London) Series A Vol. 121 p. 626 639

3.11 Burgess, Kroemer and Houston *Corrected values of Fowler-Nordheim emission functions v(y) and s(y).* 1953 Phys. Rev. Vol. 90 p. 515

3.12 Eisberg R. Resnick. R. *Quantum physics of atoms, molecules, solids, nuclei and particles.* 1985 New York Wiley.

3.13 Tipler P.A. *Physics for scientists and Engineers.* 1991. New York: Worth.

3.14 Chapter 6.

3.15 Chapter 2 section 2.3.

3.16 Cobine J.D. *Gaseous Conductors, theory and engineering applications.* 1958 New York: Dover Publications Inc.

3.17 Bugaev S.P. Litvinov E.A. Mesyats G.A. Proskurovskii D.I. *Explosive emission of electrons.* 1975 Soviet Physics Uspekhi Vol. 18 No. 1 p.51 to 61 1975.

3.18 Swanson L.W. *Electron and ion emission from liquid metal surfaces.* 1991 I.E.E.E. Transactions on Plasma science Vol 19 No. 5 p 746 to 748.

3.19 Chapter 4 Table 4.1.

3.20 Puchkarev V.F. *Estimating the electron temperature from fluctuations in a vacuum arc plasma: cathode spot operation on contaminated surfaces.* 1991 J. Phys.D: Appl. Phys. vol 24 P. 685 to 692.

3.21 Holmes A.J.T. *A theoretical model of the mercury and copper vapour arcs.* 1974 J. Phys. D. Appl. Phys. Vol 7 p. 1412 to 1425.

CHAPTER 4 THE CATHODE SPOT

4-0 INTRODUCTION

There is as much confusion over the definitions of the behaviour at the cathode electrode as there is confusion over the terminology which has evolved. As experimental observations have improved the terminology has come to have slightly different meanings. The cathode spot was originally the 0.1 mm diameter area observed under the column of the arc, from which the emission from the cathode could be seen to be coming.[4.1] As measurements have improved this cathode spot has been resolved into multiple sub-micron spots within the original cathode spot, [4.22, 4.20, 4.26]. These are now often referred to as cathode spots, but clearly have a slightly different meaning to that of the original definition of the the observed constriction in the arc column at the cathode. The issue is confused further as the mark left by the sub-micron cathode spot is often referred to as a crater, due to the likeness to a life-size crater, when observed with an electron microscope. In this section a cathode spot refers to the sub-micron size emission region and a crater refers to mark that is left by a cathode spot in the electrode material.

4-1 HEAVY CURRENT OVERLOAD EMISSION

Heavy current emission is a term used here to mean the electrode is emitting electrons at a current density which it is not possible to describe with the conventional electron emission mechanisms of thermionic, field and photoelectric emission. It is encountered in many arc electrodes as the current density required to sustain the arc is so large. The minimum current density at which this region is first encountered varies depending on the electrode material, as the maximum current obtainable from the material is dependent on the melting point and work-function of the material. When the electrode enters the heavy current overload region it displays certain characteristics which are as follows.

The electrode's conventional emission mechanisms have been overwhelmed by the demands of the system and the shortfall in electron current density is made up by vaporising the electrode material to liberate electrons into the system. This manifests itself in two forms, crater mode emission and melt mode emission. The heavy current overload region is encountered under different conditions for different electrode materials and types of electrical discharge, as the classical emission processes, such as those described in sections 3.3, 3.4 and 3.5 depend on the electric field and temperature to which the material is being subjected. For example it is possible to make copper electrodes display heavy current overload characteristics when the current of a D.C. arc is as little as 10 amps [4.38, 4.50] and the same mechanism can be seen in tungsten cathodes sustaining a 20,000 amps arc. [4.36] It is most common to see this mechanism in non-refractory material electrodes, since with low melting point electrodes, the maximum thermionic component of the emission current is much lower and therefore heavy current overload is encountered more frequently.

Melt Mode emission. Any cathode forced into heavy current overload emission region displays one of two categories of emission, melt mode or crater mode. Melt mode occurs when the shortfall in electron emission is overcome by gross melting of the electrode material, resulting in rapid destruction of the electrode. The information that can be obtained from electrodes subjected to melt mode of emission is limited because of the destructive nature of this mode; the only parameters that can be measured are the erosion rate, threshold melt mode arc current and external operating conditions of the arc. Melt mode is caused by the thermal capabilities of the electrode being exceeded. [4.38] This is determined by the power of the arc, the velocity of the arc and the cooling rate on the electrodes, which combine to exceed the thermal capabilities of the electrode material. The other form of heavy current overload emission is the cathode spot mode where the electron emission mechanisms are enhanced by the formation of distinct emission spots on the surface and not by gross melting of the electrode.

Cathode Spot Emission Mode. Crater emission occurs when electrons are emitted from point sources on the cathode surface, called cathode spots when active, rather than the broad area emission that is associated with other forms of electron emission. The craters are small pits in the surface of the cathode, varying in size from 0.1 μm to 2 μm [4.34 , 4.15] which are an indication of the presence of a cathode spot on the electrode. The geometry of these pits on the surface varies; they are not regular and the best approximation is to assume they are hemispherical [see pictures in Chapter 6, 4.24] The vapour emission is thought to come from these cathode spots [4.26] but it is not certain that the classic forms of emission occur from these sites [4.25]. Cathode spots were first observed in the 1930's when arcs were recognised to have distinct attachment points to cathodes. [4.1] The size and current density of the emission spots were initially estimated to be 0.1 mm and 10^4 A cm^{-2} respectively [4.4.] The estimates of size gradually decreased as observation techniques improved and the availability of electron microscopes enabled high magnification studies of highly polished samples exposed to short duration arcs which revealed the sub-micron craters that are described in the above paragraphs [4.22]. These crater observation studies have proved to be the only insight into the emission mechanism that does not rely on a model of the emission mechanism being assumed. The information that can be gained from these studies without assuming some sort of emission mechanism is limited to the physical size of the craters and the number density of the craters. It is therefore usual to assume some sort of model of the emission process when performing crater observation experiments. This makes assessing the information that is gathered from different experiments difficult, as results can differ because of the different assumptions that are made. When observing craters on one material, there is one definite conclusion that can be drawn which requires no assumption of a model. The formation of cathode spots is profoundly affected by the surface oxidation state of the electrode. [4.26, 4.27, 4.29, 4.30] The size, number, current density and lifetime are all severely affected by the oxidation state of the electrode and this causes

severe difficulties in measurements made on the cathode as the control on the surface oxidation state is often limited, especially in rotating arc experiments [4.34]

There are several methods of evaluating the emission site lifetime and emission site current density of a cathode spot. The experimental evidence used to make these estimates is the number of craters per unit area and the external parameters of the arc, duration, velocity (non-stationary experiments) current and arc velocity. The number density of craters is established from S.E.M examination of the sample after the arc has passed over. Depending on whether the experiment employed a stationary short duration or a moving arc, the crater density is either measured directly by counting the number of craters that can be seen in the damaged area left behind by the arc, or scaled up from the number of craters found in a sample area, to the total damage area left by the arc. Using these parameters estimates of the current density are made using various models or using extra information gathered from further observations. Guile et al [4.13] assumed that the current density distribution over the emission sites would be the same as the size distribution, which they had measured, and assumed it would range between an arbitrary maximum and minimum. Applying the same model to the site lifetime they estimated current densities and lifetimes of emission craters to be 1.4×10^4 A cm^{-2} and 4.5 nsec. Basharov et al [4.5] established the number of emission sites that were coexisting by observing the arc with a high speed streak camera. With this information they were able to establish that the lifetime of the emission craters was 2 μsec and the current density was 1×10^7 A cm^{-2}. This experiment was carried out on copper electrodes with no deliberately grown oxide layer. Augis and Grey [4.39] measured the number of craters that formed after a short duration, 20 nsec, arc had been run on a palladium electrode. They assumed the emission sites to coexist and then used an analytic model of the heating of the cathode spot to establish the current density needed to reach the melting point of palladium of 2000 °C. They found the current density to be 2×10^7 A cm^{-2}. Secker and workers [4.32, 4.7] used a model that applied to single shot experiments where the arc had been driven linearly along rail electrodes. They assumed that in a line along the direction of movement no craters had

coexisted and counted the number of craters along this arbitrary line. This resulted in a estimate of the maximum lifetime of the emission site of 0.1 μsec and a current density of 2×10^7 A cm^{-2} for copper electrodes with an un-oxidized surface. A direct measurement was attempted by Drouet and Gruber [4.9] who inserted a pick up coil in the cathode electrode and monitored the induced voltage from the emission sites. Using this, the cathode spot current density was found to be 1×10^{10} A cm^{-2} and spot lifetimes to be 1 μsec.

There are wide variations in the current densities and lifetimes that are reported. These variations have several causes; the difference in the methods of measuring the lifetime, the lack of control of other parameters that affect the lifetime and current density and the nature of the experiment, which will always produce inconsistencies as it is very difficult to generate exactly the same arc in every experiment [4.35.] It is most informative to produce a table of the lifetime values that are most often quoted. Since it is not possible to discount any of the results that have been reported, as there is no established method of evaluating the lifetime or the current density or model that accounts for the experimental differences. To make comparisons of experimental data, the lifetimes have to be calculated using the same method, and where the experimental information is given comparisons are made using the lifetime calculation described in Chapter 5.

Table 4.1 The development of current density and lifetime measurements of the cathode spot.

Cathode material	Arc type	Current density A cm^{-2} (J_S)	Site lifetime nsec (τ_S)	Technique of measurement	Ref.
Not specific	vacuum arcs	1×10^6	-	A review of the measurements completed before 1959	4.1
Cu	Air discharge	9×10^4 8×10^5 1.2×10^5	- - -	A tabulated review of measurements by von Engel 1957	4.2
W	Vacuum discharge	1×10^7 to 1 $\times 10^8$	-	Examined melt tracks on cathode optically and estimated current density to melt cathode	4.4
Cu	Pulsed discharge vacuum arc	10×10^7 9×10^7 8×10^7 8×10^7 8×10^7 9×10^7 8×10^7	2000 to 3000	Measured the number of cathode spots co-existing using high speed streak camera..Examined cathodes for the total number of cathode spots and calculated current density	4.5
Cu	rotating arc	1×10^6	-	Estimated value from erosion model.	4.6
Cu Brass	single shot linearly driven air	2×10^7 5×10^6	100 100	Examined electrode with S.E.M and estimated current density by assuming that along a line in the direction of arc movement no craters coexist and counting along an arbitrary line	4.7
Cu 0.6 µm Oxide 0.045 µm oxide	Rotated arc in air Single shot	3.3×10^7 3.3×10^7 3.3×10^7	6.5 0.05 2	Current density estimated for joule heating model and lifetime estimated from crater formation model.	4.8
Cu	Single shot	1×10^{10}	1000	Direct measurement using pick up coil	4.9
Cu	single shot vacuum arc	1×10^8		S.E.M. study of cathode spots which assumes each spot exists singularly	4.10

Cu 100 nm oxide	single shot 34 to 68 A.	5.7×10^7 to 6.5×10^8	0.36 to 4	Uses S.E.M. observations to estimate cathode spot nature. Found craters 0.1 μm in diameter.	4.11
Cu 44 nm oxide 100 nm 225 nm 340 nm	50 A Arc. 4.5 A stationary arc 12 nsec to 45 μsec duration.	3.5×10^8 4×10^8 2.95×10^8 1.28×10^8 6.15×10^7 3.7×10^7	30 1.3 3.3 4.5 23 105	Examined the cathode spots to reveal craters on the surface. Calculated a constant value for the lifetime current product. Used this information to establish current density	4.12
Cu 100 nm oxide	Stationary 4.5 A arc	1.4×10^8	4.5	Same method as above	4.13
Cu	General	1×10^8		A theoretical model used as a basis to calculated minimum current to melt cathode spot	4.15
Cu	Vacuum arc	4.3×10^7		Theoretical model	4.14
Cu	Vacuum arc	1×10^8	10	S.E.M. study and used Joule heating model to calculate spot lifetime and current density	4.16
Cu	Vacuum spark discharge	1×10^8	5	S.E.M. study adjusting length of short duration discharge until form one cathode spot	4.17
Cu 100 nm oxide	Atmospheric discharge 45 A	3.5×10^8 2.2×10^8	50 50	see reference 12	4.18
Cu	Vacuum arcs 8 to 50 A magnetically driven	10×10^8	-	A direct measurement where arc are driven over electrodes separated by a gap and as each spot is driven over the electrode the difference in current is measured.	4.19
W	Vacuum arc at different electrode temperatures	1.2×10^7	25 to 50	Decreased arc current until obtained one cathode spot. Confirmed by S.E.M. study, in which spots are assumed to exist singularly.	4.20

4-2 CATHODE SPOT FORMATION THEORIES

Theories of crater formation and their role on the emission mechanism of the electrode remain varied and unfortunately no crater formation theory has unified all the experimental and practical experience of using emitters in heavy current overload. The most eloquent theories on crater formation were made by Guile and co workers [4.13, 4.11, 4.40] who developed a series of crater formation models which have been adapted as further experimental information has become available.

Guile recognised the significant role of the oxide layer on the emission surface, and used the information from the single shot experiments with prepared electrode surfaces and the long duration rotating arc experiments, to propose a model for crater formation on oxide coated electrodes. For oxide films thicker than 20 nm Guile and co workers assumed a filamentary channel conduction mechanism through the oxide layer. [4.41] The highly resistive oxide layer is broken down by the formation of conducting channels of copper that are formed by a process of fritting or electroforming [4.42]. Fritting is a type of electrical breakdown where a thin insulating layer, such as an oxide layer, is broken down by a strong electric field. The electric field causes the formation of a filament of the metal. In the case of copper the oxide is reduced in the reaction,

$$Cu_2O \rightarrow CuO + Cu$$

to form copper channels through the oxide. The current of the arc is sustained through the oxide by these conducting channels and the destruction of these conducting filaments leaves the craters and stripped areas behind in the electrode surface as shown in Chapters 6 and 7. A channel is formed through the oxide and the crater is formed by the vaporization of the copper filament. Guile et al [4.43] substantiated this theory by investigating the time dependence of the erosion rate and found that the erosion rate was proportional to the oxide layer growth rate. In 1984, [4.40] this idea was extended and was used to relate the erosion rate to the activation energy of the reaction for copper or other reduction equations for electrodes of different materials.

The filamentary conducting channel model demonstrates a model that could account for the formation of the craters on the surface of electrodes covered in thick oxides (> 10 nm) However the empirical equations that were established to support this model have not withstood the harsh test of application to a wider set of experimental conditions, such as different materials and very high power arc applications. [4.37] The filamentary conduction mechanism does not account for the electron emission process from the surface of the oxide layer, nor clarify the implications regarding the temperature and the electric field strength at the emission surface or explain the profound effect on the performance of the electrode. The model also fails to account for the differences seen in thin oxide layers (< 10 nm), although Guile did offer an explanation for thin oxide layers by proposing a different mechanism of crater formation [4.43.]

Non oxidised electrodes. Table 4.1 lists the wide variety of experiments that have been carried out on arc electrodes, with the majority of the experiments being completed on non oxidized cathodes. In this section the theories of crater formation or the cathode spot will be examined for both vacuum arc and gaseous discharges when changes to the unoxidized state are avoided and when short duration arcs or single shot experiments are involved. Vacuum arcs differ from gaseous discharges because the discharge is more dependent on the vaporization of the electrode material to sustain them. However the formation of craters or cathode spots on these electrodes is so strikingly similar [4.26, 4.31, 4.20, 4.34] that in this section the systems are treated as one. The electrodes in vacuum and atmospheric discharges both display heavy current overload emission characteristics.

In 1957 von Engel and Robson [4.2] were among the first to recognise the paradoxical situation of the very high current densities of the arc cathode and the apparent low temperature and electric field strength causing a large disparity between the actual current density and the theoretical maximum. von Engel and Robson proposed that the impact of excited atoms on the emission surface, which is known to

be a highly efficient mechanism for electron production, could account for the shortfall in electrons. The positive ions would be accelerated by a space charge region, close to the emission surface, to provide them with enough energy to liberate the electrons. von Engel and Robson managed to prove that for a mercury vapour arc these processes could account for a current density of 1×10^5 A cm^{-2} that was thought to be the maximum current density in the cathode spot. von Engel did not examine how the cathode spot became molten; the process of electron emission was assumed to melt the cathode spot. Rich [4.3] was amongst the first to examine the mechanism of Joule heating as the cause of the cathode spot melting. Treating the cathode as a semi hemispherical region and considering the current flow into and out of the spot Rich derived an equation for the power dissipated in the cathode spot by Joule heating Pj,

$$P_j = 0.48\left(\frac{2}{3}\pi a^3\right)J_z^2\rho$$

equation 4.1

where a is the radius of the cathode spot, ρ is the resistivity of the electrode material and J_z is the current density flowing perpendicular to the electrode surface. The temperature of the cathode spot was calculated using an expression that also included the energy input from the positive ion bombardment component. The temperature equation was derived from standard thermodynamics, giving,

$$T = \frac{a^2A}{2K}\left[1 + \left[\frac{2\kappa t}{a^2} - 1\right]\mathrm{Erf}\left[\frac{a}{2(\kappa t)^{1/2}}\right] - 2\left[\frac{\kappa t}{\pi a^2}\right]^{1/2}\mathrm{Exp}\left[\frac{-a^2}{4\kappa t}\right]\right]$$

equation 4.2

where T is the temperature, A is the rate of the heat produced per unit time per unit area, K is the thermal conductivity, a is the radius of the cathode spot, κ is the thermal diffusivity and t is the time. Rich concluded that Joule heating was possibly the heating mechanism for high resistivity cathode materials when considering the current densities and lifetimes of the cathode spot that where believed to exist at that time, 10^6 A cm^{-2} and 10 µsec. Rich also found that with a lower resistivity metal, such as copper, Joule heating could be a large contributor to the total power input, if the current density were above 10^7 A cm^{-2}. Rich's conclusion becomes more believable as modern attempts

have shown the cathode spot current density have measured the crater to be smaller, becoming approximately 1 μm in diameter, and the current density larger. Whether Joule heating is a dominant heating mechanism and is responsible for the apparent melting of the cathode spot has not been resolved. Using equation 4.2. to predict the temperature of the cathode spot as a function of time shows that Joule heating could account for the melting of the cathode spot for copper electrodes, as illustrated in Figure 4.1 where the energy flow into the cathode is taken to be the Joule heating component, equation 4.1. and the temperature is predicted from equation 4.2.

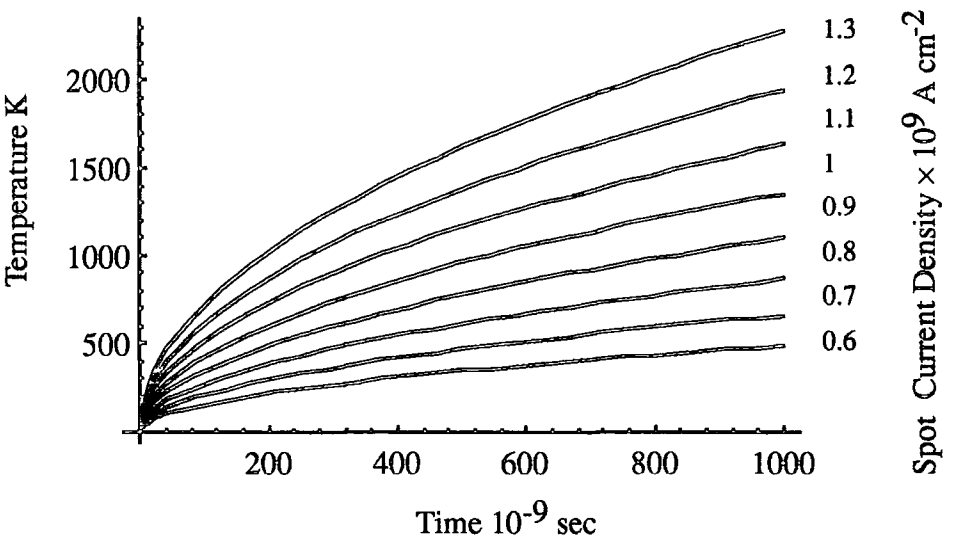

Figure 4.1. The predicted temperature of the cathode spot, equation 4.2. assuming that the spot is heated by Joule heating, equation 4.1.

In contrast Holm [4.33 page 430] suggested that compared with the energy from other heating mechanisms the Joule heating component could be ignored as it was insignificant. Holm approached the problem using an energy balance, accounting for the energy inputs to the cathode spot and balancing these against the energy losses. Energy into the cathode spot is from positive ions that enter the cathode releasing both kinetic and excitation energies; this energy is assumed to be transferred to the surrounding area by conduction. Energy losses from the cathode spot are assumed to be from the cooling that electron emission will cause. Holm derived an expression for the energy balance in the cathode spot in terms of the current density and the

dimensions of the cathode spot, and found a good correlation between the energy input and the energy output. Holm did not attempt to describe the emission processes at the cathode.

Sanger et al [4.7, 4.32] attributed the craters to initial, intense ion bombardment of the cathode spot followed by Joule heating, as the current flows from the site, and a micro explosion of the spent emission site forms a crater. Sanger believed that Joule heating was a major contributor to the heat generated in the emission site, because he was using palladium electrodes, which have a resistivity of 0.1 $\mu\Omega$m at 273 K, and because of the high current densities that he measured in the cathode spot, 10^7 A cm^{-2}. In Sanger's discussion the mechanism of electron emission to account for the high current density is assumed to be thermally enhanced field emission, and the role of the evaporating emission site is not discussed. It is possible to check the estimate of the lifetime of the emission spot in more detail as the theoretical melting time of the electrode, obtained from equation 4.2, can be compared with the estimated lifetime of the craters that Sanger et al reported.

Holmes [4.14] derived a model which incorporates many of the aspects that are lacking in the previously described models because it starts with an assumption of the emission mechanisms that supply the electrons from the cathode. Holmes used the information that the energy that is available for electron emission is relatively small. This precludes photoelectric and ion induced emission processes, which require 10^2 to 10^3 eV for a high probability of emission. Holmes found that there are two possible emission mechanisms, excited ion bombardment and thermally enhanced emission, but unlike von Engel [4.2] found that for copper, excited ion bombardment can be discounted as there is no long lived excited state which has a higher energy than the workfunction of copper. Holmes used the gas pressure to describe the electric field at the cathode, the emission mechanism equation and energy balance equations and then derived ten simultaneous equations which can be solved for the important arc parameters. The advantage of this solution is that the parameters are derived from the basic constants of the material. The method does not invoke one of the arc parameters

to calculate the others, which makes this theory not as dependent on the uncertain experimental measurements as are other theoretical calculations. Holmes found a heavy dependency of all the parameters on the arc gas density at the cathode spot as the electric field and voltage distribution at the spot are heavily dependent on the gas density and these in turn are critical parameters.

Holmes' approach to the problem of the cathode spot is useful as it shows that by combining an emission mechanism equation with energy balance exercise it is possible to arrive at a physical description that results in sensible values of the arc parameters. The current density is found to be 4.3×10^7 A cm^{-2}, the spot temperature 5490 K the cathode electric field 3.3×10^9 Vm^{-1} and a spot diameter of 8.1×10^{-9} m; experimental values can be found to support this model. Holmes' model clearly shows the value of this type of model as there is much information to be gained.

4-3 LIFETIME AND CURRENT DENSITY VALUES

For theoretical calculations it is necessary to make an estimate of the absolute value of the lifetime and current density. The methods used for making most measurements on cathode spots prevent accurate separate values of site lifetime and site current density being stated. [see Table 4.1] The product of $J*$ and $\tau*$ is what can be established from arc track examinations, where $J*$ is the current density assuming emission sites exist singularly and $\tau*$ is the lifetime of such a site. If the total arc current is known and the number of cathode spots measured, the product $J* \times \tau*$, can be calculated. [see Chapters 5 and 6] The actual lifetime and current density are then values whose product, $J_S \times \tau_S$, is equal to $J* \times \tau*$. When making theoretical calculations it is possible to set current density and a range of lifetime values to give a range of $J_S\tau_S$ that is within the experimental error of the observation.

4-4 ENERGY FLOW AT THE CATHODE

As shown in the previous section accounting for the energy input into the cathode spot, in the form of an energy balance equation, is an important step towards understanding the cathode spot phenomena. The equation can be derived for different situations, such as total energy output and ion current and used to derive some physical parameters of the arc. Figure 4.2. shows the energy flowing into and out of the cathode. To construct an energy balance equation requires quantitative estimates of the energy that is being transferred by each of these processes, which in some cases can be difficult to ascertain.

Ion Kinetic Energy. A source of energy into the cathode spot will be the kinetic energy of an incoming, positively charged, ion as it impacts on the cathode surface. The energy of the ion will be transferred to the spot. To quantify this, the amount of energy that the ion acquires as it is accelerated through the cathode voltage fall region must be estimated. Holm [4.33] assumes that the accelerating field is equal to the cathode voltage fall, which in short length arcs is assumed to be the total arc voltage, V_a, so that kinetic energy is given by $V_a I_i^+$ where I_i^+ is the ion current flowing into the spot. Other investigators [Daalder 4.12, 4.14 Davis and Miller, Plyutto et al 4.45] have found that there is a potential increase close to the cathode surface, which has obvious ramifications for the accelerating voltage of the positive ion. Direct measurements of the average kinetic energy of each ion, U_{kin} were attempted by Davis [4.44], using a mass spectrometer, and by Plyutto et al [4.45] with a voltage probe. If all in coming ions are assumed to transfer their energy to the spot then the kinetic energy transferred to the cathode spot by the impact of ions, E_i, is given by

$$E_i = I_i^+ U_{kin}$$

equation 4.3.

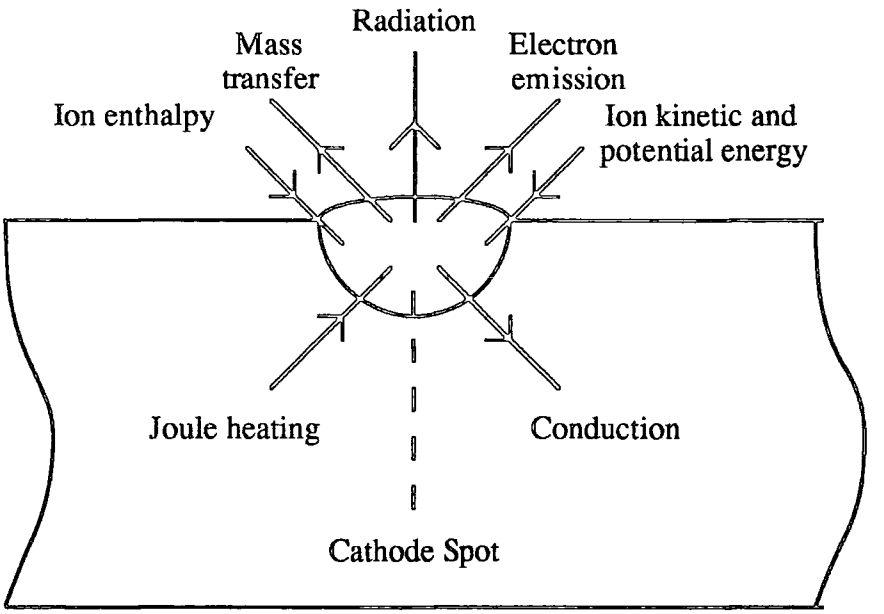

Figure 4.2. The energy flow into and out of the cathode spot.

Ion Neutralization. The liberation of an electron to neutralize the charged positive ion uses some of the potential energy that the ion possesses, so that to find the energy that is transferred to the cathode it is necessary to deduct the energy to liberate an electron, ϕ the work function, from the potential energy of the ion. The potential energy transferred to the cathode spot, E_p,is then given by

$$E_p = I_i^+(U_{ion} - \phi)$$

equation 4.4

Where U_{ion} is the average potential energy of the in coming ions.

Ion latent heat. The neutralized ion will transfer energy to the cathode spot by conduction of heat as the ion cools down to the cathode spot temperature. The latent heat of the ion can be derived from the condensation energy of the material. The energy gained is given by equation 4.5.

$$Ee = I_i^+H$$

equation 4.5.

Where Ee is the heat energy gain and H is the heat capacity of the particle.

Joule heating. The energy transferred to the cathode spot from current flow through the spot due to Joule heating, E_j, has been discussed in other sections, and the power is given by equation 4.1.

4-5 ENERGY LOSSES FROM THE CATHODE

Mass Transfer from the cathode. The mass transfer from the cathode into the arc will cause energy to be lost from the cathode spot in the form of vaporized material. Estimating the amount of energy lost from the spot requires the erosion rate of the cathode spot to be measured. There are numerous experimental investigations of erosion rate of the cathode spot [4.12 , 4.14, 4.43, 4.41, 4.6]. Daalder [4.12], measured the erosion rate for a 100 Amp arc to be approximately 50 μgC^{-1}. Bugeav et al [25] have cited an equation that can be used to calculate the mass lost from a vacuum arc cathode spot. This equation was applied to an example arc, which is described in Chapter 1, and the mass lost was calculated to be 4×10^{-8} g. If the temperature is assumed to be 2000 K the energy loss can be calculated to be

$$E_v = \gamma I_a$$

Equation 4.6

Where γ is a constant with an approximate value of 4.5×10^{-2} W A^{-1}.

Energy loss from electron emission. The energy needed to emit an electron from the cathode spot is not exactly known, because precisely how much energy is used depends on the mechanism of electron release. The maximum energy loss is when the electron is emitted by thermionic emission and is

$$W_{em} = e\phi \quad \text{per electron}$$

equation 4.7.

where e is the charge on an electron and ϕ is the work-function, provided that the electron is not ejected with appreciable kinetic and potential energy components. The high current densities of the cathode spot preclude the assumption that all the electron emission is thermionic and a large proportion must be from field emission, because the provision of high current densities from the cathode spot by thermionic emission

would require more energy than exists in the cathode spot. Unfortunately if all the emission were attributed to field emission the cathode spot would experience no energy loss as the electrons would leave by tunnelling through the work-function potential barrier from the Fermi level. In a cathode spot the emission mechanism is from an extended and intermediate region above the Fermi level where both field emission and thermionic emission occur, [see Chapter 3.] The average energy loss when an electron is emitted will then be a fraction of the normal work-function and it is necessary to include a factor α_o in the equation for the energy lost due to electron emission. Putting $\alpha_o = 0$ corresponds to 100 % field emission and $\alpha_0 = 1$ to 100 % thermionic emission. The energy loss per second, E_{em}, is given by,

$$E_{em} = \beta\alpha_o I_{el}^{-} \phi$$

equation 4.8

where β is the fraction of energy loss that is compensated for by the incoming energy flow from positive ions and I_{el}^{-} is emitted electron current.

Power loss by conduction. Daalder [4.14, 4.12] found that the heat loss due to conduction from the spot, Ec, to the bulk material is given by,

$$E_c = U_{con} I_a$$

equation 4.9

where U_{con} is the conduction loss in watts per amp and I_a is the discharge current. Daalder [4.12] showed that U_{con} could be related to the arc voltage V_{arc} by the relationship,

$$U_{con} = 0.40 (V_{arc} - \phi)$$

equation 4.10

Daalder found that his relationship holds for a wide range of materials and the conditions of a relatively low current arc, 100 A.

Power loss by radiation. The amount of radiative energy that is emitted or received by the cathode spot is an unknown factor as it is a difficult parameter to measure experimentally. There have been few attempts, but Haynes [4.46] measured the total power radiated from a cathode spot to be 2×10^{-2} W A^{-1} and this energy loss

is small compared with the other losses from the cathode spot and is therefore neglected.

4-6 ENERGY BALANCES

With the energy gains and losses to the system that have been discussed above it is possible to equate them in energy balance equations that can yield useful results, such as the power available for heating of the cathode spot [4.16] , the ionic current carrying capacity [4.14] and the feasibilities of other models for the emission process [4.33].

The variables in the above equations are difficult to estimate accurately as there is no way of making sufficiently precise measurements of them. Their value often defines whether the mechanisms they define are important in the overall cathode spot process, which makes conclusions drawn solely from energy balance equations inconclusive.

The energy balance equation for the arc spot will have the form

$$E_c + E_{em} + E_v = E_e + E_p + E_i + E_j$$

equation 4.11

This equation can only be used constructively if it can be expressed in terms of the arc current and known parameters of the arc and the electrode material. The expressions derived in the previous sections are an attempt, to quantify these energy values, to enable some conclusions to be drawn about the operation of an arc. Substituting these expressions into equation 4.11. produces the following expression

$$U_{con}I_a + \beta\alpha_o I_{el}^- \phi + \gamma I_a = I_i^+ H + I_i^+ (U_{ion} - \phi) + I_i^+ U_{kin} + 0.48\left(\frac{2}{3}\, a\right) J_z^2 \rho$$

equation 4.12.

The energy that is available for the heating of the cathode can then be estimated from this expression, by substituting values of U_{con}, β, α_o, γ, H, U_{ion}, U_{kin}, J_z and estimates of the total arc current , I_a the ion current component I_i^+ and the current carried by emitted electrons, I_{el}^- . The temperature that the cathode reaches can be

predicted from equation 4.1, but it is necessary to neglect the energy loss by conduction in the energy balance as a component for conduction losses from the spot is accounted for in the derivation of equation 4.1.

A quantitative estimate of the energy available for heating the example arc discharge, described in Chapter 1, is obtained by assuming the constants in equation 4.12 are given by Daalder [4.15]. The ionic component of the electric current is taken to be 10 % of the total arc current Sakuntala M [4.47] and the remainder carried by emitted electrons; the current density is estimated to be 1×10^7 A cm^{-2}. The appropriate constants for copper electrodes are used for a calculation of the available energy. The result is the predicted temperature versus time graph shown in Figure 4.3. This can be compared directly with Figure 4.1 where the heating energy is assumed to be from Joule heating only and it is clear that the energy available from Joule heating is comparatively small compared with the other sources of energy with positive ion bombardment being the most significant contributor.

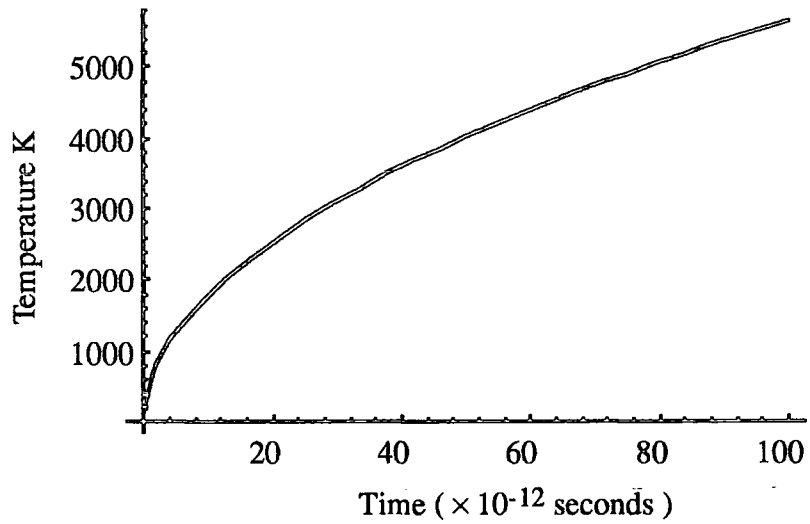

Figure 4.3. The temperature dependency on time when heated by the energy predicted as being available from the energy balance equation; the current density is estimated to be 1×10^7 A cm^{-2}.

4-7 THE CONDITIONS OF THE CATHODE SPOT

The cathode spot conditions are of vital importance to the emission processes of the cathode. Prediction of the cathode spot current density would be impossible without the electric field and temperature of the emission area being known with a fair degree of accuracy. For an unoxidized cathode the physical parameters of the cathode are well known and the only two parameters which are difficult to describe are the cathode spot temperature and the electric field strength.

Spot temperature. Estimates of the cathode spot temperature can be bounded by the lower limit of the melting point of the cathode spot material. This is because experimental investigations of the cathode emission area reveal evidence of melting of the cathode spot, Guile et al [4.26]. Figure 4.3 showed that the energy available for heating the cathode spot is capable of melting it in a time much shorter than the lifetime of the emission spot. The upper limit is much more difficult to ascertain. The assumption that the maximum cathode spot temperature is the boiling point of the material is the logical upper limit for any current density calculation. However this boiling point may be at much higher temperatures than the atmospheric boiling point as the pressure in the emission spot could be greater than atmospheric pressure. [4.32] At this point an assumption has to made of the upper limit of the temperature and for these calculations it is taken to be the boiling point of the material at atmospheric pressure. Examination of the cathode spot does not reveal any evidence of extreme values of temperature, such as distortion of the areas around the crater, however the possibilities of very high temperatures of the cathode should not be discounted.

Electric field strength. The extreme current density of the cathode spot indicates that there is a very high electric field strength in the cathode region. This is also evident from the measurement of the voltage characteristics of the arc with the cathode voltage fall indicating that there is an appreciable electric field strength. Measuring the cathode voltage fall has been achieved by many experimentalists, but

measuring the distance over which this voltage is dissipated is not a measurement that has been attempted frequently. Dickson et al [4.48] used a set of electrodes that could be mechanically separated and measured the arc voltage as they were moved apart. They reported that the cathode voltage fall region started no further than 4×10^{-8} m from the surface of the cathode. The cathode voltage fall is usually found to be of the order of 10 V and therefore the minimum cathode region electric field could be assumed to be 2.5×10^{6} V cm^{-1}. The upper limit on the cathode region electric field is once again open to conjecture. Under some conditions the formation of very large electric fields is possible and this would lead to a conclusion that an upper limit on the electric field strength might be 1×10^{8} V cm^{-1} which is an approximate upper limit on sustainable electric fields. However in the cathode region substantial numbers of charge carriers will be flowing across it making the concept of sustaining the upper limits of electric field strength a difficult one to envisage. An electric field will be sustainable because of the quasi-neutrality of the arc enabling the formation of a positive sheath between the arc column and the cathode electrode, in a manner similar to the formation of the positive column described in section 2.3 of Chapter 2. To find an upper limit on the electric field strength it is necessary to look at the work that led to defining the minimum electric field strength, and to use the lower limit of the distance over which the cathode voltage fall occurs to define the upper limit. Dickson found that a gap of approximately 1×10^{-6} cm was the limit of the inter electrode gap before some other effects come into effect, [4.48]. If this is correct the upper limit of the electric field strength in the cathode region would be 1×10^{7} V cm^{-1}.

In summary for a copper cathode in an unoxidized state the limits on the temperature are then 1400 K to 3000 K, with the electric field strength from 2.5×10^{6} V cm^{-1} to 1×10^{7} V cm^{-1} for a work function taken to be 4.5 eV [4.49]. The emission equation to be used for this range of temperatures and electric field is found from figure 3.5 which shows clearly that this regime falls within that of field enhanced thermionic emission, for which the solution is described in section 3.3 of Chapter 3, equation 3.21. The results of plotting current density versus temperature in equation

3.21 for the temperature range defined above, with the electric field strength as apparent over the range described above, are shown in figure 4.4. The curves demonstrate that current densities of the order of magnitude that is believed to be emitted from the cathode spot are possible with this type of mechanism.

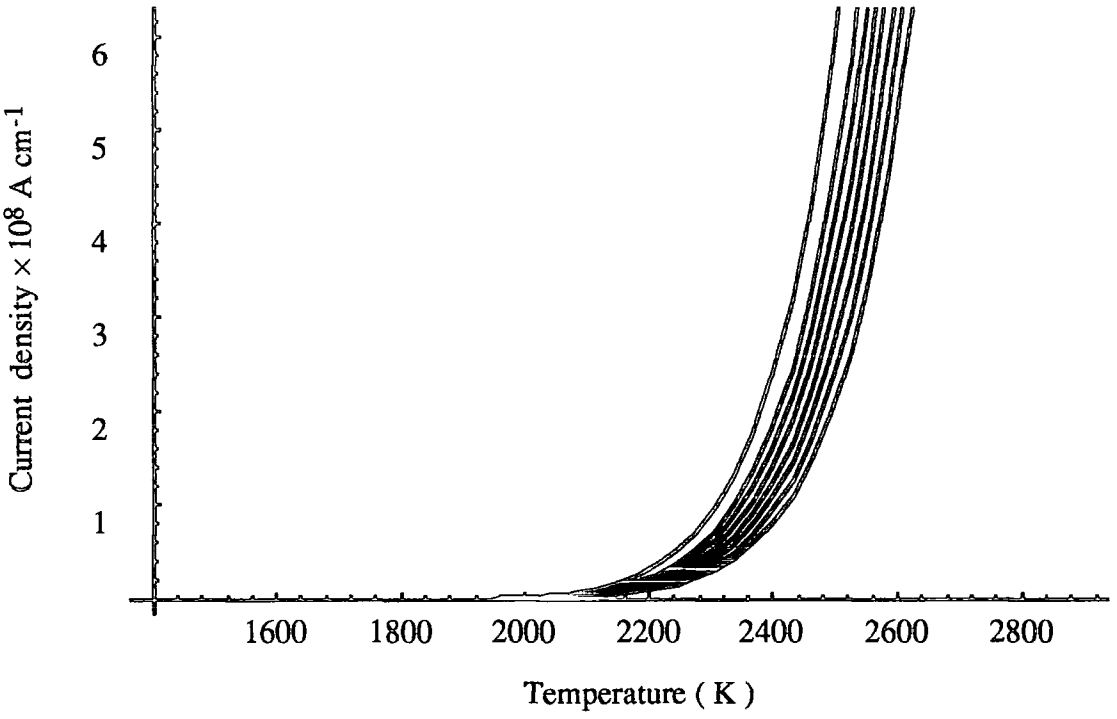

Figure 4.4. Equation 3.21 showing the predicted current density over the range of temperatures and electric field strengths defined in section 4.7 with curves for increasing electric field strength from 2.5×10^6 to 1×10^7 V cm^{-1}.

4-8 REFERENCES

4.1 Somerville J.M. *The Electric arc.* London: Methuen and New York: Wiley. 1957

4.2 von Engel A. Robson A.E. *The excitation theory of arcs with evaporating cathodes.* 1957 Proc. Roy. Soc. London Series A Vol. 242 p. 217 to 236.

4.3 Rich J.A. *Resistance heating in the arc cathode spot zone.* 1961 Journal of Applied Physics. Vol. 32 No. 6 p. 1023 to 1031.

4.4 Wroe. H. *Vacuum arcs on Tungsten cathodes.* 1958 Nature Vol. 182 p. 338 to 339.

4.5 Basharov R. Gavnlovskaya E.N. Malkin O.A. and Trekhov A. *An investigation of cathode spots in a pulsed discharge between parallel electrodes.* 1966 Sov. Phys.; Tech. Phys. 10 p. 1428

4.6 Harry J.E. *The measurement of the erosion rate of the electrodes of an arc rotated by a transverse magnetic field.* 1969 Journal of Applied Physics. Vol. 40 No. 1 p. 265 to 270.

4.7 Sanger C.C. Secker P.E. *Arc cathode current density measurements.* 1971 J. Phys. D. Appl. Phys. Vol 4 p 1940 to 1945

4.8 Guile A.E. *Model of emitting sites on non-refractory cathode arcs with thickish oxide films.* 1974 Proc. I.E.E. Vol. 121 No.12 p 1594.

4.9 Drouet M.G. Gruber S. *Dynamic Measurements of cathodic emission in a moving arc.* 1976 I.E.E.E. trans. on Power apparatus and systems. Vol PAS-95 No. 1 p. 105 to 112.

4.10 Daalder J.E. *Diameter and current density of single and multiple cathode discharges in a vacuum.* 1974 I.E.E.E. Trans. Power Apparatus and Systems PAS. 93 p. 1747 to 1757.

4.11 Guile A.E. Hitchcock A.H. Barlow *Transition in size and number of emitting sites with increase in arc speed over copper cathodes.* 1977 Proc. I.E.E. Vol. 124 No. 4 p. 406 to 410.

4.12 Daalder E. *Energy dissipation in the cathode of a vacuum arc.* 1977 J.Phys. D: Appl. Phys. Vol. 10 p.2225 to 2234

4.13 Guile Hitchcock Stephens G.W. *Emitting site lifetimes , currents and current densities on arc cathodes with 100 nm thick copper oxide films.* 1977 Proc. I.E.E. Vol 124, No. 3, 273 to 276.

4.14 Holmes A.J.T. *A theoretical model of the mercury and copper vapour arcs.* 1974 J. Phys. D. Appl. Phys. Vol 7 p. 1412 to 1425.

4.15 Daalder J.E. *A cathode spot model and its energy balance for metal vapour arcs.* 1978 J. Phys. D. Appl. Phys. Vol. 11 p. 1667 to 1682.

4.16 Jüttner B. *Formation time and heating mechanism of arc cathode craters in vacuum.* 1981 J. Phys. D. Appl. Phys. Vol. 14 p. 1265 to 1275.

4.17 Hantche E. Jüttner B. Pucharov V.F. Rohrbeck W. Wolff H. *Erosion of metal cathodes by arcs and breakdowns in vacuum.* 1976 J. Phys. D. Appl. Phys. Vol. 9 p. 1771 to 1781.

4.18 Guile A.E. *Joule heating in emitting sites on various non-refractory arc cathodes.* 1977 Proc. I.E.E. Vol. 127 No. 7 P 452 to 457.

4.19 Jüttner B. Pursh H. Anders S. *On the current density at the cathode of vacuum arcs.* 1984 J. Phys. D. Appl. Phys. Vol. 17 L. 111 to 114.

4.20 Puchkarev V.F. Murzakeyer A.M. *Current density and the cathode spot lifetimes in a vacuum arc at threshold currents.* 1990 J. Phys. D. Appl. Phys. Vol. 23 p. 26 to 35.

4.21 Hess H. *The vacuum arc spot - a high pressure phenomenon.* 1991 J. Phys. D. Appl. Phys. Vol.24 p. 36 to 40.

4.22 Augis J.A. Gibson F.J. Gray E.W. 1971 Int. J. Electron. Vol. 30 p 533

4.23 A H. Hitchcock A.E. Guile. *A scanning electron microscope study of the role of copper oxide layers on arc cathode erosion rates.* 1977 Journal of Material science 123 p. 1095 to 1104 ,

4.24 Grey E.W. Pharney J.R. *Electrode erosion by particle ejection in low current arcs.* 1974 Jour. Appl. Phys. Vol 45 No. 2 P 667 to 671]

4.25 Heylen A.E.D. Guile A.E. Morgan D.V. *Electron field emission from copper with various thickness of oxide film.* 1984 I.E.E. Proceedings Vol 131 pt A no.2 p. 111 to 117 .]

4.25 Bugeav S.P. Litvinov E.A. Mesyats G.A. Proskarovskit *Explosive emission of electrons* 1975 Sov. Phys. Usp Vol. 18 No. 1 p 51 to 61.

4.26 Guile A.E. Jüttner B. *Basic erosion processes of oxidized and clean metal cathodes by electric arcs.* 1980 I.E.E.E. Trans. on Plasma Science Vol. PS-8 No.3 p. 259 to 268.

4.27 Anders S. Jüttner B *Influence of residual gases on cathode spot behaviour.* 1991 I.E.E.E. Transactions on Plasma science Vol 19 No. 5 p 705 to 712.

4.29 Puchkarev V.F. *Estimating the electron temperature from fluctuations in a vacuum arc plasma: cathode spot operation on a contaminated surface.* 1990 Jour. Appl. Phys. vol. 24 p. 685 to 692.

4.30 Szente R.N. Munz R.J. Drouet M.G. *Cathode erosion in inert gases: the importance of electrode contamination.* 1989 Plasma Chemistry and Plasma Processing, vol 9 no.1 p. 121 to 132.

4.31 Augis J.A. Gray E.W. *Scanning electron microscope study of electrode damage due to nanosecond arcs.* 1971 Jour. Appl. Phys. vol. 42 No. 6 p. 3367 to 3368]

4.32 Secker P.E. George I.A. *Preliminary Measurements of arc cathode Current Density.* 1969 Jour. Phys. D: Appl. Phys. Vol 2, p 918 to 920.

4.33 Holm R. *Electric Contacts Theory and Application.* 1967 (Berlin: Springer Verlag)

4.34 Hitchcock A.H, Guile A.E. *A scanning electron microscope study of the role of copper oxide layers on arc cathode erosion rates.* 1977 Jour. of Material science Vol. 12 p. 1095 to 1104.

4.35 Pfender E, Boulos M. and Fauchais P. 1987 *Plasma Technology in Metallurgical Processing.* ed Feinman J. (Iron and Steel Society ISBN 0-932897-12-6.) p. 37.

4.36 Bebber H. [Private Communication.]

4.37 Hare A.L. [Private Communication]

4.38 Guile A.H . *Arc-electrode phenomena* 1971 Proc. I.E.E., I.E.E. Reviews Vol. 118 No. 9R p. 1131 to 1154.

4.39 Augis J.A. Gray E.W. *Scanning electron microscope study of electrode damage due to nanosecond arcs.* 1971 Jour. Appl. Phys. vol. 42 No. 6 p. 3367 to 3368

4.40 Guile A.E. Hitchcock A.H. *Physical implication of an effective activation energy for arc erosion on oxidized cathodes.* 1984 J. Phys D: Appl. Phys. Vol 15 p 2341 to 2355

4.41 Guile A.E. Hitchcock A.H. *The effect of rotating arc velocity on copper cathode erosion.* 1974 J. Phys D: Appl. Phys.Vol. 7 p. 597 to 606.

4.42 Guile A.E. Morgan D.V. *Electroforming or fritting in surface films on contacts.* 1975 Proc I.E.E. Vol. 122 no. 12 p 1454 to 1455

4.43 Guile A.E. Hitchcock A.H. *Time variations in copper cathode erosion rates for long duration arcs.* 1975 Jour. Phys D: Appl. Phys. vol 8 p 427 to 433 1975.

4.44 Davis W.D. Miller H.C. *Electrode products emitted by d.c. arcs.* 1969 Jour. of Appl. Phys. Vol. 40 no. 5 p. 2212 to 2221

4.45 Plyutto A.A. Ryzhkov V.N. Kapin A.T. *High speed plasma streams in vacuum arcs.* 1965 Soviet Phys. J.E.T.P. Vol. 20 No. 2 p. 328 to 337.

4.46 Haynes J.R. *The production of high velocity Mercury vapour jets by spark discharges.* 1948 Phys. Rev. Vol 73 No. 8 p. 891 to 903.

4.47 Sakuntala M. von Engel A. Fowler R.G. *Ionic conductivity of highly ionized plasmas.* 1960 Phys. Rev. Vol. 118 No. 6 p. 1459 to 1465.

4.48 Dickson D.J. Engel A. von *Resolving the electrode fall spaces of electric arcs* 1967 Proc. of the Roy. Soc. Series A Vol. 300 p. 316 to 325.

4.49 Kaye G.W.C Laby T.H. *Table of physical and chemical constants and some mathematical functions.* 1973 London: Longman

4.50 Anders S. Anders A. *On modes of cathode operation.* 1991 I.E.E.E. Trans. on Plasma Science Vol. PS-19 No.1 p. 20 to 24.

CHAPTER 5. EXPERIMENTAL WORK

5-1 INTRODUCTION.

This chapter describes the apparatus and techniques that were developed to enable an experimental investigation of electron emission processes of a cold cathode thermal arc to be made. Before experimental investigations of the emission mechanisms of thermal arcs could begin reliable apparatus for generating, manipulating and characterizing a thermal arc had to be constructed.

The first task in generating a thermal arc was to develop a suitable power supply that could deliver the current-voltage characteristics of an arc in the time scale of a discharge. Initially the arc maximum discharge time was estimated as approximately 10 msec, therefore the power supply had to be capable of a rapid release of energy. When designing such a power supply it has to be noted that there will be two electrical circuits that will be equivalent to the power supply. The first being the desired state when the arc is conducting between the electrodes and the second when there is no conduction between the electrodes. These two circuits have to be examined in detail before any power supply is built, if unexpected results are to be avoided.

There are several methods of achieving the required power performance such as; high power A.C. transformers and solid state rectification, three phase A.C motors coupled to D.C. generators and charge storage devices. These methods were discounted as either they could not deliver the necessary current-voltage characteristics, were prohibitively expensive or contained large capacitative elements. High value capacitors are avoided in arc power supplies as they cannot sustain large current discharges for a long periods, require modification to alter the discharge time and prohibit the use of some ignition systems. The solution used in these experiments provided a power supply that was capable of delivering a current voltage waveform that would generate a thermal arc over a wide range of discharge time scales and was cost effective.

5-2 ARC GENERATION

The power supply. The power supply circuit diagram is shown in figure 5.1. The E.M.F. is provided by six lead acid cells that are connected in series. The lead acid cells used have large surface area electrodes which enable rapid discharge. This enables short time scale discharge experiments to be completed, but the high charge storage capacity of the cells enables long duration arcs to be sustained, to a maximum of 1 hour. The current output of the power supply is controlled by a resistor connected in series with the negative rail of the power supply. This unusual configuration was used to enable monitoring of the voltage across the test resistance part of the limiting resistor without using a floating input circuit with the oscilloscope.

The limiting resistor consisted to two parts, the test resistance used to measure the current output of the power supply and load resistance which could be adjusted to alter the output of the power supply. The limiting resistor had to have a range of values from approximately 0.05 Ω to 10 Ω, with a power capacity of 8 kW and because of the small time scale of the discharge, a low impedance value. A linear geometry was chosen for the resistor using a rectangular resistance wire, 0.75 mm by 7 mm, approximately 10 m in length, wound around an H shaped frame. Terminations were made every 20 cm along the wire giving a wide range of resistance values and hence a wide range of available current outputs.

The open circuit voltage of the power supply could not be altered as simply, but was most easily adjusted by the addition or removal of cells. The original power supply had an open circuit voltage of 76 volts; this was chosen to enable the power supply to overcome any circuit resistance and provide an arc voltage of approximately 10 volts.

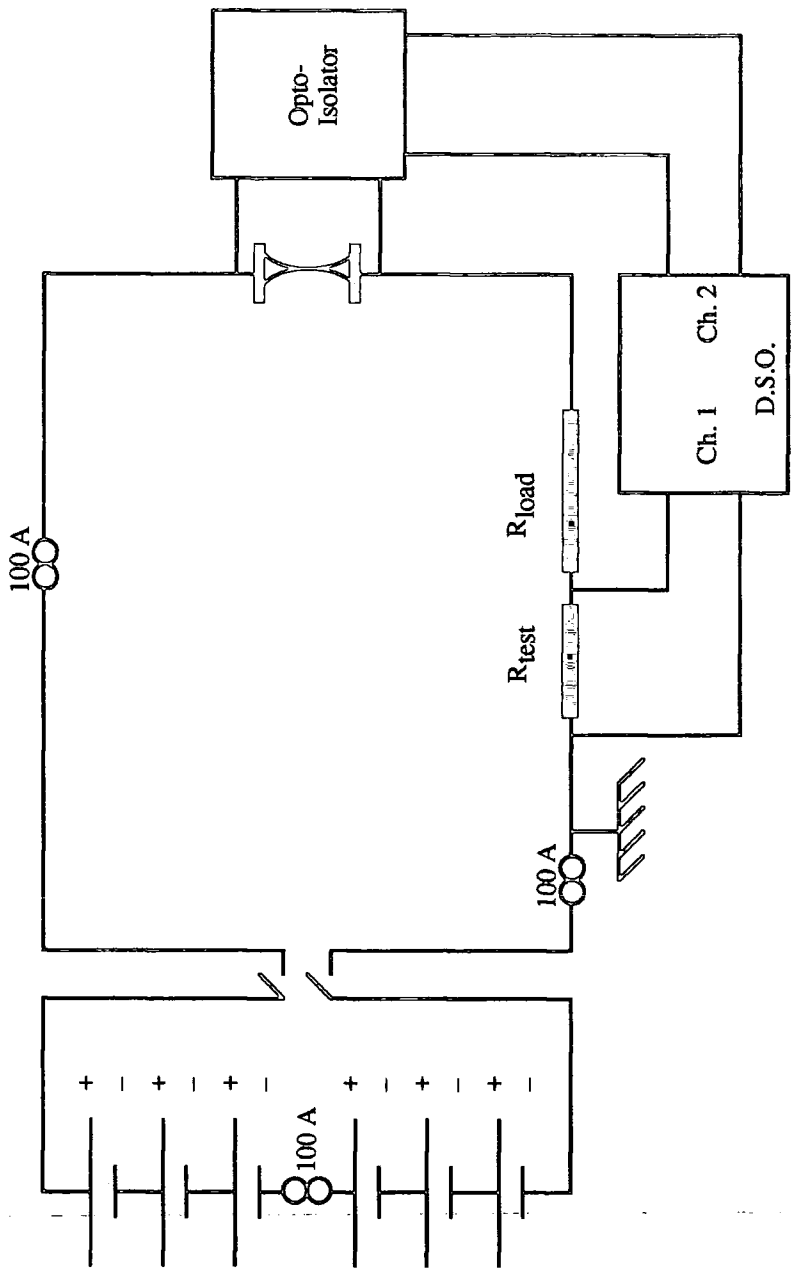

Figure 5.1. The power supply circuit diagram.

The maximum current output of the power supply was determined by the switch gear bought to control the power supply. (A Santon C 10 H 28 four pole D.C. switch.) This had a maximum rating of 110 amps and the apparatus was fused for 100 amps to allow an adequate safety margin. Additional fuses were included in the apparatus as circuit breakers which had to be removed before access to the potentially live parts power supply could be achieved. The lead acid cells were contained in a ventilated metal acid cabinet and the limiting resistor housed in an separate insulated cabinet. The internal resistance was measured to be 0.12 Ω and the open circuit voltage was measured to be 78 volts, which would give a theoretical maximum current output of 650 amps. The high power capability and flexibility of discharge times demonstrated the suitability of this power supply for sustaining experimental D.C. thermal arcs.

Arc Initiation. Striking an arc requires some mechanism to overcome the high resistance of the gas to enable current to flow, i.e. the gas has to be initially ionized by some external means. There are two established mechanisms to achieve this and the choice depends on the experimental apparatus. If the electrodes can be initially brought into contact with each other a short circuit can be established. This provides enough vaporized material and generates enough heat to allow the electrodes to emit thermionically and the gas to conduct sufficiently for an arc regime to take hold when the electrodes are separated. This method is only suitable when it is possible to move the electrodes and if the power supply is sufficiently powerful enough to melt the electrodes in a short circuit. A more flexible method is to pre-ionize the electrode gap by some external means to a level where the threshold voltage for striking the arc is equivalent to the arc voltage. This can be achieved by reducing the pressure of the discharge gas or changing the discharge gas to another with a lower Päschen voltage. Alternatively an external source of ionization, such as a focused laser beam, high frequency high voltage spark or a thin fuse wire stretched between the electrodes can be used to provide enough pre-ionization for the arc to initiate. In these experiments

two methods of pre-ionization were employed, a high frequency spark or a fuse wire technique. The former was possible because the power supply contained no capacitative elements, which enabled a high impedance, low resistivity inductor to be included in the power supply. The high impedance isolates a high frequency signal from the D.C. power supply, enabling a high frequency, high voltage ignition power supply to be in parallel with the D.C. circuit. It was used as it was believed it would be necessary to strike the arc without contaminating the electrode with other metal particles, from exploding fuse wire between the electrodes. Arcs could successfully be struck between the electrode with this apparatus, but it was difficult to strike a single arc and to isolate the high frequency pulse from the other instrumentation of the apparatus.

The problem of contamination of the experiment with other materials from an exploding fused wire approach was overcome by using a thin strand of copper wire, 30 swg, between the electrodes instead of fuse wire. The wire was vaporized when the power supply was switched on and this provided the initial ionization for the arc regime to be struck. This method was a simple way of striking a single arc, which was used in all the damage experiments with a 96 % success rate.

Electrode design. The arc was struck between rail electrodes with an inter electrode gap of 2.5 mm. The holder was made from a ceramic material to withstand the heat produced by the arc. The anode electrode was vee shaped, with tapered ends to ensure the arc ran over the centre of the cathode electrode. Figures 5.2 show the construction of the electrodes, the electrode holder, the joint between the sample and run on electrodes, and figure 5.3 illustrates the connection to the power supply.

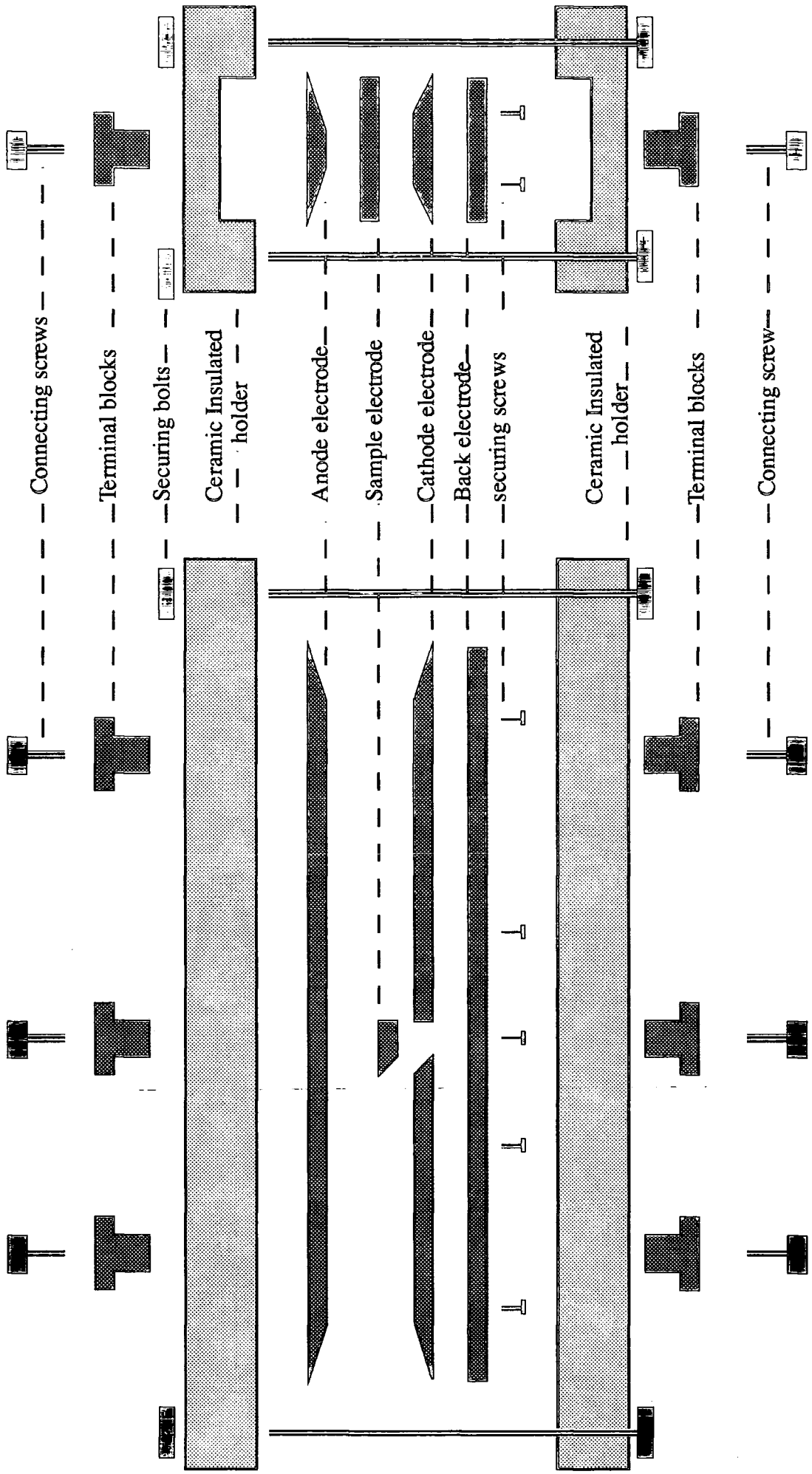

Figure 5.2. The electrode assembly

The cathode electrode was split into three sections, a run-on electrode, on which the arc was ignited, a sample electrode, the surface of which could be specially prepared, and a run-off electrode on which the arc would be extinguished. The three sections of the electrode had to be carefully machined for a close fit as any gaps or appreciable cracks in the surface of the cathode electrode caused the arc to deviate from the required path. The run on and sample electrodes were joined by a 45° edge to ensure the arc traversed onto the sample electrode. It was not found to be necessary to join the sample electrode to the run-off electrode, in the same way, as few problems were encountered with the arc transferring onto the run-off electrode provided the electrodes were butted together. To ensure good electrical conduction between the three electrodes they were connected by a back electrode which was also used to ensure a strong mechanical joint between the three electrodes. The edges of the run-on and run-off electrodes were bevelled to minimize any increase in the electric field strength that would occur at the edges of the electrode.

Arc manipulation. The arc experiments required that the arc could be driven down the rail electrodes at a chosen velocity. If there is no external driving force the arc spot does not remain stationary in attachment to the electrode, moving with a random velocity, V_{spot}, but for the experiments it was necessary to impose a velocity component along the rail electrodes V_z. This could be superimposed on V_{spot} by subjecting the arc to an external driving force such as a magnetic field, B_z, induced in a plane perpendicular to the direction of the current flow, I_x, or by striking the arc in a gas flowing with a velocity G_z. Figure 5.4 shows how the external forces were applied singularly and simultaneously.

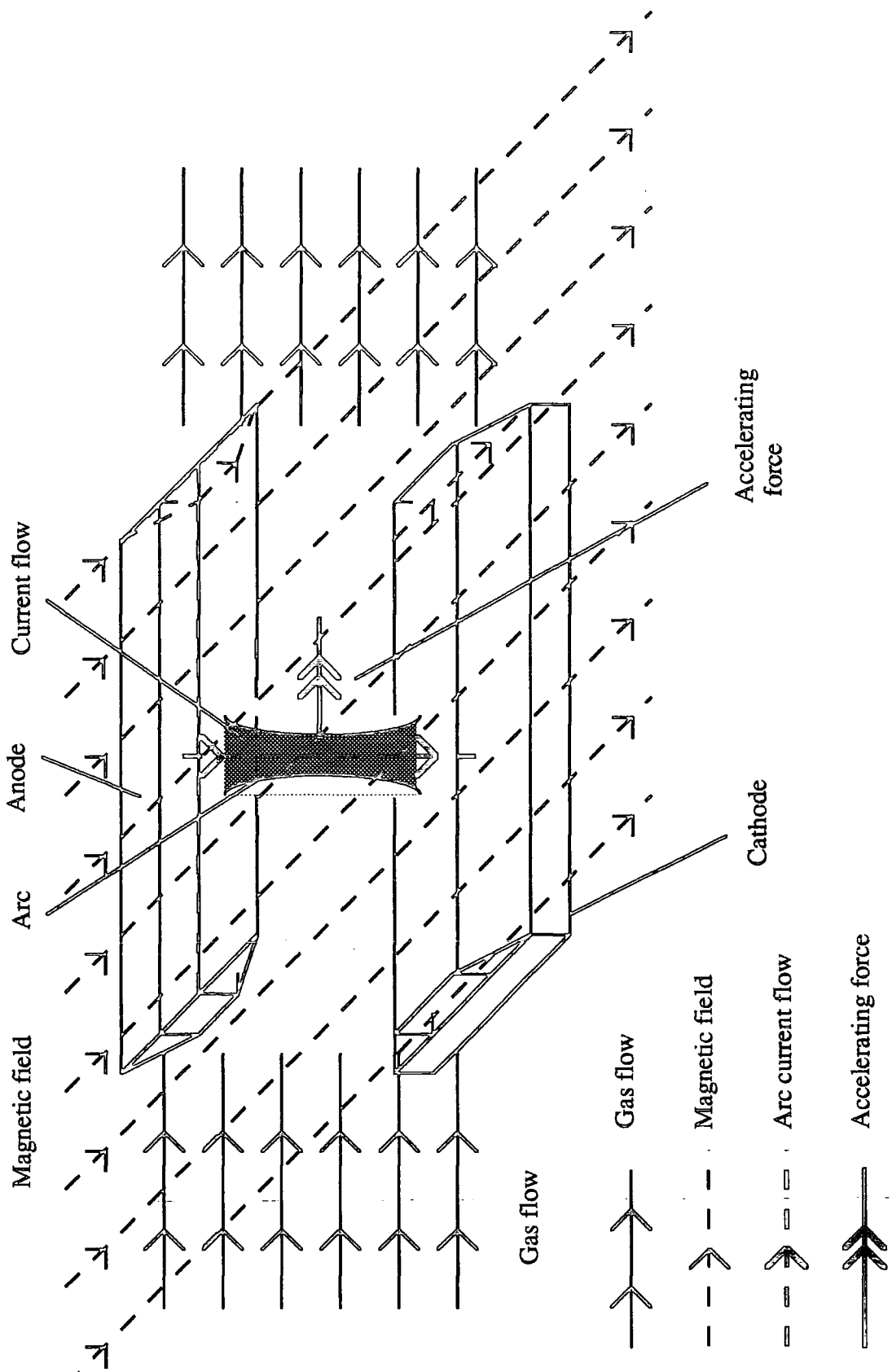

Figure 5.4. The application of driving forces to the arc.

The external magnetic field was provided by an electromagnet (Newport Instruments type A) powered by a 3 kW D.C. power supply (Newport Instruments type D 104,) which is capable of delivering chosen magnetic fields of up to 0.650 Tesla. The magnetic field was applied by placing the electrodes holder between the poles of the magnet with the sample electrode at the centre of the pole pieces.

The driving aerodynamic force was generated by a cylinder of compressed air, with a cylinder pressure of 200 atm. The gas was obtained from B.O.C. and had a water content of less than 50 vpm (volume parts per million). The gas flow was controlled by a pressure regulator which maintained a constant pressure despite the gas flow rate, and as it was flowing into the atmosphere this was an effective method of controlling the gas velocity and ultimately the arc velocity. The gas is fed between the electrodes by a 4 mm diameter pipe which is held between the electrodes by an insulating P.T.F.E. former. For field free measurements the electrode assembly was not put between the pole pieces of the electromagnet as there was a permanent residual magnetic field in the pole pieces which would have interfered with the experiments. The gas driving pressure used was varied from 5 to 15 bar. The experiments were difficult because it was possible to create a vortex stabilized stationary arc where the gas flow forms an equilibrium with the self induced magnetic field of the arc. This could be prevented if the electrodes were as smooth as possible, therefore it was necessary to replace the run on and run off and anode electrodes frequently.

These two external driving forces could be used in conjunction with each other or independently from one another to drive the arc along the rail electrodes at a chosen velocity in the range of 4 to 70 ms^{-1}, for a magnetically driven arc and 3 to 15 ms^{-1} for an aerodynamically driven arc. In Chapter 2 section 2.3 it was shown that arc behaves as an aerodynamic solid body, when driven by both magnetic field and aerodynamic driving forces. Thus when damage experiments were completed it was valid to compare the two differently driven arcs as the forces act on the arc in the same way.

Superimposing a linear velocity on the arc also served to control the arc. When a rail electrode arrangement was used the arc could be extinguished by driving it

beyond the end of the electrodes, blowing the arc out. The arc velocity also controls the amount of damage that is done to the electrodes and it was possible to prevent melt mode emission from the electrodes without introducing external cooling to the electrodes or altering the arc current. These characteristics of single shot, driven arc, experiments, make them suitable for crater formation studies.

5-3 ARC CHARACTERIZATION.

Crater formation studies require a few basic characteristics of the arc to be measured, to enable them to be accounted for in any damage experiments. The two primary parameters that have to be controlled are the linear arc velocity V_z and the arc current.

Current Instrumentation. Measuring the arc current was done by monitoring the current output of the power supply. The current pulse was of a relatively short duration so the current instrumentation had to have a high frequency response, i.e. a low reactance. Since low impedance was also a requirement of the load resistance, the two resistors were combined in one low impedance resistance assembly, which was described in section 5.2. The voltage signal, generated by the current flowing though the test resistance, was captured on a digital storage oscilloscope. (Gould 20 MHz Digital storage oscilloscope type 14 25.) The frequency response of such a system was found to be adequate to measure the current signals that were being generated by the arc. The test and load resistance were placed in the negative rail of the circuit, despite it being safer in the positive side, because this enabled the oscilloscope to be attached directly to the circuit without either isolating the oscilloscope from earth or using a floating input circuit. The oscilloscope was triggered on the voltage signal itself and the signal captured with 75 % pre-trigger. The value of the test resistance was 0.062 Ω.

Discharge voltage instrumentation. In later experiments it was found desirable to measure the voltage across the arc and this was achieved by measuring the

voltage formed across the arc itself. The two states of the circuit, as described in section 5.2, would not allow the second channel of the oscilloscope to be attached directly across the electrodes of the arc. The input resistance of the oscilloscope had to be very large to prevent the power supply shorting through the earth connection of the oscilloscope. The was achieved by using a opto-isolator circuit on the input channel of the oscilloscope. The circuit diagram is shown in figure 5.5. The input signal is modulated onto a light source by an LED. This light is then converted into an electrical signal, replicating the original signal, by a photodiode, thus achieving total electrical isolation of the two circuits. This circuit enabled the oscilloscope to be safely attached even when the arc was not burning between the electrodes. The voltage and the current of the arc were then measured simultaneously on the two channels of the oscilloscope.

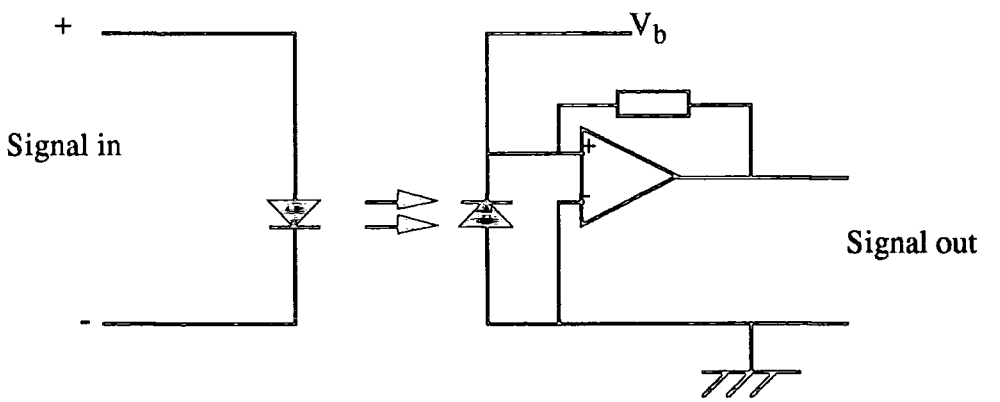

Figure 5.5. The opto-isolator.

Arc velocity measurements. The superimposed linear velocity of the arc, V_z was an important characteristic of the damage experiments that had to be measured. An established procedure for measuring the arc velocity was to time the passage of the arc past photovoltaic detectors and an elaborate experimental apparatus was designed to detect the passage of the arc as shown in figure 5.6.[5.11] The light generated by the arc was directed, via a mirror, collimator and fibre optic cable to a photodiode. Several detector circuits were placed along the rail electrodes and the outputs from these were fed into a storage oscilloscope. The time between the leading edges of the voltage

pulses produced by each detector being triggered could then be resolved. The distance between the detector circuits was known and the velocity of the arc calculated.

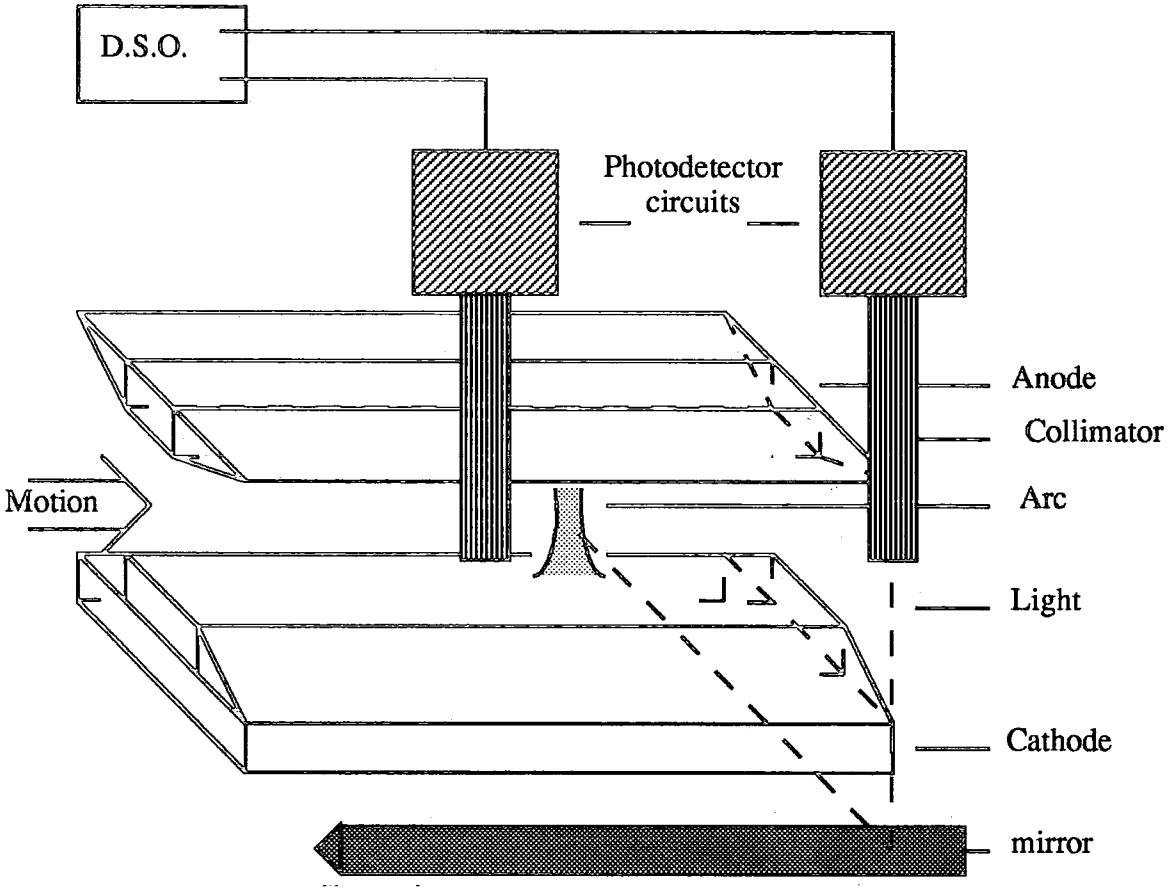

Figure 5.6. The photo detector apparatus used to measure the velocity of the arc.

This system could be used to establish the approximate velocity of the arc, but was prone to many experimental difficulties. The primary causes of problems were the high intensity light that the arc generated which triggers the detectors prematurely and the large amount of noise that was generated by the experiment which interfered with the electronics of the detector circuits. The collimators were intended to resolve the problem of premature triggering of the detector circuits, but these revealed a further fundamental problem with attempting to measure the velocity of the arc in this way. The arc does not take the geometry that is suggested in figure 5.6. High speed photography of an arc running along rail electrodes shows it has a drawn out appearance that can be several cm long and emits light all along this length, Mai [5.1] , Munz [5.2]. This

makes optical assessment of the arc velocity in small gap rail electrode arc experiments uncertain.

Alternative methods of measuring the velocity were then explored. The first was to measure the duration of the current waveform of the arc, that was recorded to monitor the current of the arc. This gave the total duration of the arc as it travelled the length of the electrodes and therefore the average velocity of the arc. The mass of the arc will be negligible, in terms of the accelerating force and therefore the deviation from the average velocity will depend on the uniformity of the accelerating force. In aerodynamic driving force experiments the force will be very uniform and therefore the average velocity measurements will be sufficiently accurate for the experiments. In magnetic driving force experiments the accelerating field is less uniform and the deviation of the actual velocity, over the sample, to the average velocity will be larger.

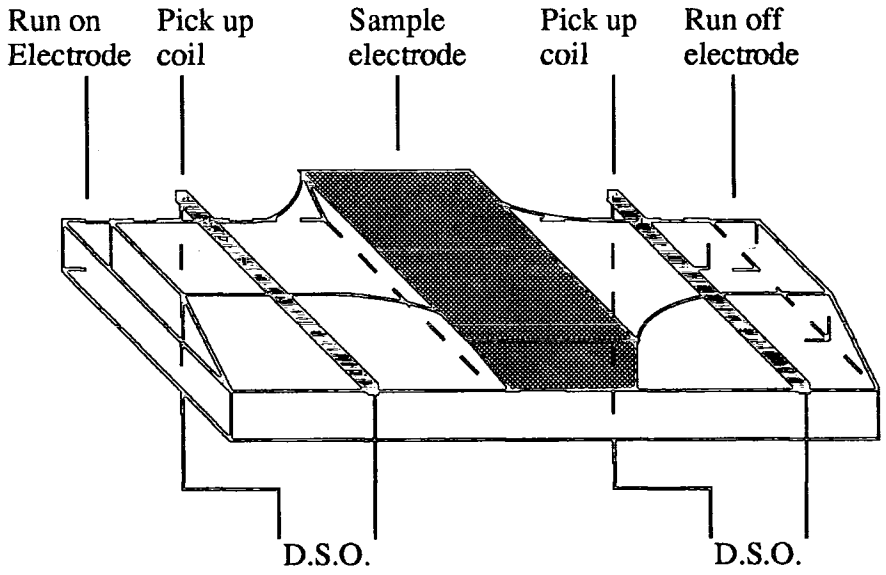

Figure 5.7. Two pick up coils mounted just below the surface of the cathode generate a voltage when the arc passes over them, enabling velocity measurements.

The other method of measuring the velocity of the arc was to use an adaptation of the pick up coil apparatus Drouet et al, [5.3] used to measure the current of the arc. Two axially wound coils were inserted into the cathode electrode just below the surface of the electrode, as shown in figure 5.7. The coils were electrically insulated from the

electrode and the outputs were attached to a digital storage oscilloscope. As the arc ran over the surface of the electrodes a voltage would be induced in the pick up coils, which would be detected on the oscilloscope. The time delay of peaks of the induced voltages could be used to determine the velocity of the arc.

This apparatus was of only limited success as the coils were prone to pick up stray R.F. noise that was generated by the apparatus. However measuring the velocity by this method was possible, but the results obtained were close to the values of the average velocity obtained by monitoring the current waveform. Due to the uncertainty in the exact time that the induced voltage peaked, (caused by the noise) and close agreement with the results from the current waveform method, the measurements obtained by this method were not used in any crater study experiments.

The generated arc. Despite the careful design of the apparatus, there are many unforeseen parameters that affect the generated arc, therefore it is important to characterize the type of arc that has been generated in the experiment. The current voltage waveform of an arc generated by the power supply is shown in figure 5.8. The arc was struck using a thin strand of copper wire between the rail electrodes and the current and voltage of the arc were measured using the instrumentation described in this section. Despite the high current of the arc the short arc column length enabled the electrode regions to limit the current within the arc column, thus ensuring the arc was of a low intensity nature. Low intensity arcs have a tendency to be unstable, but they can be stabilized by an external force.

The high current and low voltage of the discharge indicate that it is an arc type discharge, with electrical characteristics like those shown in figure 2.5. The discharge column was observed to have a high luminosity, which is also a characteristic of thermal arcs. The low discharge voltage showed that the emission mechanisms of the arc were very efficient, but the measured voltage, 4 V was lower than expected, 10 V. The voltage instrumentation was carefully re-calibrated and was found to be accurate. The lower voltage of the discharge could only be accounted for by the short arc length

minimizing the voltage dropped across the arc column. The low discharge voltage reiterates the efficiency of the electron emission mechanism.

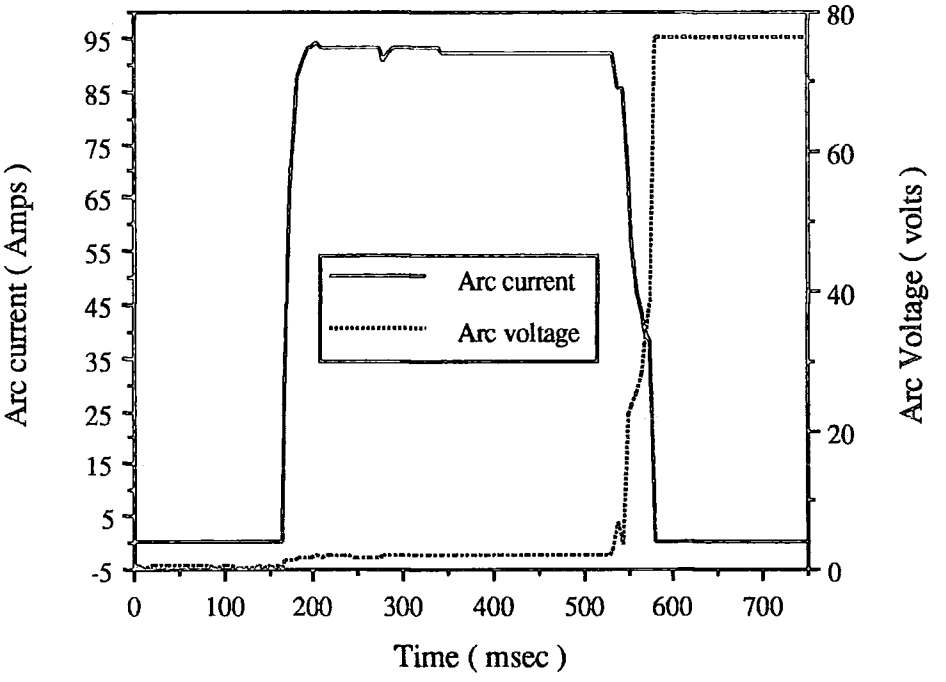

Figure 5.8. The current and voltage waveforms of a generated arc. The arc was generated on copper rail electrodes and driven along them with a magnetic field.

The arc velocity was measured using the time of the current discharge. The arc velocity dependency on magnetic field was plotted, for an arc current of 90 amps, and is shown in figure 5.9. The results highlight one of the problems that occurred in the experiments that could not be solved. The jump in velocity from 15 ms^{-1} to 35 ms^{-1} for a negligible increase in the driving magnetic field strength. This problem occurred in all later experiments, and caused a gap in the experimental data. A possible explanation of this was that jets of molten material from the anode could cause the arc velocity to be reduced, with low field driven arcs. It has been suggested that the arc velocity, V_Z, is a function of the magnetic field, B_Z (Tesla), [5.8, 5.12.] The relationship is

$$V_Z = \alpha I^{0.4} B_Z^{0.6}$$

equation 5.1

where α is a constant that is dependent on the experiment and I is the arc current in amps. As the arc current and other experimental variables were kept constant, $\alpha \times I^{0.4}$ was established by taking the average of the measured velocity divided by $B_z^{0.6}$. The theoretical results are also shown in figure 5.9 with high velocity and slow velocity arcs having being treated as separate experiments and the data fitted to the theory independently.

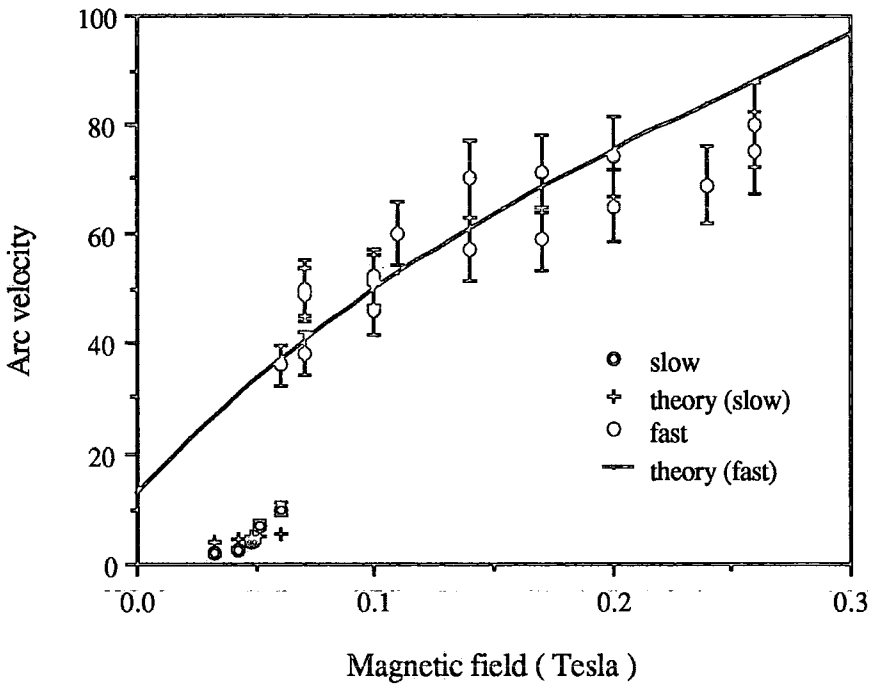

Figure 5.9. The average arc velocity as a function of the magnetic field.

The experimental and theoretical results would seem to be compatible at intermediate velocities, but the experimental values are appreciable lower at high velocities. This may be accounted for in one of two ways, either the theory did not extend to these velocities, or the error in measuring the velocity became appreciable at high velocities. It is more likely that the detection system was at fault as the theory has been tested to higher velocity and current ranges than those used in this experiment, [5.9.] The errors in the velocity measurement will be caused by inaccuracies in the measurement of the duration of the arc, the distance the arc travelled, the non uniformity of the accelerating force and deviations in the burning of the arc, such as the arc being momentarily stationary or a secondary arc being generated. Equation 5.1

does not fit the slow velocity regime which is also an indicator of irregular behaviour occurring in this velocity range. The arc could not be made to run with a velocity of 20 to 35 ms^{-1} by the application of an external magnetic field. There was no reason to suspect an error in the instrumentation, but this was a peculiarity of the experiment. No other evidence of this type of problem was encountered in the literature and no satisfactory explanation could be found for this phenomenon. It is possible that the slow speed of the arc caused jets of liquid electrode to be injected into the arc column leading to changes in the characteristics of the arc. However no evidence of excessive jetting was seen on the same electrode.

The duration of the arc was measured by an oscilloscope, which when used in single shot mode had a maximum time resolution of 0.05 msec. The error in the timing circuit was therefore ± 0.025 msec. The arc was always struck from the same point on the electrode, a hole 1 mm in diameter and ran the length of the electrodes, a distance of 140 mm. The error in the distance travelled was therefore ± 0.5 mm. The errors that occurred when the arc did not burn as predicted were so large that the situation became obvious. The discrepancy in the actual applied accelerating force was more difficult to access, the magnetic field measured the peak field at the centre of the pole pieces. To find the average field strength the magnet was re-calibrated with the average magnetic field measured along the length of the electrodes, at a given peak field strength . The error was found to be systematic with an error of 7 % and the total error in the velocity readings was then taken to be 10% to account for all the errors in the measurement.

A similar graph of arc velocity versus gas pressure was produced, the arc velocity was measured in the same way, the driving pressure being recorded from the pressure regulator. The error in the measurement of the velocity was less than that occurred in the magnetically driven experiments as the accelerating force was more uniform along the length of the electrodes. The measurements shown in figure 5.10 are the average of the arc velocity versus gas pressure, obtained over three readings.

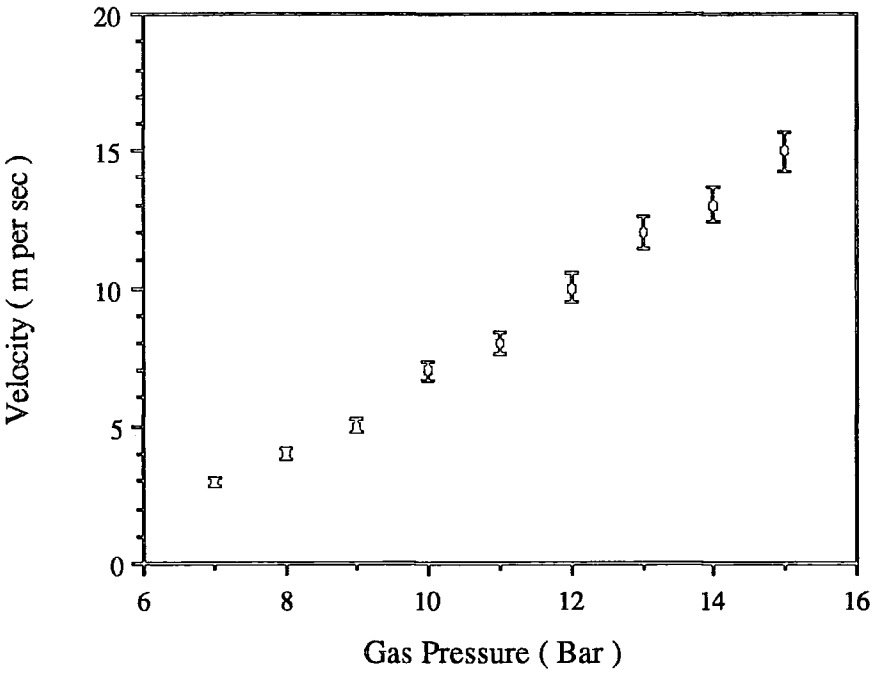

Figure 5.10. The average arc velocity as a function of the driving gas pressure.

5-4 ELECTRODE PREPARATION

Electrode polishing. To enable the microscopic structure of a crater to be observed in the electrode, the electrode has to be polished to a high quality optical finish (surface flatness of approximately 0.1 μm)so that the crater is not lost in the background of irregular features of the surface of an unpolished electrode. This is one of the most important parts of any damage experiment as it is very time consuming and determines the number of experiments that can be completed in an research programme. For these reasons it was imperative that a reliable polishing recipe was developed and that was not prohibitively time consuming. The electrodes were fabricated from oxygen free high conductivity (O.F.H.C.) copper, which displays the mechanical and chemical properties of normal copper. The ease with which soft metals can be scratched during a polishing process make them difficult to polish. Conventional forms of polishing, using progressively smaller particle grinding pastes, are not the most effective form of polishing to an optical finish. The surface is too soft to withstand the

polishing action of the grinding particles and therefore many stages of polishing, with progressively smaller particles, have to be used to reach a high degree of polish.

This approach to polishing the electrodes proved to be so time consuming that it was not viable for the damage experiments and an alternative recipe for polishing copper was sought. The method used to polish the electrodes to an optical quality finish in a reasonably short time period involved a two stage process of traditional mechanical and chemical polishing. The electrode was mounted on a polishing jig, a device that supports the electrode at the required angle for the duration of the polishing process. It was then polished with an aqueous suspension of 10 % 3 μm alumina powder on a polishing pad using a polishing machine (Logitech PM 10). This stage was used to grind the electrode surface to a flat finish with no large surface deformities, leaving the surface with a dull finish; this took approximately 8 hours. The sample was then polished with a suspension of 0.3 μm alumina particles in an aqueous solution of sodium hypochlorate, for approximately 10 minutes. This solution is a mild chemical etch of copper and the polishing action was to etch the surface of the electrode and remove the debris produced by the action the alumina particles. This stage was completed on a soft fibre pad, using a mechanical polishing machine. These materials are available commercially from Logitech Ltd Glasgow. The polished electrode had an optical quality finish, with features less than 0.1 μm. The process was completed in two working days which was an acceptable time scale for the project.

Characterization of the polished copper sample. The quality of the polishing of the sample was illustrated by the ability to distinguish the craters in surface of the polished electrodes, as shown in chapter six. The crystalline structure of the polished samples was investigated to find the grain structure of the samples. The grain size of samples that had been damaged were measured using the Stephenson and Barnes X ray technique, [5.13.] The grains in the copper were found to have an average grain size of 0.3 mm. This was confirmed by etching the surface of an undamaged polished sample with 10 % nitric acid and measuring the size of the grains

that were revealed with an optical microscope and a graticule. The work on grain size characterization was carried out by Ms. L.M. O'Tool as part of her honours degree.

Surface preparation. The polished copper surface was oxide free when removed from the polishing machine. This state would not persist unless elaborate steps were taken to keep the electrode from oxidizing agents. This was not possible as the experiments were conducted in air, therefore the degree of initial oxidation that occurred to the sample was controlled. All samples were removed from the polishing jig and re-polished, by hand, in the polishing suspension to remove oxidation that occurred in removing the sample from the polishing jig. The sample was washed in a cleaning agent (10 % Decon 90) rinsed in de-ionized water and dried. At this stage the sample was left for 30 minutes in atmospheric air to allow the natural 2.5 nm oxide layer to form on the surface. [5.4] The next stage of the preparation, or the final experiment was completed 30 minutes later; this simple step ensured that each sample started with the same oxidation state.

In some experiments is was necessary to grow an oxide layer of known morphology and thickness on the surface of the electrode. The desired oxide of copper was Copper I oxide, Cu_2O (Cuprous Oxide) and it was established that thin films of this could be grown at 200 ^oC in atmospheric air. [5.4, 5.5, 5.6 and 5.7.] Polished electrodes were placed in an oven at 200 ^oC, for from 1 to 75 minutes.

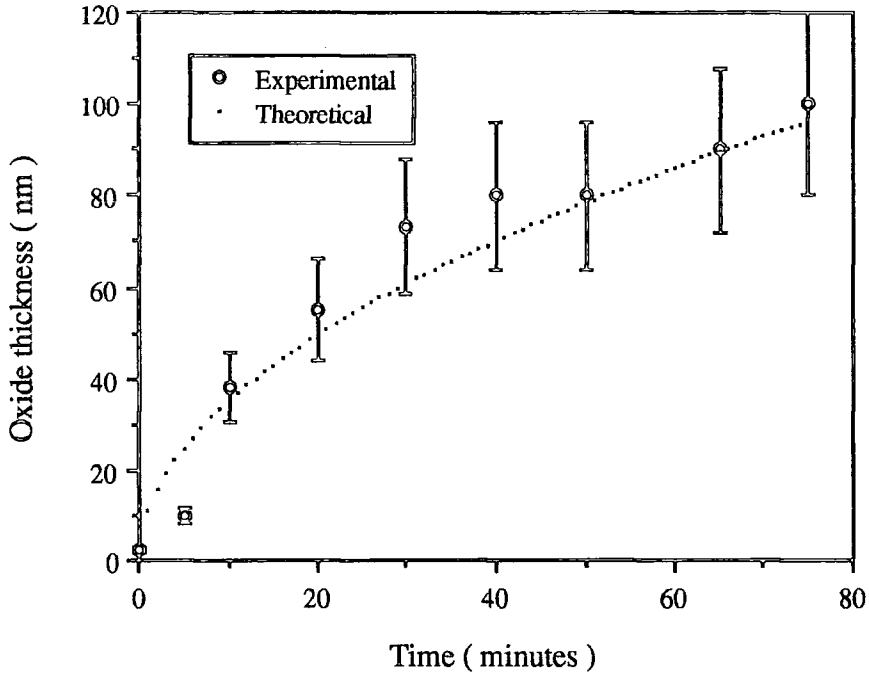

Figure 5.11. The oxide layer thickness calibration curve, for growth in air at 200 °C. The thickness of specially prepared samples was measured using a Talisurf.

The thickness of the oxide layers was established by several techniques. The interference colours of the oxide were used as a non-destructive check to ensure that the electrode being used in an experiment had the same thickness of oxide on the surface of other electrodes used in the experiment. Talisurfs and ellipsometers were used to establish a temperature versus thickness calibration chart that was used to determine the actual oxide thickness. These measurements usually resulted in the destruction of the sample for experimental purposes. The Talisurf required that a step in the oxide layer was fabricated. This was achieved by covering half the electrode in a protective film that prevented oxidation of the surface. The Talisurf was able to measure that thickness of the oxide with close agreement with expected results. Ellipsometer measurements were non destructive, but the time taken to complete measurements eliminated the electrode from further experiments. The oxide thickness calibration was compared to a theoretical curve generated by using a parabolic growth law. The thickness of oxide

layers are often found to follow a parabolic function with time and this was found to be true in this case, as illustrated by the theoretical curve, [5.4.]

The morphology of the films was investigated using the Laué x ray back reflection technique, to examine the lattice spacing of the oxide that was grown. Although the oxide films had a maximum thickness of 100 nm, a long exposure back reflection photograph could reveal the grain structure of the layer, if the more distinct copper rings were filtered out from the photograph. Figure 5.11 shows the calibration growth curve, the thickness values were taken from Talisurf measurements of polished electrodes where a step has been fabricated in the oxide layer. This graph was then used to gauge the thickness of oxide on electrodes that were used in the crater experiments. The work on x ray characterization of oxide layers was carried out by Mr. M Horne as part of his honours degree.

Electrical characterization of copper oxide. The oxide films were characterized in another way by examining the electrical characteristic of oxides prepared in the same way as the samples. For electrical characterization the samples need to be prepared on insulated substrates. This was achieved by first evaporating copper onto clean glass slides. The thickness of the oxide was controlled by timing the length of the evaporation and calculated the amount of material that would be deposited on the area of a sphere. The radius of the sphere is the distance of the sample from the evaporation boat. This theoretical thickness was compared to Talisurf measurement and was found to be highly accurate.

The sample was then oxidized, in air at 200 ^{o}C, for the time that corresponded to the thickness of the evaporated layer, and this gave thin copper oxide film of the same morphology as the sample oxide layers. The oxide layer could then be characterized electrically and the results compared with those known for Cu_2O thin films. A 100 nm thick oxide layer was found to be a p type semi conductor with a room temperature resistivity of $0.003 \pm 0.002\ \Omega^{-1}\ cm^{-1}$, when measured using Van der Pauw technique. The temperature dependency of the D.C. conductivity of the sample was measured which enabled the activation energy of the oxide layer to be calculated.

In the temperature range of 20 to 200 °C this was found to be 0.26 eV. The electrical characteristics could be compared with measurements made on single crystal Cu_2O in 1970 by Kuzel and Weichmann , [5.10.] They reported a value of the conductivity, as 0.001 Ω^{-1} cm^{-1}, which was dependent on the surface preparation and the detailed oxidation procedure. The difference in the room temperature conductivity value was due to the different preparation technique, but was within an acceptable range of values reported in the literature, [5.7.] The activation energy of 0.26 eV was found to be in agreement with the range of values found by Kuzel and Weichmann. The D.C. electrical characteristics of the thin films confirmed that the grown layers were Cu_2O. The work on D.C. electrical characterization was carried out by Mr. R. Jones as part of his honours degree.

5-5 DAMAGE EXPERIMENTS

Crater formation experiments. The electrodes were cleaned and smoothed by rubbing with a fine grade of emery paper. This removed any surface defects caused by the previous experiment and any residual oxide growth. The sample electrode was placed in the cathode electrode and secured with a 2 BA screw in the back of the sample electrode, see figure 5.2. The two electrodes were assembled and the strand of copper wire, placed between the electrodes at the ignition point. To ensure electrical contact between the ignition wire and the electrodes the wire was connected to the electrode terminals. The electrode assembly was placed in the relevant driving force apparatus and the power supply connected. The measurement instrumentation, consisting of current waveform apparatus, in all experiments, and voltage instrumentation, in some experiments was connected and the oscilloscope was armed. The oscilloscope was set to trigger on the current waveform signal and capture a 50 msec waveform. The power supply was set to deliver 90 amps to the arc in all damage experiments. The apparatus was activated by throwing the D.C. switch, the ignited arc was driven down the electrodes and blown out by the driving force. The power supply was switched off and disconnected from the electrode assembly. The oscilloscope signal was recorded and

the sample electrode removed for analysis. This technique was used to form craters on the surface of sample electrodes with differently prepared surfaces and with alternative driving forces. These experiments are described in the next paragraphs.

Magnetically driven arcs with 2.5 nm thick oxide sample electrodes. When no attempt to grow an oxide was made the polished sample electrodes were allowed to grow a natural 2.5 nm oxide layer. These electrodes were then used in with the crater formation experiment described in the previous paragraph. The arc was driven by a magnetic field, in the range of 30 to 500 mTesla, which produced an arc velocity, V_z, values between 3 to 80 ms^{-1}.

Magnetically driven arcs with sample electrodes with oxide layers 100 nm thick. Sample electrodes were polished and then placed in an oven at 200 ^oC in air for 75 minutes. This produced a 100 nm thick oxide layer and these were then used in a crater formation experiment in a velocity range of 30 to 70 ms^{-1}.

Magnetically driven arcs with sample electrodes with oxide layers 50 nm thick. Sample electrodes with a 50 nm thick oxide layer were also used in crater formation experiments in a velocity range of 30 to 70 ms^{-1}.

Aerodynamically driven arc damage experiments on sample electrodes with a 2.5 nm oxide layer. Crater formation experiments were completed on sample electrodes with a 2.5 nm layer oxide with an arc driven aerodynamically in the velocity range of 3 to 15 ms^{-1}.

Constant arc velocity experiments. The effect of a driving force on the formation of craters cannot be distinguished from the effect of velocity in the magnetically or aerodynamically driven experiments. If there is a second order effect due to the magnetic effect it will be hidden by the effect of the linear velocity. An experiment using an aerodynamically and magnetically driven arc, with a constant velocity of 7 ms^{-1} can be used to study the effect of magnetic field directly. The magnetic field was gradually increased, while the gas pressure was decreased to enable crater formation versus magnetic field to be studied. This experiment was completed using sample electrodes prepared with a 2.5 nm oxide layer.

5-6 CRATER DAMAGE ASSESSMENT

Damage assessment was carried out by examining a damaged polished electrode using various microscopy techniques. An area where the arc had traversed was carefully marked out in a 1 mm^2 area and then examined in a scanning electron microscope. A typical electron micrograph of a large crater formation contrasted against the polished sample surface, is shown in figure 5.12. This technique was used as it is very difficult to search for such small features over the comparatively large and featureless area of the polished sample electrode. The 1 mm^2 area was chosen as in a number of experiments it was found that the width of a typical arc track was 1 mm. The number of craters present in a 1 mm^2 area was sufficiently large for any experimental difference to be evident. The sample area was scanned for crater type features, by starting in one corner of the marked out area and moving across the area in the microscope keeping one feature of the previous frame in the next frame to ensure correct orientation in the area. The scan had to be completed in one session as this dead reckoning technique was only accurate if the original orientation of the sample was not changed. When craters appeared on the surface a micrograph of the features was taken, at a fixed magnification. The resulting photograph was then examined and the number of craters in the total area of the micrograph counted. The number of craters per unit area could then be established by examining several of these micrographs and averaging the results.

The samples were then examined optically and the percentage area of oxide removed by the arc was measured by over-laying a grid and estimating the number of squares in which the oxide had been removed. Unfortunately the samples degraded after a few days making craters more difficult to see as they became obscured by a fresh growth of oxide. Keeping the samples in an inert atmosphere increased their shelf life to a few weeks, but it was difficult to keep them indefinitely. For this reason it was necessary to make all crater observations at the time of the crater experiment to ensure the results are as accurate as possible.

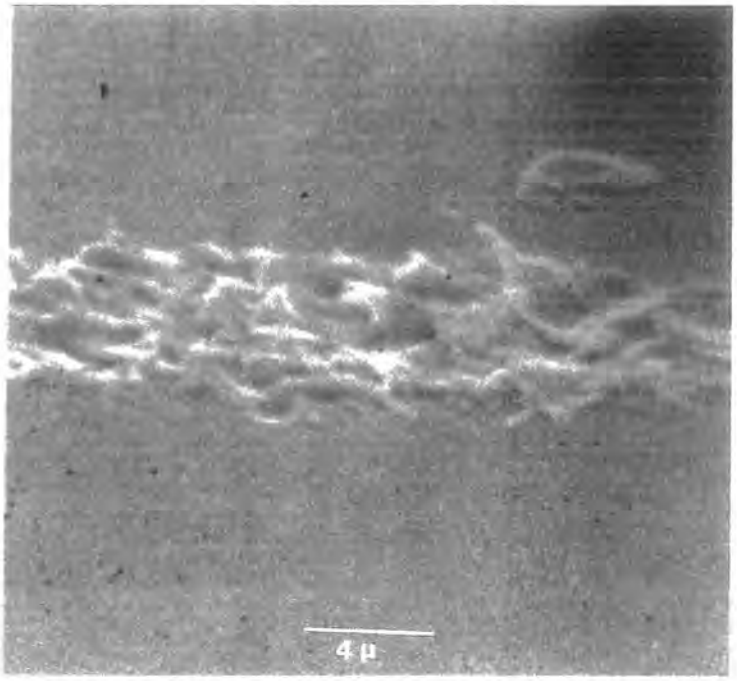

Figure 5.12. A crater formation on the surface of a polished sample electrode

With the area of damage on the electrode and the number of craters per unit area established, it was possible to estimate the total number of craters on the surface.The time at which the arc was present at each crater, assuming there was only one site active at any one time, could be calculated and this was known as the minimum site lifetime, $\tau*$. The duration of the arc over the sample, D_S, was calculated from the average velocity, V_Z and the number of craters in 1 mm^2 was scaled up to the whole of the damaged surface, N_T. The site lifetime, $\tau*$. was then calculated from

$$\tau* = \frac{D_S}{N_T}$$

equation 5.2

The maximum current density of the emission sites was calculated by finding the average diameter of the craters over the 1 mm^2 sample area and making the following assumptions; the craters were circular and so their area can be estimated and that the craters do not coexist.

5-7 SAFETY PRECAUTIONS

The arc experiments were potentially dangerous for a number of reasons and it was necessary to design the experiment with some safety devices included in the apparatus. The power supply presented a danger of electrocution and as the E.M.F was obtained from lead acid cells it was never possible to totally isolate the power supply making elaborate safety precautions necessary. Circuit breakers, in the form of fuses, were placed in the circuit in such a way as to isolate the end terminals from the battery terminals, and to serve as a back up against failure of the switch gear. This enabled connection to the electrodes to be completed with double insulation. It was also possible to totally isolate the load resistance from the batteries making current adjustment of the apparatus possible without risk of electric shock. The batteries were housed in a metal acid cabinet which was shut and secured before charging and discharging so that in the event of a battery exploding there would be no excessive spillage of acid. The cabinet ventilation was fan assisted to prevent any build up of explosive or poisonous gases when charging and discharging the batteries. The arc experiments were completed in an insulated cabinet, which was ventilated externally. The cabinet had perspex viewing windows which enabled observation of the experiment, but filtered out any U.V. radiation that might be emitted by the arc. The entire experiment was grounded via a high current earthing lead with all the apparatus, including the instrumentation, being earthed via the same route. All experimental activities were assessed for their C.O.S.H.H. risk and were carried out in such a way as to comply with C.O.S.H.H. regulations.

5-8 REFERENCES.

5.1 Mai H.H. Dimoff. K. Jean B. *Optical analysis of the interface between a moving arc and air at atmospheric pressure*. 1979 Jour. appl. Phys. Vol. 50 No. 6 p. 3944 to 3955.

5.2 Munz R.J. Private communication

5.3 Drouet M.G. Gruber S. *Dynamic Measurements of cathodic emission in a moving arc*. 1976 I.E.E.E. trans. on Power apparatus and systems. Vol PAS-95 No. 1 p. 105 to 112.

5.4 Kubaschewski O. Hopkins B.E. *Oxidation of metals and alloys*. 1962 London: Butterworths.

5.5 Hitchcock A.H, Guile A.E. *A scanning electron microscope study of the role of copper oxide layers on arc cathode erosion rates*. 1977 Jour. of Material science Vol. 12 p. 1095 to 1104.

5.6 Jian J. Mayer J.W. *Oxidation and reduction of copper oxide thin films*. 1992 Mat. Chem. Phys. Vol. 32 No. 1 p. 1 to 24.

5.7 Rakhshani A.E. *Preparation, characteristics and photovoltaic properties of cuprous oxide. A review*. 1986 Solid State Electronics Vol. 29 p. 7 to 17.

5.8 Guile A.E. Hitchcock A.H. *The effect of rotating arc velocity on copper cathode erosion*. 1974 J. Phys. D. Appl. Phys. Vol. 7 p. 597 to 606.

5.9 Guile A.E. Naylor K. A. 1968 Proc. I.E.E. Vol. 115 p. 335 to 342.

5.10 Kuzel R. Weichmann F.L., 1970 Jour, Appl. Phys. Vol 41 p. 271

5.11 Guile A.E. Hitchcock A.H. *The effect of rotating arc velocity on copper cathode erosion*. 1974 Jour. Phys D: Appl. Phys. vol. 7 p. 597 to 606.

5.12 Drouet M.G. Comments on " *Optical analysis of the interface between a moving arc and air at atmospheric pressure*. 1980 Jour. appl. Phys. Vol. 51 No. 7 p. 3963 to 3967.

5.13 Klug H.P. Alexander L.E. *X-ray diffraction procedures for polycrystalline and amorphous materials*. 1974 New York: Wiley.

CHAPTER 6 EXPERIMENTS ON ELECTRODES WITH 2.5 NM OXIDE LAYERS

6-1 INTRODUCTION

In this Chapter the results from experiments with sample electrodes with no deliberately grown oxide are shown. The preparation of sample electrodes was described in section 5.4 of chapter 5 and the experiments that were completed were briefly described in section 5.5. The results of this chapter are displayed in a graphical format, with some micrographs to illustrate crater formation on the surface of the electrodes.

6-2 MAGNETICALLY DRIVEN ARCS

In the initial experiment it was found to be possible to drive the arc along the electrodes with a minimum velocity of 30 ms^{-1}, as slower moving arcs were found to melt the electrode surface. Craters were formed by using the experiment described in section 5.5. of Chapter 5. The highest velocity at which the arc could be driven at was 80 ms^{-1}, and initially the crater formation on the surface of non oxidized electrodes was studied in the 35 to 80 ms^{-1} velocity range. This was done by varying the magnetic field so that the crater formation was not only a function of the arc velocity but also of the magnetic field.

The surface layer of the electrode was removed by the action of the arc in a track approximately 2 mm wide along the centre of the electrode. The arc track was positioned in the centre of the electrode deliberately by making the cathode electrode a vee shape The track was continuous in all 2.5 nm oxide layer electrodes examined with no evidence of a hopping motion or of multiple arc tracks. The stripped area was readily visible on the run-on and run-off electrodes, but was difficult to observe on the polished samples as the oxide layer on the surface was thin and and there was little difference in the colour of the stripped area and the remainder of the polished area, however it could seen by careful observation.

In the velocity range of 35 to 80 ms^{-1} the craters appeared relatively infrequently on the surface of the electrode. To observe craters on the surface of these samples the centre of the arc track was marked with a 1 mm^2 area (as described in section 5) as the surface of a polished electrode was essentially featureless except for the 1 μm^2 craters in the surface was difficult. High magnification was needed to reveal them. The scratched marking enabled the stripped area to be found when observing in the S.E.M. Micrographs of the craters are shown in figures 6.1, 6.2, 6.3 and 6.4. The micrographs show the emission spot of these sample electrodes to be small, with an average size of 0.7 μm diameter and an approximate depth of 0.5 μm.

The range of velocities was increased using the aerodynamically driven arc and experiments showed that destruction of the electrodes could be prevented by diligent experimental technique. It was found possible to drive 3 ms^{-1} arcs along the electrodes with the arc still remaining in crater mode emission. The arc velocity range was then increased to include these points. Figure 6.9 shows the inverse crater area density, which is the average area, in m^2, that each crater occupies, as opposed to the actual area of the crater. The lower the inverse crater area density the easier analysis becomes as the number of craters that are observed in a micrograph increases. Figures 6.5, 6.6, 6.7 and 6.8 are examples of the crater formation that occurs on slow moving arc samples. It is clear that the number of the craters is increased which makes analysis statistically more reliable and easier to complete.

The current density of the emission sites was determined by measuring the average size of the crates that appear in the micrographs. The potential for error in this measurement is large as the sample is placed in an electron microscope at an angle, to maximize the number of secondary electrons that are detected. There will be a geometrical difference in the apparent size on the (flat) micrograph compared to the actual size of the (angled) sample. This error was minimized because the arc track was formed on the centre line of the sample, and care was taken to position the electrode on the centre of the microscope stage. This was the axis of rotation, to angle the secondary electrons into the detector, therefore this would minimize the error in the measurement.

However the crater diameters are not absolute measurements, but every effort was made to keep the error consistent in the experiment. The average size was then used to calculate the current density of the emission site, J_* A cm^{-2}, assuming that each emission site exists singularly. Figure 6.10 shows J_* as a function of the arc velocity, the slower moving arcs have a higher J_* value. The high number of craters means that there is a large size distribution and the average size is smaller which causes a higher average current density.

Figure 6.11 shows the single emission site lifetime, τ_* in nanoseconds, as a function of the arc velocity. This was calculated using the technique described in section 5.6. The number density of the craters was established from the micrographs and the duration over the sample was calculated from the velocity of the arc. This results in a minimum lifetime value, which does not take into account for the number crater that exist simultaneously. There is a trend for the lifetime to decrease as the velocity is increased, with the lifetime decreasing from 8×10^{-9} to 1×10^{-10} s, but the reason for this may not be apparent at first. If the actual lifetime of an emission site τ_s is believed to be in the region of 1×10^{-7} to 1×10^{-9} s then the driving velocity would not be expected to change the site lifetime as the change in velocity from 3 to 80 ms^{-1} only changes the duration of the arc's passage over the sample electrode from 2.5 ms to 0.125 ms. A duration much longer than the lifetime would not be expected to be mirrored in the emission site lifetime.

There are two errors that can be made when making such an estimate that both increase as the sample velocity increases. The crater density (the average area each crater occupies) in figure 6.9 shows that as the velocity increases the crater density is lower. Any measurement of the number of craters formed on a sample will always involve a statistical approach to counting the number of craters, with error in the number of craters that are counted increasing the higher the crater density. The slower moving arcs result in a higher crater density which makes establishing the statistical number of craters more accurate than on faster moving arc samples. The other error is due to the nature of the emission sites. The small size of the craters and the relatively

enormous area in which they are formed (1×10^6 larger) necessitates a high magnification search for craters, which can result in some of the craters being missed. These two errors are illustrated by comparing figures 6.4 and 6.5 which are micrographs of fast and slow moving arcs respectfully as the micrograph of the faster moving arc shows a crater in the centre of a featureless polished sample. The slower moving arc, in contrast, shows numerous craters in the small area of a micrograph.

The first error can be expressed as a function of the crater density. The second error will be more dependent on the experimenter. It will depend on meticulousness of the search of the sample for craters and is not systematic, but the faster the arc velocity the higher the probability of error. The actual counting of craters from the micrograph is assumed to be completed with 95 % degree of certainty. The error in finding the craters on the sample is expressed as a linear function of the velocity. The constant is assumed to be $\pm$ 0.1. The sums of these errors are the total error in the measurement which are shown as the y coordinate error bars. The x coordinate error bars come from the velocity measurement error discussed in chapter 5. This shows how the slower moving arc experiments were more accurate than the faster moving experiments. However despite the error in the measurement, the site lifetime undoubtedly decreases as the velocity increases, in the velocity range of 3 to 15 ms^{-1}.

The reason for the lifetime decrease could be linked to the charge density emitted from each site, as shown in figure 6.12, calculated by multiplying the current density by the site lifetime. A slow moving arc will need to extract more charged particles per m^2 than a fast moving arc. The difference in the number of emission sites can be explained by this simple fact. Figure 6.13 shows the total charge of the arc, i.e. the total duration of the arc $\times$ the current of the arc as a function of the arc velocity. The comparison between figures 6.12 and 6.13 clearly shows the similarity between the trend of the two curves. The charge density of the emission sites appears to follow a reciprocal trend, which is directly comparable to the total arc charge, which is a reciprocal of the arc velocity.

In the velocity range of 35 to 80 ms^{-1} there is not such a clear trend with velocity, even allowing for the errors in the measurement, the lifetime is relatively uniform. The charge density does appear to follow the reciprocal trend, but this could be a distortion of the graph. Figure 6.12 was re-plotted in the velocity range of 30 to 80 ms^{-1} to reveal the trend in this region, as shown in figure 6.14. It is clear that there is no particular trend, but it is difficult to establish if this is due to the measurement being beyond the resolution of the experiment or if the lifetime has reached a minimum value. The resolution of the experiment is hard to determine because, in this velocity range it is a function of the crater area density not the lifetime itself. The ultimate resolution of the duration of an emission spot would occur when the number of craters on the surface was too numerous for them to be resolved by microscopy techniques, or when the emission site lifetime was too short to cause damage that could be detected. Figure 6.9 shows that the crater area density is not too small for the number of craters to be observed and examination of the micrographs reveals craters which are clearly detected in an electron microscope. The minimum resolution of the experiments in these terms has not been reached in these experiments.

If the lifetime is approaching a minimum value the crater area density would increase to a level where it would be impossible to find the micron sized craters in the large areas of undamaged electrode and the error in the measurement would increase. The crater area density would increase with arc velocity in the fashion that is suggested in figure 6.9. The crater density would not be expected to depend on the velocity in this way if there were not minimum resolution on the lifetime. This supposition is not supported by the theoretical calculations of the time taken to melt the crater spot, the only physical argument for a minimum lifetime value. The calculations completed in section 4.6 of Chapter 4 demonstrate that a maximum emission current density of 50×10^8 A cm^{-2} and a minimum lifetime of 1×10^{-10} seconds would provide sufficient charge input to melt the cathode spot. Unfortunately the experiments are inconclusive, but they suggest that there may be a minimum value of the product of $J*$ and $\tau*$.

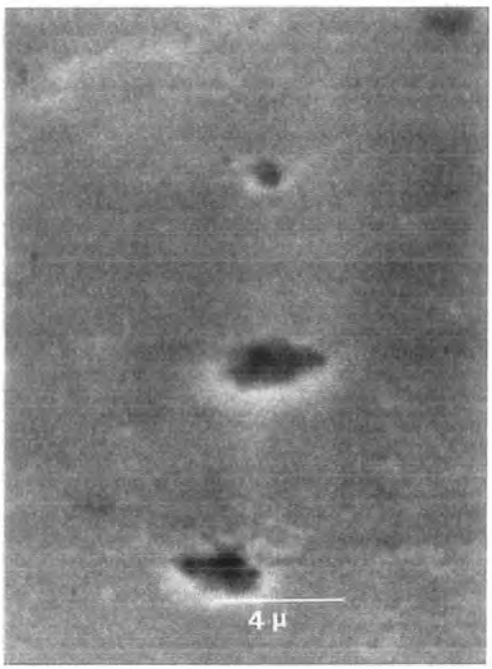

Figure 6.1. Crater formation on copper electrodes. Magnetically driven with an arc velocity 35 ms^{-1}.

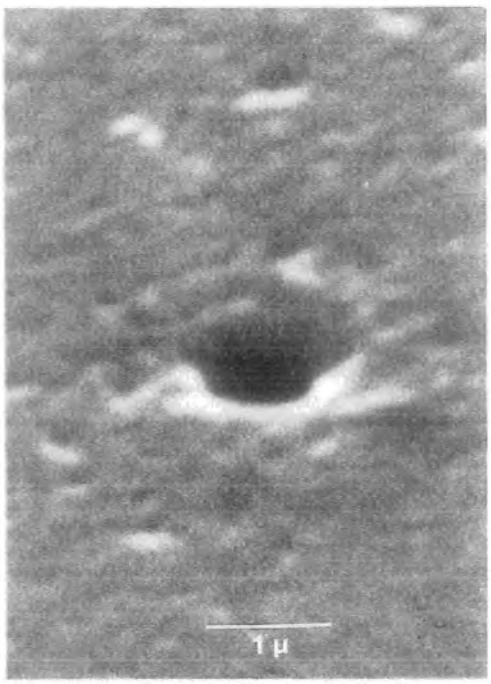

Figure 6.2. Crater formation on copper electrodes. Magnetically driven with an arc velocity 48 ms^{-1}.

Figure 6.3. Crater formation on copper electrodes. Magnetically driven with an arc velocity 70 ms^{-1}.

Figure 6.4. Crater formation on copper electrodes. Magnetically driven with an arc velocity 80 ms^{-1}.

Figure 6.5. Crater formation on copper electrodes. Magnetically driven with an arc velocity 4 ms^{-1}.

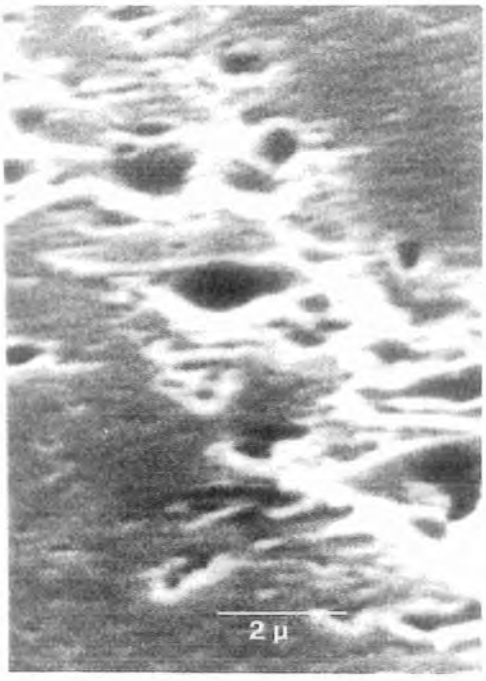

Figure 6.6. Crater formation on copper electrodes. Magnetically driven with an arc velocity 7 ms^{-1}.

Figure 6.7. Crater formation on copper electrodes. Magnetically driven with an arc velocity 10 ms^{-1}.

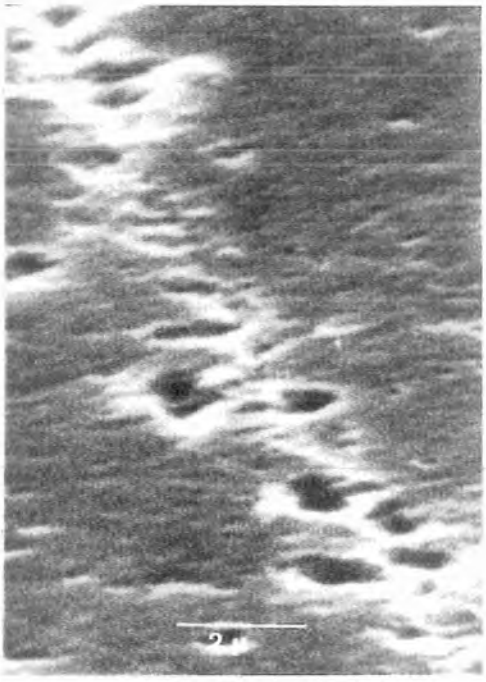

Figure 6.8. Crater formation on copper electrodes. Magnetically driven with an arc velocity 16 ms^{-1}.

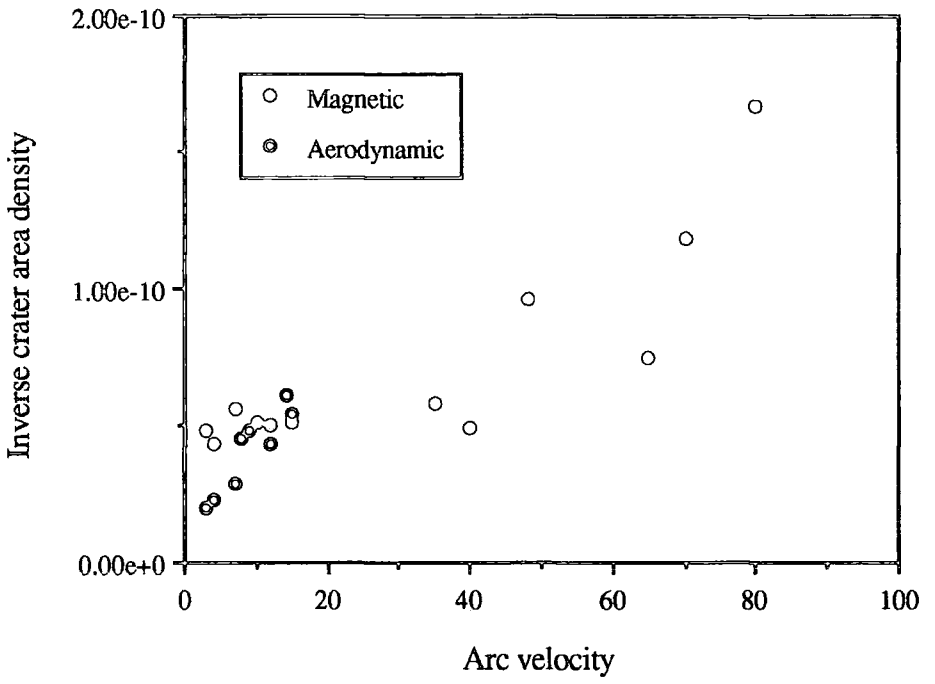

Figure 6.9. Inverse crater area density. The fraction of the damaged area each crater occupies in m^2 as a function of the arc velocity.

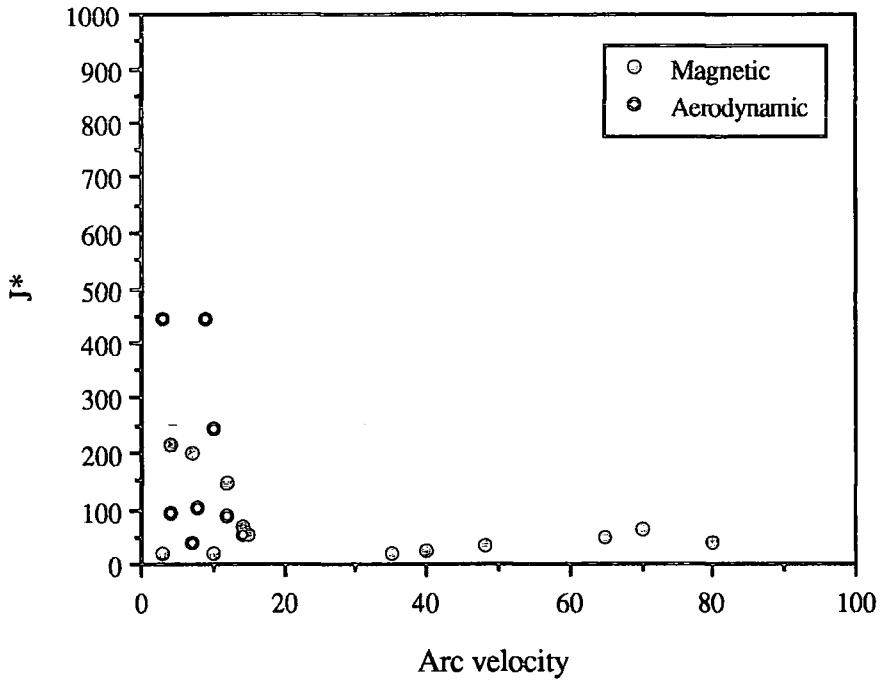

Figure 6.10. The single emission site current density, $J_* \times 10^8$ A cm^{-2}, versus arc velocity, ms^{-1}.

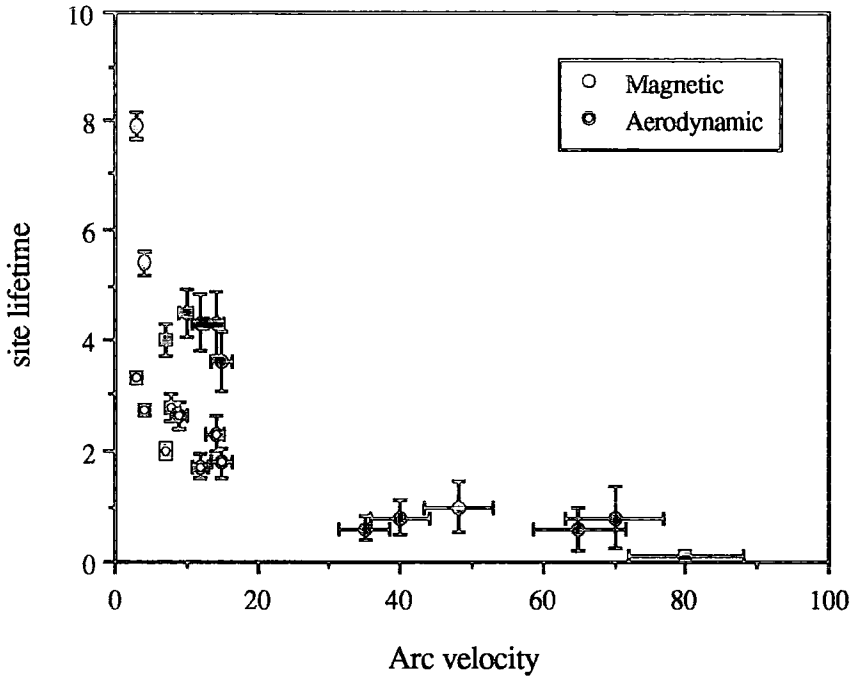

Figure 6.11. The single site emission site lifetime, $t*$, in nano seconds, versus the arc velocity,in ms^{-1}.

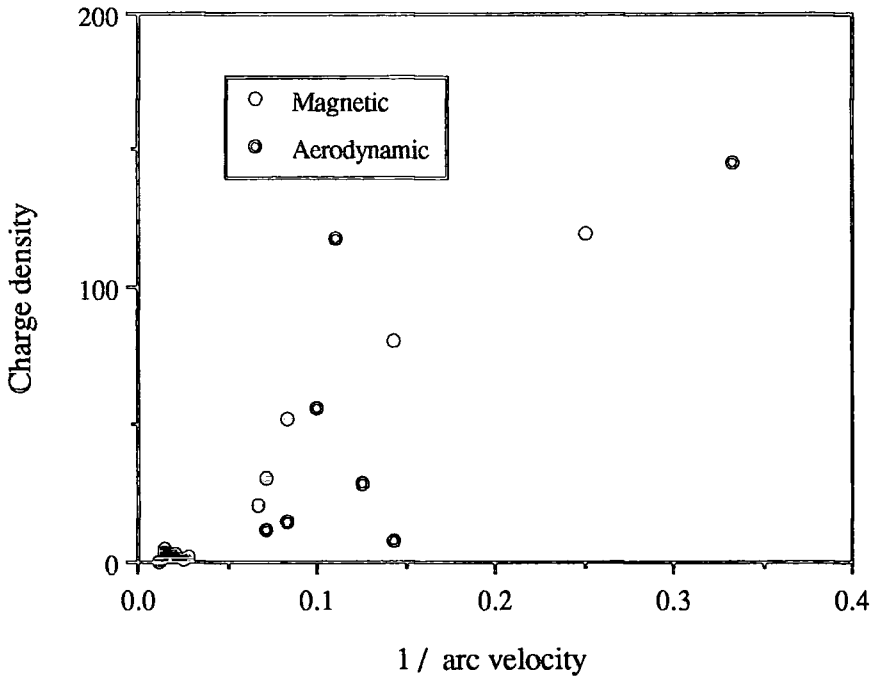

Figure 6.12. The charge density, ($\tau_* \times J_*$) in Coulombs cm^{-2}, versus reciprocal of the arc velocity.

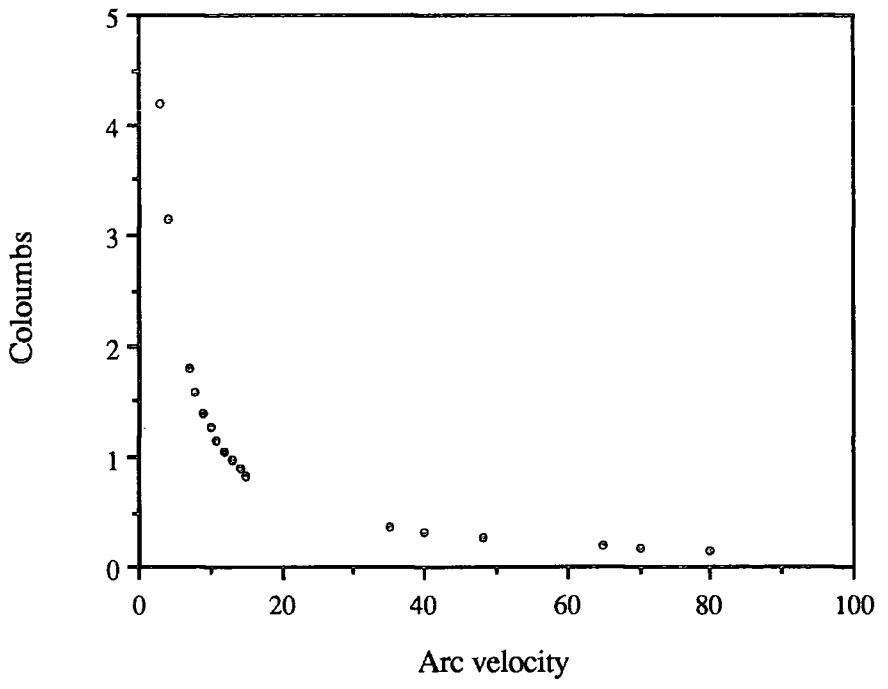

Figure 6.13. The total charge of the arc as a function of the velocity.

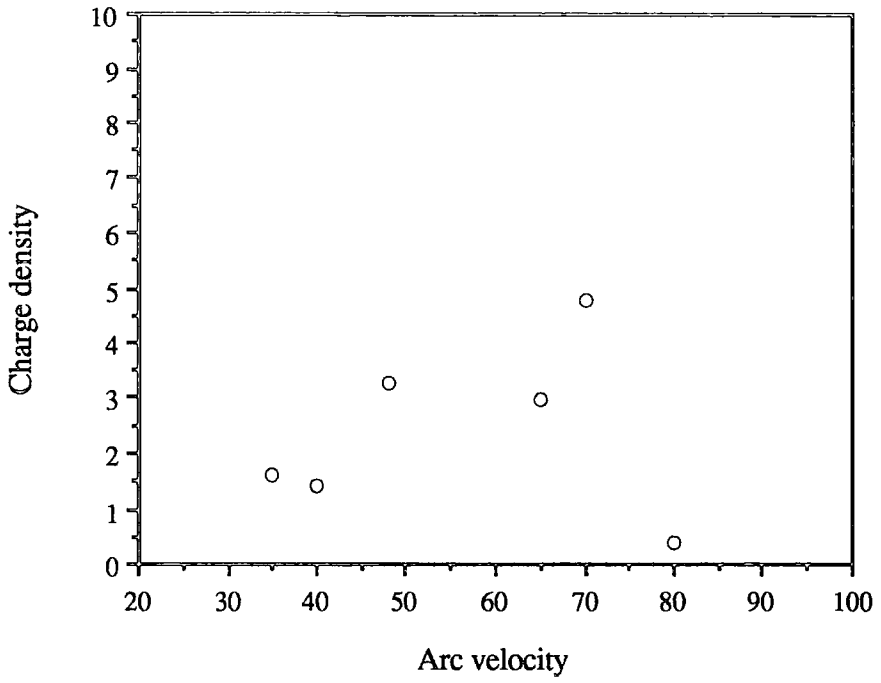

Figure 6.14 The charge density, ($\tau* \times J*$) in Coulombs cm^{-2}, versus arc velocity, in ms^{-1}, for the velocity range of 35 to 80 ms^{-1}.

Comparison with other data. Table 4.1, in Chapter 4 summarises previous experimental investigations of crater formation in various materials subjected to a heavy current overload emission mode. To make a comparison of the present experiments with other data it is necessary to convert the single emission site lifetime, $\tau*$ and current density $J*$ to actual values, τ_S, J_S. These values are interlinked as each is calculated assuming that one emission site sustains the arc. If two sites were to exist simultaneously then the actual site lifetime would be a factor of two larger than $\tau*$ and the current density half $J*$.

In table 6.1 the results of some comparable experimentation is shown, with the product of the lifetime and the current density calculated where possible. If the trend of the lifetime following a reciprocal relationship with velocity is correct then $\tau_S \times J_S$ values should compare favourably with the average value of $\tau* \times J*$. If the results of reference 6.4 is neglected then the average of the values of $\tau_S \times J_S$ in the table is 23

Coulombs. This average value ignores the trend of the lifetime with the current density, which can be seen in figure 6.12, where the charge density, $\tau_* \times J_*$, is plotted versus the arc velocity. The estimates of spot temperature and electric field at the cathode spot, made in Chapter 4, were based on a theoretical range of current densities from 1×10^7 A cm^{-2} to 1×10^9 A cm^{-2}. This range of current densities can be used to define a range of emission spot lifetimes, τ_s, by dividing the charge density in figure 6.12 by them. The maximum range of the lifetime is then 0.01 μs to 15 μs and the minimum range from 0.015 μs to 0.0001 μs. The range of the average lifetime value is from 2.4 μs to 0.024 μs over the arc velocity range of 3 to 80 ms^{-1}. These lifetimes are comparable with those listed in table 6.1 which means that the method and theoretical calculations used to make these estimates are valid.

Cathode material	Arc type	Current density A cm^{-2} (J_s)	Site lifetime nsec (τ_s)	$\tau_s \times J_s$	Reference number.
Cu	Pulsed discharge vacuum arc	10×10^7 9×10^7 8×10^7 8×10^7 8×10^7 9×10^7 8×10^7	2000 to 3000	200	6.2
Cu	single shot linearly driven air	2×10^7	100	2	6.3
Brass		5×10^6	100	0.5	
Cu	Single shot	1×10^{10}	1000	10000	6.4
Cu	single shot vacuum arc	1×10^8		-	6.5
Cu	50 A Arc.	3.5×10^8	30	10.5	6.6
	4.5 A stationary arc 12 nsec to 45 μsec duration.	4×10^8	1.3	0.52	

Cu	General	1×10^8		-	6.7
Cu	Vacuum arc	4.3×10^7		-	6.8
Cu	Vacuum arc	1×10^8	10	1	6.9
Cu	Vacuum spark discharge	1×10^8	5	0.5	6.10
Cu	Atmospheric discharge 45 A	3.5×10^8	50	17.5	6.11
Cu	Vacuum arcs 8 to 50 A magnetically driven	10×10^8	-	-	6.12
W	Vacuum arc at different electrode temperatures	1.2×10^7	25 to 50	0.3 to 0.6	6.13

Table 6.1. Comparison of experimental data.

6-3 AERODYNAMICALLY DRIVEN ARCS

It has been suggested by Guile [6.1] that the external applied magnetic field, B_Z, might have an effect on the formation and duration of emission sites. The previous investigations of crater formation used an external magnetic field to drive the arc along the electrodes and the effect of removing the external magnetic field has hitherto not been thoroughly investigated. The effect of a magnetic field can never be eliminated from arc experiments because the current flowing through the arc will generate an internal magnetic field. The arc can be driven by an aerodynamic force, a technique described in Chapter 5, to provide a direct comparison with the data obtained from the magnetically driven experiment. The arc could not be driven over the full range of arc velocities obtained in the magnetically driven experiments, but an overlap in velocities was achieved. The results of this experiment have been included in figures 6.9, 6.10, 6.11, and 6.12 as the points denoted by an 'o' symbol. Micrographs of the craters formed by an aerodynamically driven arc are shown in figures 6.15 to 6.19. It can be seen that the slow moving aerodynamically driven arcs produced damage on the surface of the sample electrode of the same nature as that formed by slow moving magnetically driven arcs. Figure 6.10 shows a wide spread of values for the current density, but the values obtained are of the same order of magnitude as those for magnetically driven arcs. The crater area density values illustrate the benefits of using slow moving arcs as the small area each crater occupies enables more accurate analysis. Corresponding to

this smaller area density the single emission site lifetime, τ_*, has a lower value comparable to those for magnetically driven arcs in the same velocity range, as illustrated by figure 6.11. The emission characteristics of the aerodynamically driven arcs did follow the same trend with velocity. The charge density does appear to follow a reciprocal trend with velocity, albeit less definitely than magnetically driven arc as illustrated by figure 6.9. When the comparison between the charge density measurements, in figure 6.12, are made it can be seen that the lifetime and current density of aerodynamically driven arcs are comparable with those found for magnetically driven arcs.

The experiment was not truly free from a magnetic field as there is a self generated magnetic field present in all arc experiments. The non ferrous electrodes minimize the effect as they are not magnetized by the passage of the arc. However Guile argues that the presence of a small external magnetic field alters the conduction mechanisms in the emission surface layers of the electrode and to test for such an alteration a further experiment was designed. The magnetic and aerodynamic driving forces were combined to drive the arc at a constant velocity of 17 ± 1 ms^{-1}. The gas pressure was reduced as the magnetic field was increased which enabled the crater formation versus magnetic field to be studied without any velocity effect being involved. Crater formation versus magnetic field was studied in a range of magnetic field from 38 to 130 mT. A small magnetic field was used because the effects suggested by Guile had been observed when 100 mT had been applied.

The single emission site current density for a constant velocity is shown in figure 6.20, calculated using the same technique as described in section 5.6. It shows that at a constant velocity the current density was constant as the magnetic field was increased, within the errors that are encountered in the experiment. There was no apparent fluctuation with the magnetic field. The single emission site lifetime, τ_* versus the magnetic field, shown in figure 6.21 illustrates that in these experiments the magnetic field did not have any effect on the emission characteristics of the arc with these sample electrodes. The uniformity of the results does illustrate the consistency of

the measurements. This experiment demonstrated conclusively that the magnetic field had no effect on the mechanism of crater formation on non oxidized electrodes.

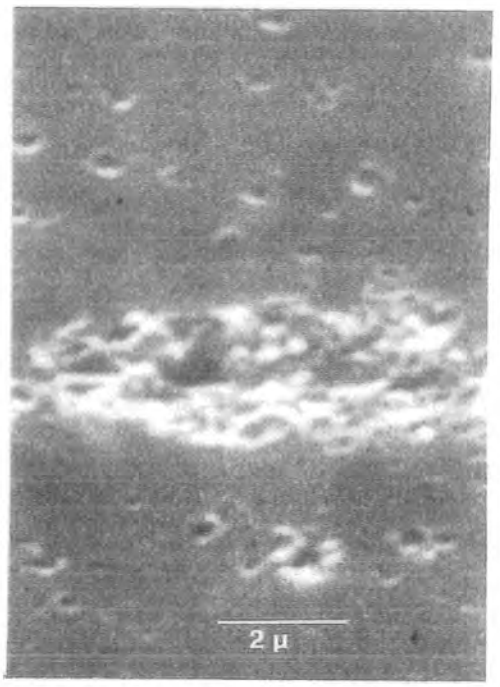

Figure 6.15. Crater formation on copper electrodes. Aerodynamically driven with an arc velocity 3 ms^{-1}.

Figure 6.16. Crater formation on copper electrodes. Aerodynamically driven with an arc velocity 8 ms^{-1}.

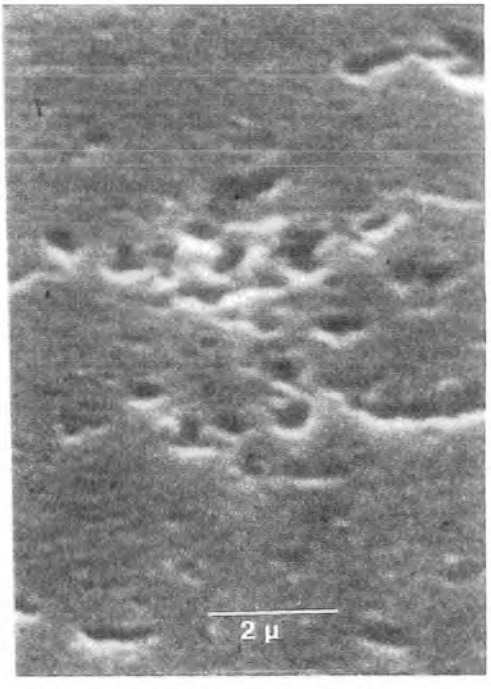

Figure 6.17. Crater formation on copper electrodes. Aerodynamically driven with an arc velocity 12 ms^{-1}.

Figure 6.18. Crater formation on copper electrodes. Aerodynamically driven with an arc velocity 16 ms^{-1}.

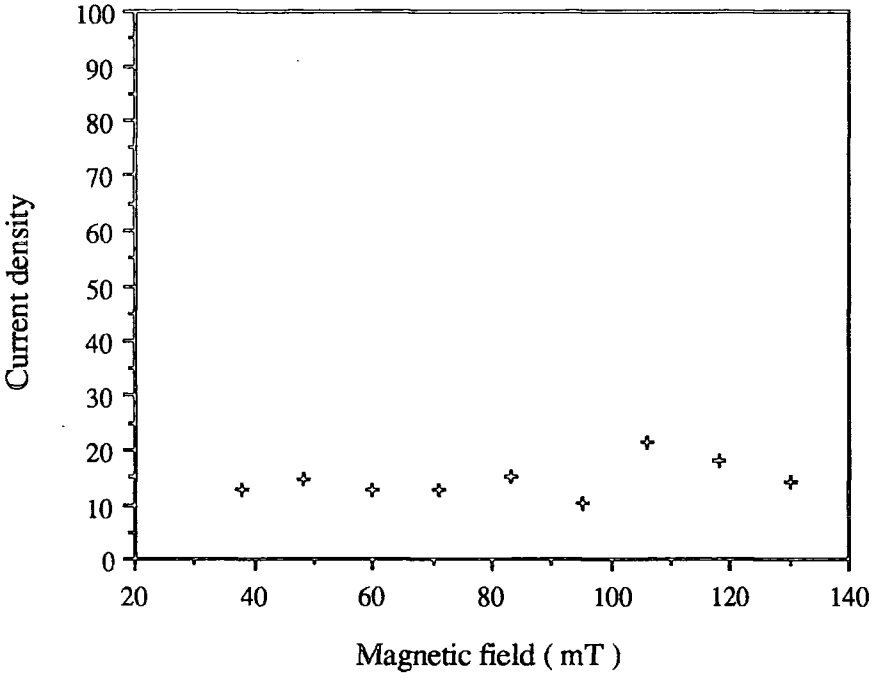

Figure 6.20. The single emission site current density, $J* \times 10^8$ A cm^{-1}, versus magnetic field, with a constant velocity of 17 ± 1 ms^{-1}.

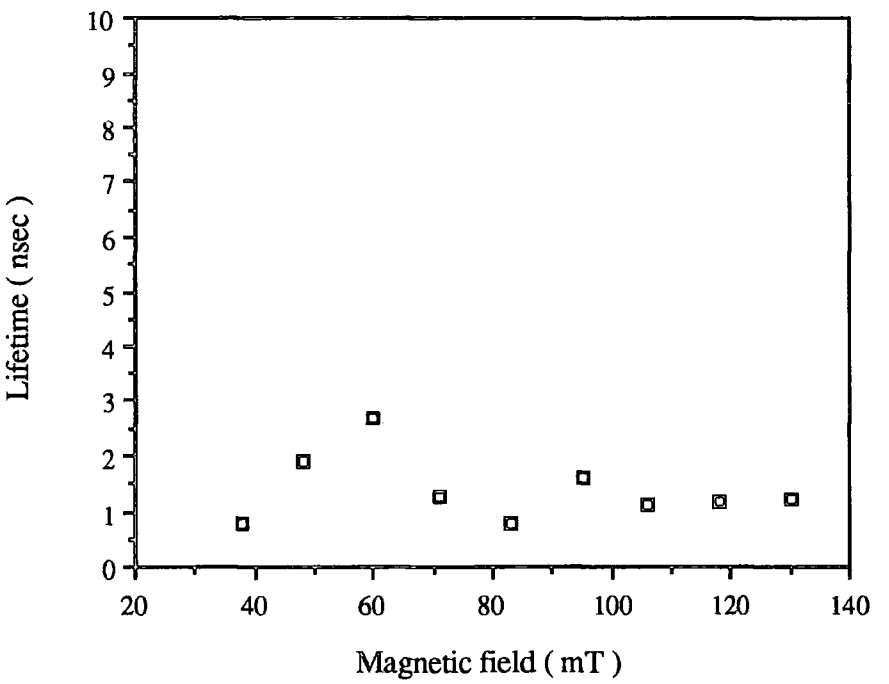

Figure 6.21. The single emission site lifetime, $t* \times 10^{-9}$ sec versus the magnetic field, with a constant arc velocity of 17 ± 1 ms^{-1}.

6-3 REFERENCES

6.1 Guile A.E Hitchcock A.H. *Effect of transverse magnetic field on erosion rate of cathodes of rotating arcs.* 1981 I.E.E. Proc. Vol. 128, Pt. A. No. 2 p. 117 to 122

6.2 Basharov R. Gavnlovskaya E.N. Malkin O.A. and Trekhov A. *An investigation of cathode spots in a pulsed discharge between parallel electrodes.* 1966 Sov. Phys.; Tech. Phys. 10 p. 1428

6.3 Sanger C.C. Secker P.E. *Arc cathode current density measurements.* 1971 J. Phys. D. Appl. Phys. Vol 4 p 1940 to 1945

6.4 Drouet M.G. Gruber S. *Dynamic Measurements of cathodic emission in a moving arc.* 1976 I.E.E.E. trans. on Power apparatus and systems. Vol PAS-95 No. 1 p. 105 to 112.

6.5 Daalder J.E. *Diameter and current density of single and multiple cathode discharges in a vacuum.* 1974 I.E.E.E. Trans. Power Apparatus and Systems PAS. 93 p. 1747 to 1757.

6.6 Daalder E. *Energy dissipation in the cathode of a vacuum arc.* 1977 J.Phys. D: Appl. Phys. Vol. 10 p.2225 to 2234

6.7 Daalder J.E. *A cathode spot model and its energy balance for metal vapour arcs.* 1978 J. Phys. D. Appl. Phys. Vol. 11 p. 1667 to 1682.

6.8 Holmes A.J.T. *A theoretical model of the mercury and copper vapour arcs.* 1974 J. Phys. D. Appl. Phys. Vol 7 p. 1412 to 1425.

6.9 Jüttner B. *Formation time and heating mechanism of arc cathode craters in vacuum.* 1981 J. Phys. D. Appl. Phys. Vol. 14 p. 1265 to 1275.

6.10 Hantche E. Jüttner B. Pucharov V.F. Rohrbeck W. Wolff H. *Erosion of metal cathodes by arcs and breakdowns in vacuum.* 1976 J. Phys. D. Appl. Phys. Vol. 9 p. 1771 to 1781.

6.11 Guile A.E. *Joule heating in emitting sites on various non-refractory arc cathodes.* Proc. I.E.E. Vol. 127 No. 7 P 452 to 457.

6.12 Jüttner B. Pursh H. Anders S. *On the current density at the cathode of vacuum arcs.* 1984 J. Phys. D. Appl. Phys. Vol. 17 L. 111 to 114.

6.13 Puchkarev V.F. Murzakeyer A.M. *Current density and the cathode spot lifetimes in a vacuum arc at threshold currents*. 1990 J. Phys. D. Appl. Phys. Vol. 23 p. 26 to 35.

CHAPTER 7 THICK OXIDE LAYERS

7-1 INTRODUCTION

The presence of an oxide layer on the electrode surface is believed to affect the way in which the emission sites of the arc are formed on the electrode. To investigate this a series of experiments were carried out using electrodes that had been deliberately under controlled conditions. The results were then compared with those obtained from electrodes with only a natural 2.5 nm oxide layer in order to try and elucidate the role played by the oxide coating.

The experiments were carried out in the 35 to 80 ms^{-1} arc velocity range, a procedure that was subsequently, when experimenting on non-oxidized samples, found to be less appropriate than using a slower velocity range. However the experiments were completed accurately and the collection of data was meticulous enough for sufficient information to be gathered to enable the analytical technique described in Chapter 5 to be undertaken, although the analysis was carried out at a much later stage. Oxide layers with thicknesses of 50 and 100 nm were examined in these experiments.

When an appreciable oxide layer was present on an electrode the damage resulting from the passage of an arc along the electrode was radically different, to that observed on non oxidized electrodes. The visible difference was the discontinuous motion of the arc across the electrodes. The electrode would hop from one stripped area on the electrode to another leaving a gap of up to 3 mm of unblemished oxide between arc tracks as described below.

7-2 ARC MOTION EXPERIMENTS

During the crater formation experiments the discontinuous motion of the oxide was noted and the experimental observations are summarized in Table 7.1. It was observed that as the linear motion was superimposed on the arc, the distance that the arc appeared to extend itself was fairly constant as a function of the velocity. This

suggested that the maximum length to which the column could be stretched was a function of the electrical characteristics and not the velocity of the arc.

The arc began to leave discontinuous tracks when the oxide layer exceeded about 20 nm thick. A continuous track was left on thinner oxides. Below 50 nm discontinuous motion was not always observed, but above 50 nm it was found to be prevalent at a constant velocity of 16 ms^{-1}. In the discontinuous mode there is no apparent switching of the arc current, the current waveform shows a continuous flow of charge. This would suggest a multitude of emission sites existing at any one time, because the arc appears to be able to hop from one stripped area to another without interruption of the charge flow.

Figure 7.1 shows a trace of the passage of an arc with the current voltage waveform (scaled to the same length.) (Unfortunately photographic representation of the arc track does not reveal the information in sufficient detail.) The rail electrode had a 70 nm oxide layer on the surface and the multiple arc tracks are the result of one arc passing along the electrode at 16 ms^{-1}. In table 7.1 the maximum distance that the arc jumped was 2.5 mm and in figure 7.1 the arc track showed a jump of approximately 1.5 mm. As the arc gap was 2.5 mm then the length of the arc could be extended, without the voltage distribution being adversely affected, to was 3.5 mm, assuming the arc connected by the shortest route.

It was apparent from the experiments with 2.5 nm oxide layers that the the arc removed the oxide layer from the surface of the electrode, but with a 2.5 nm layer the arc track was single and always continuous. The multiple tracks illustrated in figure 7.1 were not observed. Table 7.1 gives the percentage stripped area, which is the area of oxide that was stripped from a 150 mm^2 sample electrode. There was no detectable trend with velocity, but it is significant that with 2.5 nm oxide layers the arc track was approximately 8 % of the total area, with little variation whereas with thicker oxide layers the percentage stripped area varied considerably from 3.7 % to as much as 25 % in a seemingly random manner. This may have been due to the way in which the experiments were conducted rather than the actual nature of the oxide stripping.

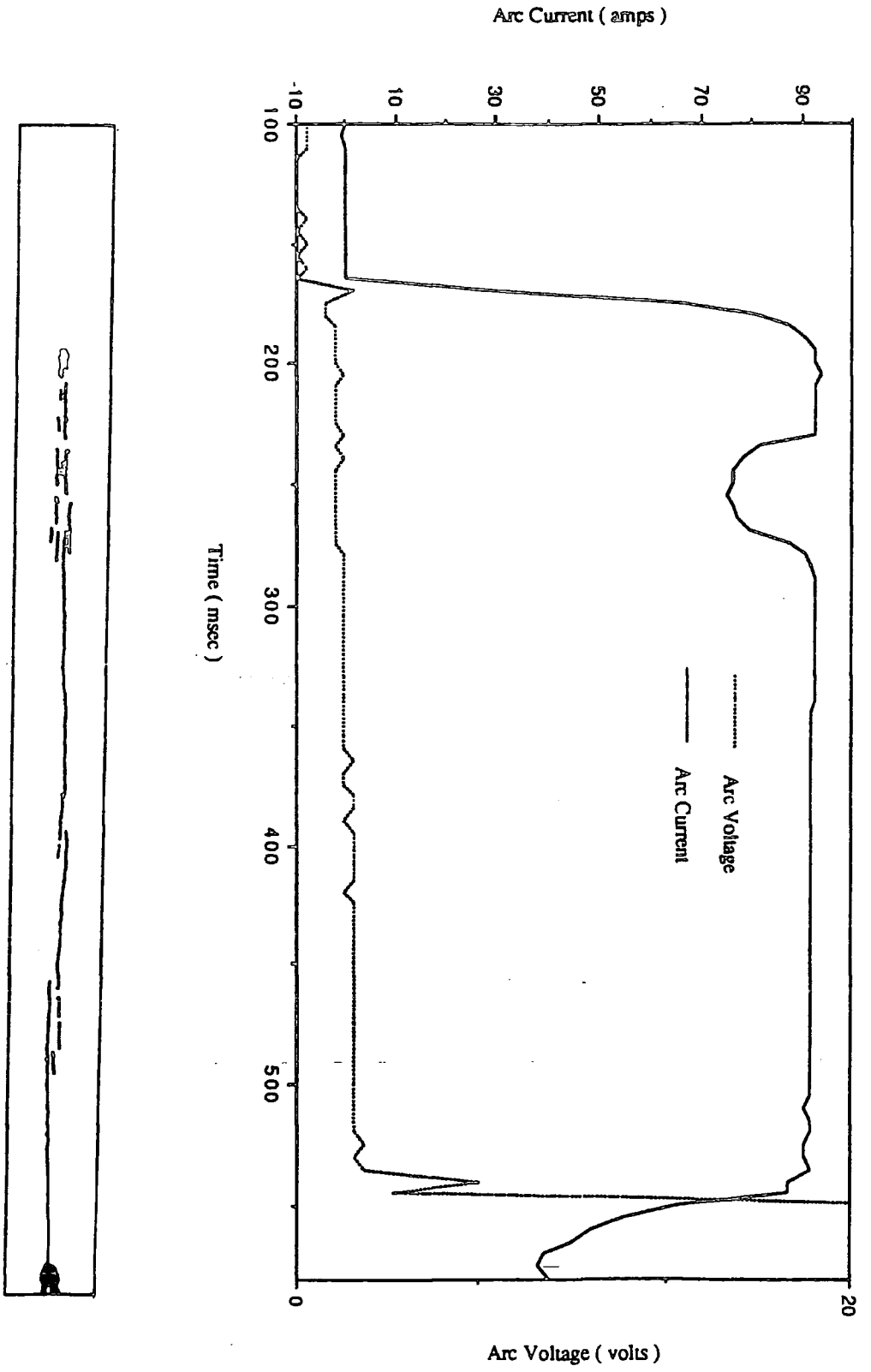

Figure 7.1. i. The The current voltage waveform of the arc, as it ran along a copper cathode with an 80 nm oxide layer on the surface.

ii. The trace of the macroscopic burn mark left by the arc. The trace shows multiple tracks and jumping of the arc along the electrode.

The study of the oxide layers listed in table 7.1 was completed on sample electrodes, placed in the cathode electrode apparatus described in chapter 5, but where the run-on and run-off electrodes did not have any deliberately grown oxide layer. The apparent random nature of the stripping may possibly have been caused by the sudden transition from a non-oxidized electrode to oxidized one.

Thickness of oxide (nm)	Arc velocity (ms^{-1})	Type of motion	percentage of stripped area	Maximum hop length (mm)
100	30	Discontinuous	5.5	1
100	37	Discontinuous	3.7	0.1
100	46	Discontinuous	11.1	1.1
100	49	continuous	16	-
100	49	Discontinuous	10	2
100	50	Discontinuous	16	0.3
100	52	Discontinuous	7	2.5
100	60	Discontinuous	15	1
100	70	Discontinuous	25	0.5
100	71	Discontinuous	11.1	0.3
100	74	Discontinuous	9.25	0.2
50	30	Discontinuous	14	1
50	38	Discontinuous	11	2
50	51	Discontinuous	10	0.5
50	55	continuous	5	-
50	57	Discontinuous	10	0.3
50	59	Discontinuous	9	1
50	65	Discontinuous	8	0.5

Table 7.1. The motion of the arc on thick oxide electrodes.

The problem of the sudden transfer from non oxidized electrode to the oxidized sample was overcome by using one piece electrodes with a uniform oxide film, to investigate the motion of the arc. This electrode arrangement was used to produce figure 7.1. ii, an arc with a velocity of 17 ms^{-1} was used to damage a one piece electrode with a progressively thicker oxide layer.

7-3 CRATER FORMATION STUDIES ON ELECTRODES WITH THICK OXIDE LAYERS

The arc tracks left on electrodes with oxidized surfaces were markedly different to those observed on non-oxidized samples. Multiple parallel tracks, separated by regions of undamaged electrode were seen, which confirms the observations made by Guile in his 1971 review paper, [7.2.] As described above the multiple tracks were associated with the removal of substantial areas of the oxide, leaving strips of the exposed copper. The difficulty in using the same analytical techniques as described in section 5.4 of chapter 5 was presented by the process of oxide stripping. The small features in the surface could have been caused by the growth process, as this involved heating the sample. The effect that heating the sample had was examined, by placing polished samples in furnaces with inert atmospheres at 200 ^{o}C and no change in the surface was found. However , it was more probable that the damage was attributable to the arc. The process of arc stripping can be seen in figures 7.2 - 7.9. These micrographs illustrate arcs removing a variety of thicknesses of oxide layers, leaving the electrodes with an indeterminate film , if any, of oxide with the crater formation occurring in this surface. The stripped area had a uniform dark grey colour, which was independent of the original thickness of the oxide. The uniform colour would suggest that the oxide was always removed down to the same thickness, but this could not be used to determine the thickness of this layer as it was beyond the resolution of an interference technique. Figure 7.6 shows that when examined closely some of the micrographs reveal features that could be interpreted as craters on the surface. This

enabled some of the sample electrodes to be analyzed using the technique described in chapter 5, to enable comparison with the results obtained in Chapter 6. However crater like formations could not be found for all the micrographs and these samples were not used in the lifetime measurements. The technique had to be modified slightly to account for the different size of stripped areas found on the sample electrodes. The total number of craters on the electrode was obtained by multiplying the number of craters per metre squared by the area of the stripped area on the electrode.

The principal results of the experiments show that the craters formed were smaller and more numerous, which resulted in an increased single emitting site current density, $J*$, and a shorter site lifetime, $\tau*$, when compared to non-oxidized samples. The thickness of the oxide layer apparently had little effect on these two parameters, as similar values were obtained for layers 50 and 100 nm thick.

The size of the craters is reflected in the inverse crater area density shown in figure 7.10, as each crater occupies a smaller area of the stripped electrode than was found in chapter 6. However completing the experiment at slower velocities would have been beneficial as a more heavily damaged electrode would have been easier to analyze with more certainty. Figure 7.11 shows the single emission site current density, $J* \times 10^8$ A cm^{-2}, versus the arc velocity, ms^{-1}. This was a reflection of the smaller average size of the features found on the samples. There does not appear to be a trend with the arc velocity, as was found for non oxidized electrodes in Chapter 6, although the small size of the craters made determining the actual size more uncertain than for non oxidized samples.

The single emission site lifetime, $\tau* \times 10^{-9}$ sec, as a function of velocity is shown in figure 7.12, for the velocity range of 30 to 75 ms^{-1} on electrodes with 50 and 100 nm oxide layers. The graph shows that there is little difference in the values obtained for 50 and 100 nm layers, but in comparison with the results for non oxidized electrodes lifetimes are an order of magnitude shorter.

Figure 7.2. Crater formation on copper electrodes, with a 100 nm oxide layer. Arc velocity 30 ms^{-1}.

Figure 7.3. Crater formation on copper electrodes, with a 100 nm oxide layer. Arc velocity 45 ms^{-1}.

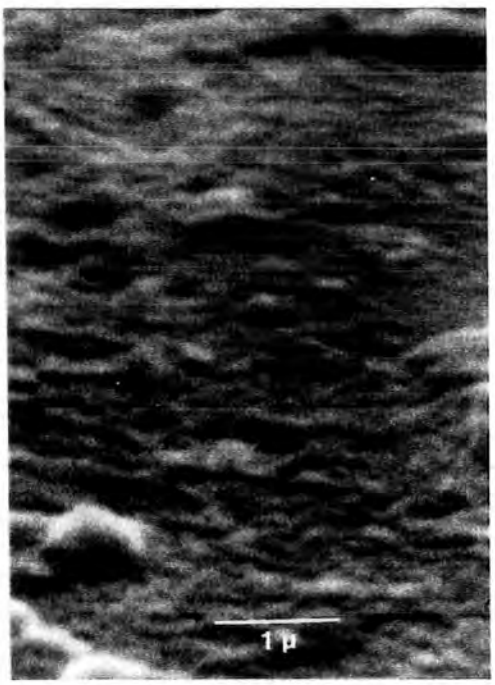

Figure 7.4. Crater formation on copper electrodes, with a 100 nm oxide layer. Arc velocity 70 ms^{-1}.

Figure 7.5. Crater formation on copper electrodes, with a 100 nm oxide layer. Arc velocity 80 ms^{-1}.

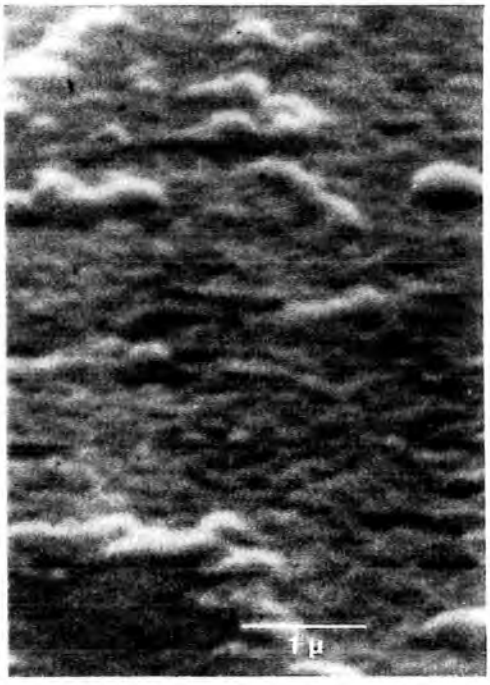

Figure 7.6. Crater formation on copper electrodes, with a 50 nm oxide layer. Arc velocity 30 ms^{-1}.

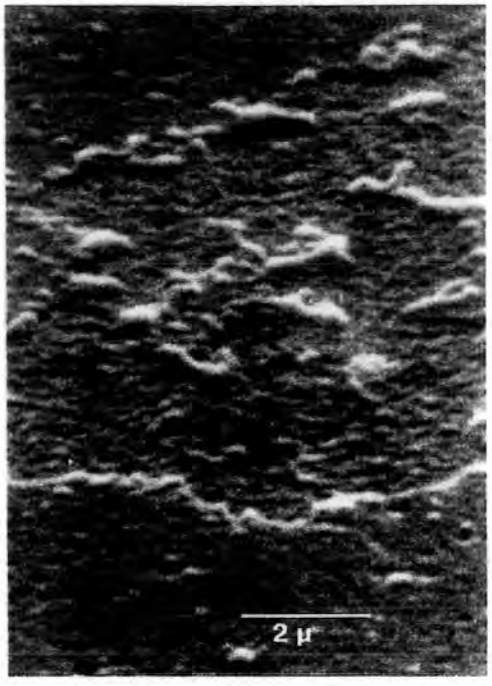

Figure 7.7. Crater formation on copper electrodes, with a 50 nm oxide layer. Arc velocity 40 ms^{-1}.

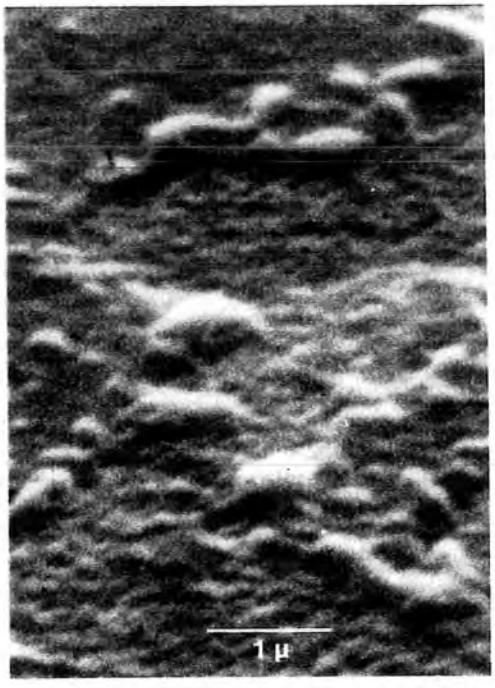

Figure 7.8. Crater formation on copper electrodes, with a 50 nm oxide layer. Arc velocity 52 ms^{-1}.

Figure 7.9. Crater formation on copper electrodes, with a 50 nm oxide layer. Arc velocity 60 ms^{-1}.

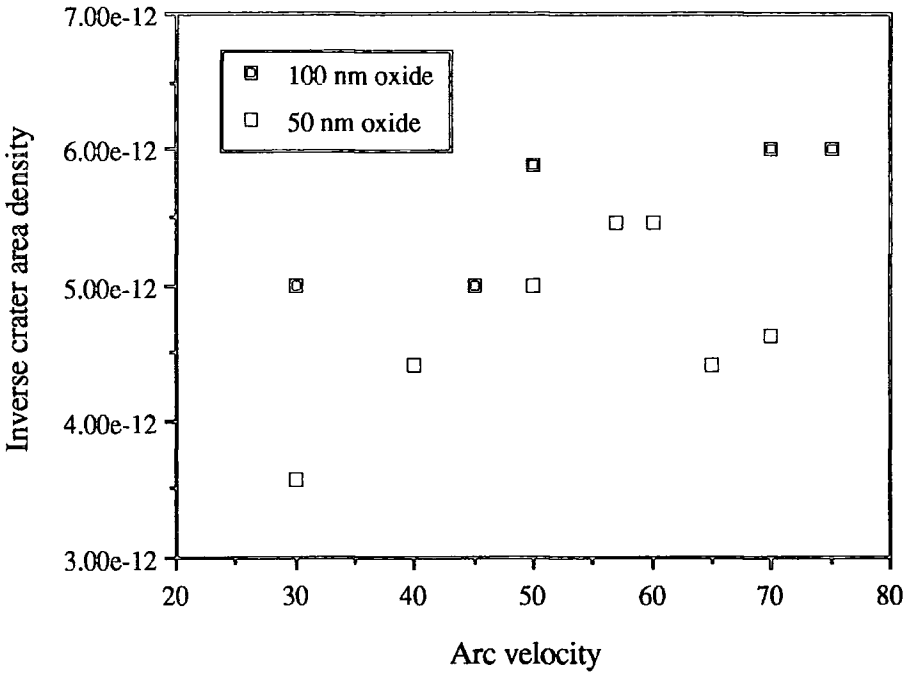

Figure 7.10. Inverse crater area density. the fraction of the damaged area each crater occupies in m^2, as a function of arc velocity.

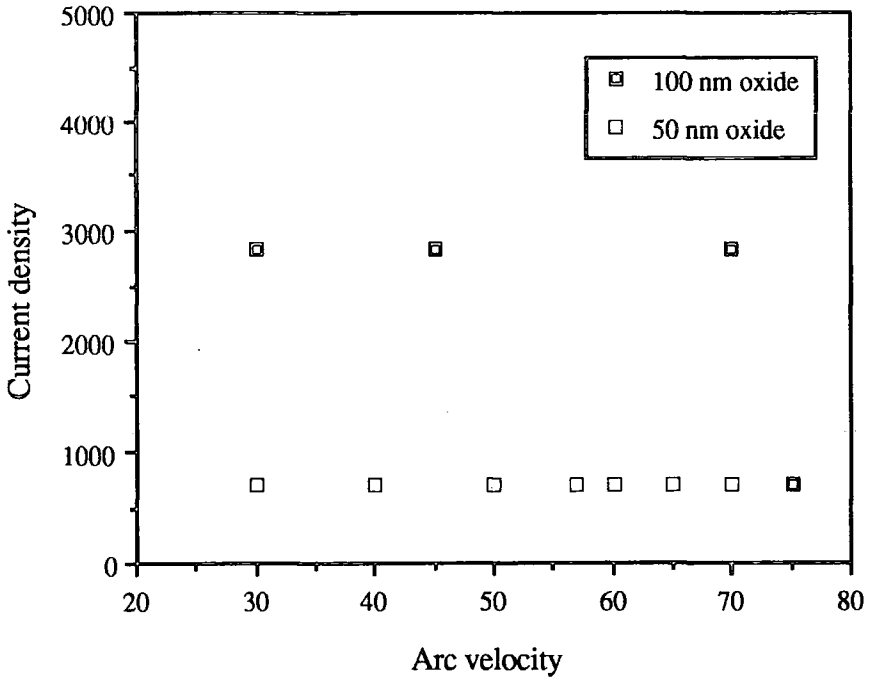

Figure 7.11. The single emission site current density, $J* \times 10^8$ A cm^{-2}, versus arc velocity, ms^{-1}.

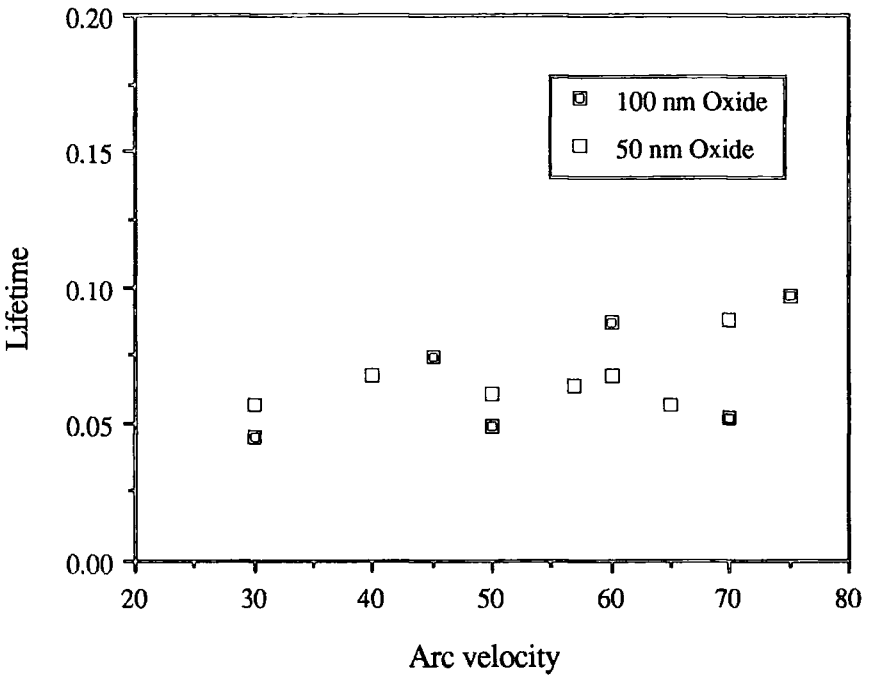

Figure 7.12. The single site emission site lifetime, $t*$, in nano seconds, versus the arc velocity, in ms^{-1}.

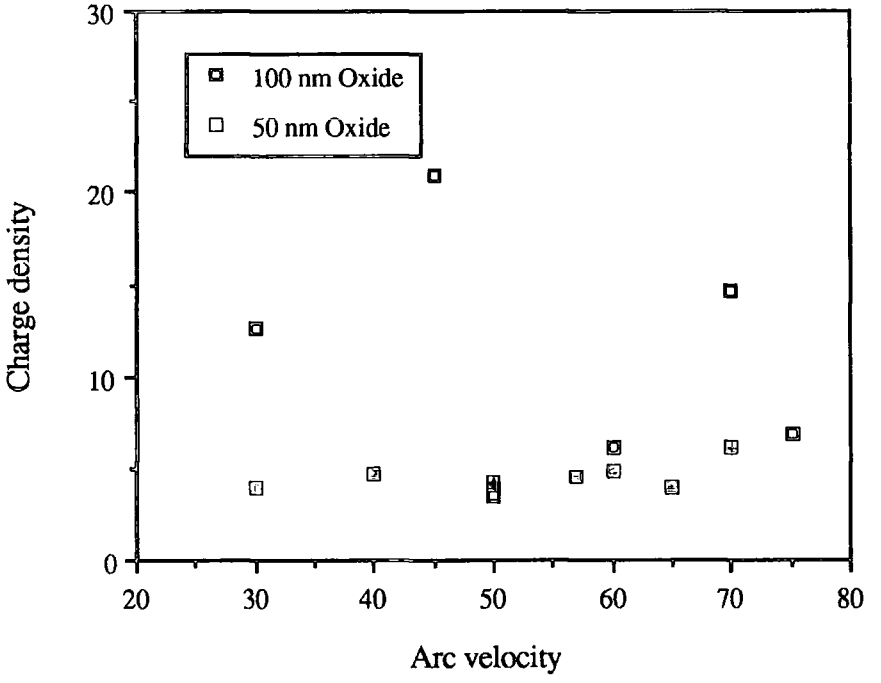

Figure 7.13. The charge density, ($\tau* \times J*$) in Coulombs cm^{-2}, versus arc velocity.

Cathode material	Arc type	Current density A cm^{-2} (J_S)	Site lifetime nsec (τ_S)	$\tau_S \times J_S$	Reference number.
Cu with					7.3
0.6 μm Oxide	Single shot	3.3×10^7	0.05	1.6×10^{-3}	
0.045 μm		3.3×10^7	2	0.066	
oxide					
Cu with	single shot 34 to 68 A.	5.7×10^7	0.36	0.021	7.4
100 nm oxide		to	to		
		6.5×10^8	4	2.6	
44 nm oxide	4.5 A stationary arc 12	2.95×10^8	3.3	0.97	7.5
100 nm	nsec to 45 μsec duration.	1.28×10^8	4.5	0.56	
225 nm		6.15×10^7	23	1.41	
340 nm		3.7×10^7	105	3.89	
Cu 100 nm oxide	Stationary 4.5 A arc	1.4×10^8	4.5	0.63	7.6
Cu	General	1×10^8	-	-	7.7
Cu	Atmospheric discharge	3.5×10^8	50	17.5	7.8
100 nm oxide	45 A	2.2×10^8	50	11	

Table 7.2. A summary of other experimental data.

Comparison with other data. Experimental studies of crater formation on electrodes with deliberately grown oxide layers appear relatively infrequently in the literature, probably due to the difficulties in reliably overcoming the difficulties of assessing crater formation. The role of oxidation on the performance of cathodes is more often investigated by measuring the erosion rates of cathodes used to sustain rotating arcs. [7.9 - 7.13.] The oxidation state of the cathode can be altered by the external parameters of the experiment such as arc rotation speed, electrode cooling rates, arc current and the discharge gas. These changes in the surface oxidation state of the electrode are then reflected in the erosion rate of the electrode. Few directly comparable experiments have been completed and these are summarized in table 7.2 . It is possible to compare the product, $J* \times \tau*$ with the values of $J_S \times \tau_S$ shown in table

7.2. As there is no evidence of a trend in the lifetime with the arc velocity the average values of the $J_* \times \tau_*$ product can be used to make the comparisons with the values found in table 7.2. The charge density plot, $J_* \times \tau_*$ versus arc velocity, is shown in figure 7.13. With the 100 nm oxide layer there is a wider spread of values, but the 50 nm results emphasize the apparent independence of the lifetime and current density with the arc velocity. The average value of the $J_* \times \tau_*$ for the 100 nm layer is 10 coulombs , for the 100 nm layer and 4 coulombs for the 50 nm layer. Using the same theoretical range of current density values as in Chapter 6 the lifetime, τ_*, is in the range of 1 μs to 0.01 μs for a 100 nm layer and 0.4 μs to 0.004 μs for a 50 nm layer.

7-4 AERODYNAMICALLY DRIVEN ARCS

Figure 7.9 is a micrograph of the damage caused when the arc is driven over an oxide coated electrode by an aerodynamic force rather than by magnetic field. This illustrates that there was little difference between it and the other micrographs of damage to the electrode. The uncertainty in establishing the damage caused by an arc to oxide coated electrodes made it difficult to assess the difference caused by the presence of an oxide layer. It has already been determined that in an external magnetic field does not alter the formation of craters on with no oxide layer. However it has been suggested that the external magnetic field altered the conduction of the oxide layer via a magneto resistance effect, [7.10.] This is a semiconductor effect involving the development of Landau levels in electron conduction bands in by the presence of large external magnetic fields at low temperatures. This phenomena is only seen in exotic materials when subjected to very large magnetic field. A control experiment where the the effect of an external magnetic field was studied on thin film oxide layers was devised. The fabrication of these oxide films and the conductivity experiments carried out on them are described in Chapter 5. This experiment was carried out by Mr R. Jones as part of his undergraduate degree under the supervision of the author. The conductivity of oxide films was measured over a range of magnetic fields. Even at the highest available magnetic field strength of 0.7 Tesla, far in excess of the fields used to

drive the arc, no change in the conductivity of the sample occurred. It was concluded, therefore that there was no evidence to suggest that the conductivity of the oxide layer was affected by the presence of an external magnetic field, (over the range of fields strengths to the present study.) This implies that the suggestion made in [7.10] that crater formation might be altered by an external magnetic field does not in fact seem to be the case.

7-5 REFERENCES

7.1 Guile A.E. *Processes ar arc cathode roots on non refractory metals having films of their own oxide*. Arc physics and weld pool behaviour International conference 1979, p. 79 to 86.

7.2 Guile A.E. *Arc electrode phenomena*. 1971 Proc. I.E.E., I.E.E. Reviews, Vol. 118, No. 9R, p. 1131 to 1154.

7.3 Guile A.E. *Model of emitting sites on non-refractory cathode arcs with thickish oxide films*. 1974 Proc. I.E.E. Vol. 121 No.12 p 1594.

7.4 Guile A.E. Hitchcock A.H. Barlow *Transition in size and number of emitting sites with increase in arc speed over copper cathodes*. 1977 Proc. I.E.E. Vol. 124 No. 4 p. 406 to 410.

7.5 Daalder E. *Energy dissipation in the cathode of a vacuum arc*. 1977 J. Phys. D: Appl. Phys. Vol. 10 p.2225 to 2234

7.6 Guile Hitchcock Stephens G.W. *Emitting site lifetimes , currents and current densities on arc cathodes with 100 nm thick copper oxide films*. 1977 Proc. I.E.E. Vol 124, No. 3, 273 to 276.

7.7 Daalder J.E. *A cathode spot model and its energy balance for metal vapour arcs*. 1978 J. Phys. D. Appl. Phys. Vol. 11 p. 1667 to 1682.

7.8 Guile A.E. *Joule heating in emitting sites on various non-refractory arc cathodes*. Proc. I.E.E. Vol. 127 No. 7 P 452 to 457.

7.9 Harry J.E. *The measurement of the erosion rate of the electrodes of an arc rotated by a transverse magnetic field*. 1969 Journal of Applied Physics. Vol. 40 No. 1 p. 265 to 270.

7.10 Guile A.E Hitchcock A.H. *Effect of transverse magnetic field on erosion rate of cathodes of rotating arcs*. 1981 I.E.E. Proc. Vol. 128, Pt. A. No. 2 p. 117 to 122

7.11 Szente R.N. Munz R.J. Drouet M.G. *Arc velocity and cathode erosion rates in a magnetically driven arc burning in nitrogen*. 1987 J. Phys. D: Appl. Phys. Vol. 212 p. 909 to 913.

7.12 Szente R.N. Munz R.J. Drouet M.G. *Cathode erosion in inert gases: the importance of electrode contamination.* 1989 Plasma chemistry and plasma processing Vol. 9 No. 1 p. 121 to 132.

7.13 Brown I.G. Shiraishi H. *Cathode erosion rates in vacuum arc discharges.* 1990 I.E.E.E. Trans. on Plasma Sci. Vol. PS-18 No. 1 p. 170 to 171.

CHAPTER 8 RESISTIVITY EFFECTS

8-1 INTRODUCTION

In the previous two chapters the results from electron erosion experiments have been catalogued. In this chapter an attempt will be made to collate these results and present a working model to describe the observations that have been collected. In the experiments crater formation was evident, crater formation being the consequence of electron emission. As such it should provide some indication of the mechanism by which electrons are emitted from distinct molten microscopic points on the surface.

The micrographs of damage caused by an arc are very similar to the ones previously reported in the literature [8.1, 8.2.] Crater formation on electrodes with 2.5 nm oxide natural layers were very similar to the type seen on copper electrodes damaged with atmospheric and low pressure high current arcs. [8.4] Oxide coated electrodes exhibited stripping of the oxide which has also been seen in other experimental investigations, [8.1.] Direct comparison, (where that has been possible) between micrographs of arc damage in other studies and those of this work has served to confirm the observations made in this research programme.

Comparison of the micrographs in Chapters 6 and 7 illustrates that the oxide layer had a considerable effect on emission crater characteristics. On oxide coated electrodes the craters were more numerous, which implied that for a given site lifetime, τ_s, of 1×10^{-9} sec there were approximately ten more active emission sites than on non-oxidized electrodes. In figure 8.1 the data is combined to compare the single site lifetime, $\tau*$ in nsec, for electrodes with three different thicknesses of oxide layer.

Variations in the nature of the motion of the arc, occur when a thick oxide is present. Oxide stripping features in both, but with very thin oxide coated electrodes the phenomena of hopping and multiple tracks was not observed. On an electrode with a separate thick oxide layer more of the oxide was removed over a wider area of the electrode although the colour of the stripped area indicated that the oxide was not completely removed and a thin uniform coating of oxide did remain. The colour of the

remaining layer was found to be the same in a series of experiments, which would suggest that the arc removed the oxide to the same depth, independently of the original oxide thickness.

These characteristics imply that the arc will be adapted to create the optimum, available conditions for electron emission from the cathode. Both the stripping down to a characteristic level and the discontinuous motion directly related to the presence of an oxide layer on the surface, and are clear indications of the critical importance of this layer on the emission process.

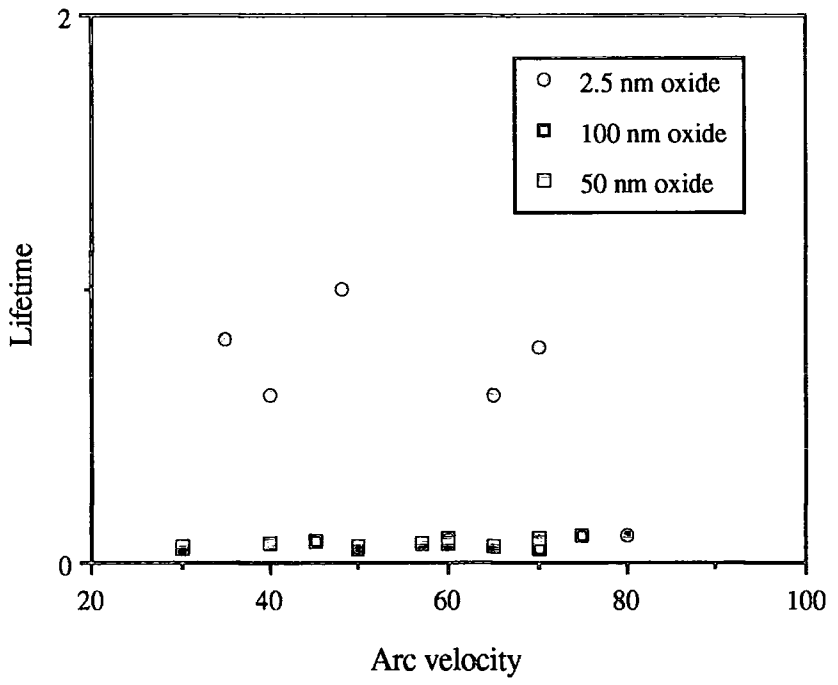

Figure 8.1. A comparison of 100, 50 and 2.5 nm oxide layer lifetime values obtained over the velocity range of 30 to 75 ms^{-1}.

In the theoretical calculation of Chapter 3 it was obvious that the estimates of current density made in Chapter 6 and Chapter 7 (based on a single emission site) are very large in the terms of the normal currents that can be extracted by thermionic, field and photoelectric emission. The electron current density from photoelectric emission

was so much lower that it was possible to discount this form of emission as playing a significant role in sustaining thermal arcs. In contrast it was shown that the explosive emission of electrons from vaporization of the electrode would be able to sustain the arc. This would obviously result in the electrode being melted at a rapid rate. It was shown in Chapter 4 that it is possible to extract current densities of the same order of magnitude as those estimated in Chapters 6 and 7 if the cathode temperature is high enough, but in the case of a non refractory or cold cathode the temperature required is much higher than the material can withstand. Crater structures, of the type seen in the micrographs of Chapter 6, suggests that such high temperatures could be achieved in small local areas. The micro spot attachment of the arc to these micron sized points enables the electrode material to be heated to very large temperatures, and because the heating time is so short the heating is very localized and the local pressure exerted by the positive ions enables the melted emission spot to reach boiling point. The local temperature coupled with the high electric field strength found in the cathode region can then be shown to be able to produce current densities of the same order of magnitude as the estimated values in Chapters 6 and 7. The efficiency of this localized heating of cathode spots minimizes the energy needed to extract electrons and hence the overall voltage of the electric arc can be much lower than in other forms of electric discharge.

8-2 RESISTANCE MEASURING EXPERIMENTS

If the resistance of the oxide has such an effect on the emission surface conditions of the plasma then it should be possible to observe the consequences in an experiment other than crater formation studies. In single shot experiments where the thickness of the oxide can be artificially controlled the effects of increasing oxide thickness should be reflected in measurement of arc resistance.

Using the experimental apparatus described in Chapter 5, single shot arcs were run over cathodes with oxide layers varying from 2.5 nm to 80 nm thick. The cathode electrode was modified into a continuous length of O.F.H.C. copper which was polished to a high surface flatness, 1 μm, and the oxide layer was grown on the

surface as described in Chapter 5. The arc was driven over the surface at a constant velocity of 30 ms^{-1} by an external magnetic field. The arc current and voltage waveforms were captured on a digital storage oscilloscope as described in Chapter 4. A typical waveform was shown in figure 7.1. The resistance of the arc was then calculated by dividing the arc voltage by the arc current, sampled at various times along the waveform and averaging over the duration of the arc.

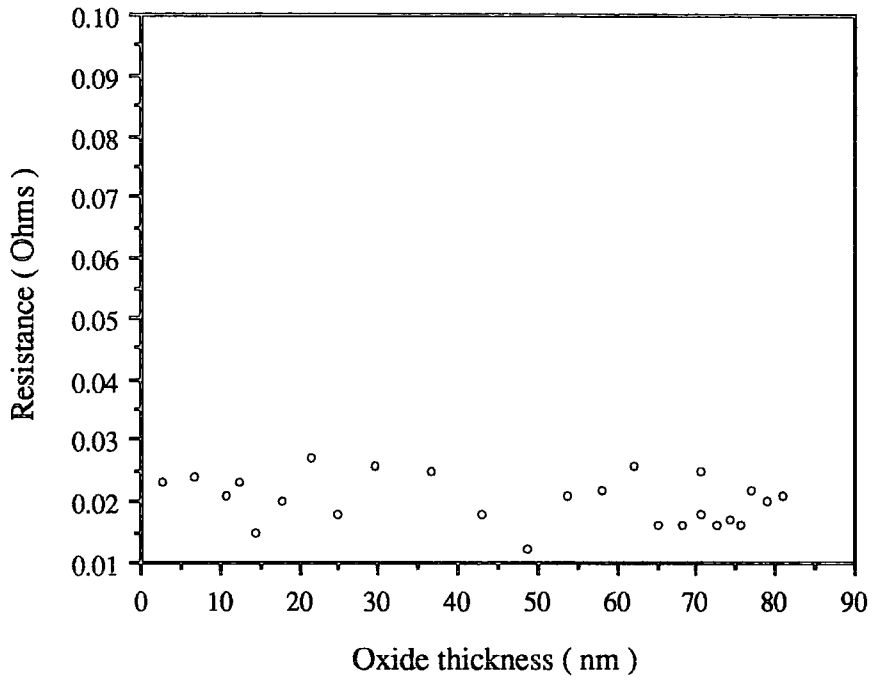

Figure 8.2. The resistance of the arc as a function of oxide thickness.

The resistance of the arc was measured in this way for a range of oxide thickness from 2.5 to 80 nm. The arc resistance has been plotted as a function of the oxide thickness, in figure 8.2. If the oxide layer is assumed to add a resistive layer to the emission surface, then it might be expected to be revealed by an increase in the overall resistance of the arc. However figure 8.2 shows no appreciable trend in the resistance of the arc due to the presence of an oxide layer.

An oxide layer 80 nm thick would be expected to add approximately 0.01 Ω to the resistance of the electrode. The resistance of the arc was measured to an accuracy of $\pm 2.5 \times 10^{-3}$ Ω therefore the additional resistance was within the capabilities of the apparatus. The measurement was made with a time constant of 0.1 msec, in which it was be hoped was sufficient to record any increase in the resistivity.

One possible explanation is that the oxide stripping in effect restored the surface to the oxide free condition prior to the arc / crater formation. If this were the case, then no additional resistance would be observed, and the following discussion lends support to this idea.

8-3 THE ROLE OF THE OXIDE LAYER

There are three candidates for the parameters that an oxide layer changes to alter crater formation: the overall work function, the electric field strength in the cathode region and the thermal characteristics of the emission spot. The work function of copper oxide is higher than that of copper, (4.7 compared to 4.45 eV [8.5, 8.15]) therefore any reduction in the work function would have to come about via a semiconductor effects such as that seen in oxide coated thermionic emitters. [8.5] It is believed that these phenomena can be discounted in crater mode emission, as they rely on the combination of energy levels forming a semiconductor type energy band structure. The current densities that are sustainable by crater mode emission are far in excess of the current densities that can be sustained by a semiconductor. The maximum current densities obtained from oxide cathodes, using rare earth metals are in the region of 1×10^3 A cm^{-2}, [8.5] Such small dimension semiconductor structures that would be found on the cathode would not be capable of withstanding the high currents observed to flow through them.

Alternatively if the oxide layer is assumed to be an insulating layer then the electric field strength in the cathode region could be increased. Charge on the surface of the oxide, which would result in an increase in the electric field and a subsequent change in the electron emission mechanism. In chapter 4 the electric field strength of

the cathode was discussed and was thought to be in the range of 2.5×10^6 V cm^{-1} to 1×10^7 V cm^{-1}, which is a very high electric field strength. The insulating properties of a 50 nm thick oxide layer would be broken down by the presence of such an electric field, making charge storage ineffective and unlikely as a method of increasing the electric field strength of the cathode region.

The oxide layer would also significantly affect the heating processes at the cathode. If it is assumed to be a conducting layer, with a high resistivity, then this will alter the Joule heating component of energy balance of the cathode. The energy balance of the cathode spot is discussed in chapter 4 where it was demonstrated that an emission site could be heated to melting point within the lifetime of that emission site, in a situation where the majority of the heating energy coming from positive ion bombardment, but an oxide layer would shift the emphasis to a Joule heating mechanism.

8-4 JOULE HEATING IN THE CATHODE SPOT

The calculation of heating in Chapter 4 assumed that the Joule heating was given by

$$P_j = 0.48\left(\frac{2}{3}\pi a^3\right)J_z^2\rho(t)$$

equation 8.1

where a is the diameter of the crater in metres, $\rho(t)$ is the temperature dependent resistivity in Ωm, J_z is the normal current density at the surface in A m^{-2} and p_j is the Joule heating in watts. It can be seen from equation 8.1 that the resistivity of the cathode material has a direct effect on the magnitude of the Joule heating. For a copper cathode the resistivity is temperature dependent and will increase as the temperature of the spot increases, therefore, for a given current, Joule heating will increase with temperature [8.6.] In Chapter 4 the Joule heating power was calculated using the average resistivity value of copper in the temperature range of 300 to 1400 K.

To demonstrate the effect of increasing the resistivity of the cathode spot an alternative method of calculating the cathode spot temperature to that used in Chapter 4 will be used. The temperature will be estimated by iteration of the Taylor expansion, of equation 8.2, where the resistivity value from the previous temperature is used to estimate the next temperature and iterating over a short period of time, using the routine,

$$\text{Temp} + \Delta\text{temp} = \Delta H \times P(\text{Temp})\ \Delta\text{time}$$

equation 8.2

where Temp is the temperature at time t and Temp + Δtemp is the temperature at time t + Δtime, ΔH is the specific heat capacity and P(temp) is the resistive power developed at temperature Temp, calculated using equation 8.1. The model is a relatively simple one in which heat losses are ignored, but it demonstrates the importance of the current density and the resistivity of the cathode material.

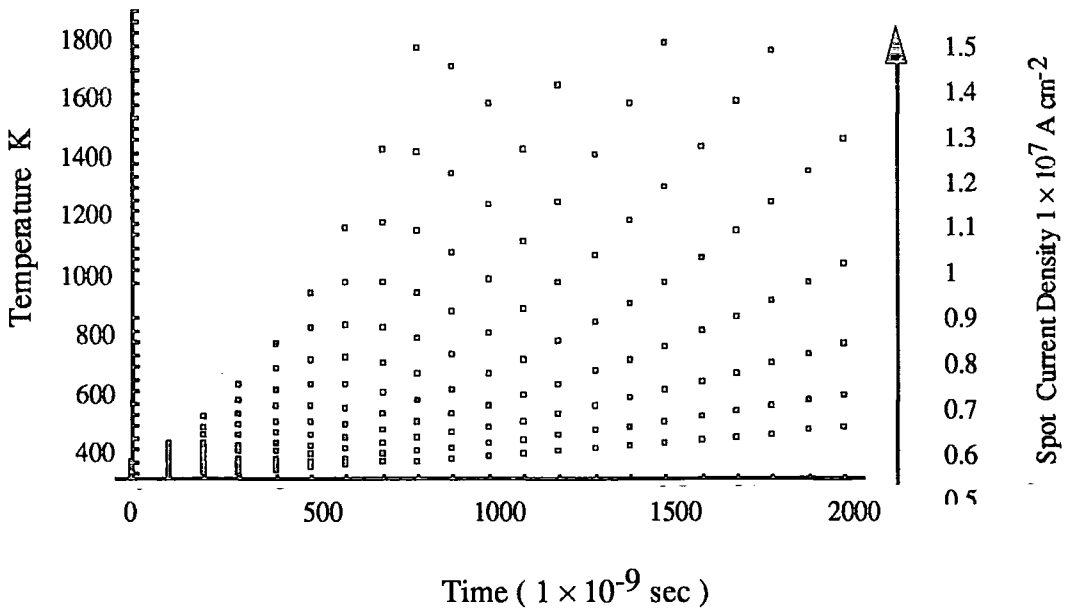

Figure 8.3. The cathode spot temperature dependency on the time and current density. Assuming the cathode spot resistivity is that of copper.

The iteration was carried out for a range of current density values from 0.5×10^7 to 1.5×10^7 A cm^{-2} underlining the importance of making accurate estimates of the current density. The results are shown in figure 8.3 for a copper electrode with no oxide layer The graph demonstrates that if the current density of the cathode spot is taken as 1×10^7 A cm^{-2} then the arc will melt an emission spot in approximately 1.5 μs. This would not be sufficient to melt the emission site within its lifetime, therefore Joule heating would not be responsible for melting the emission site.

The equivalent circuit model. The equivalent circuit represents that part of the arc from the start of the cathode voltage fall region [8.9], [8.10] to the copper electrode through any surface that emission takes place. The conduction mechanism in this region is assumed to be ohmic conduction. There is no strict physical precedence for this, however the assumption that Joule heating occurs at the cathode has been made by many workers Rich [8.8] Nemirovskii [8.12] Hare [8.7] Daalder [8.11] and the present model is then only an extension of this assumption to include oxide layer. The equivalent circuit is shown in figure 8.4.

The emission surface is divided into three regions: the current carrying electrode which is deemed to be at the potential of the negative terminal of the power supply, the copper emission surface, where Joule heating power is dissipated and has a temperature dependent resistance and the oxide layer which has a much higher resistivity than that for the copper region, but which is much thinner.

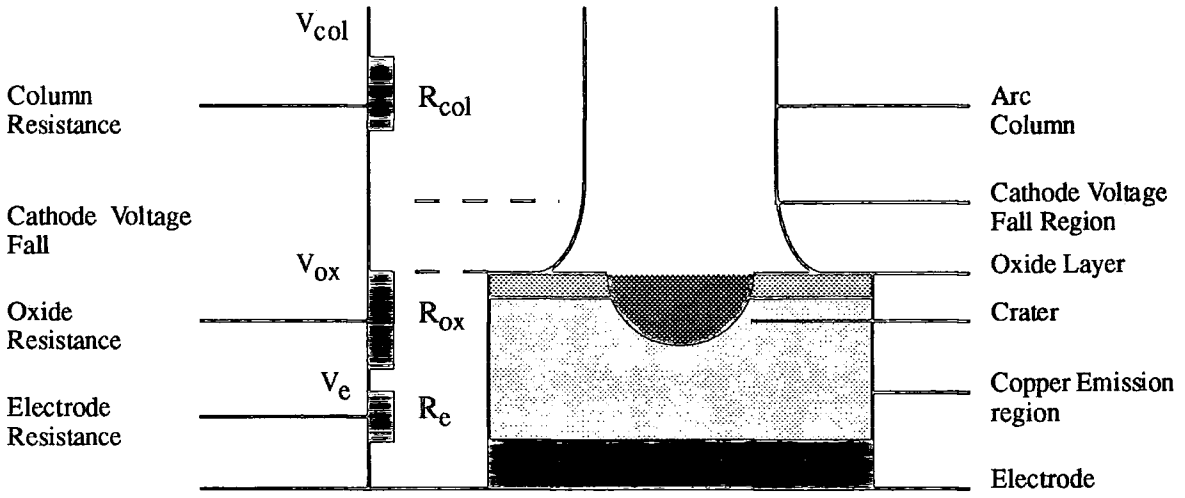

Figure 8.4. The Electrical Equivalent Circuit of the Emission.

For surface heating calculations the crater was assumed to be hemispherical with a diameter of 1 μm, and therefore it extends through the oxide layer and into the underlying copper. Consequently both the oxide and the copper would be expected to be involved in its formation. The equivalent circuit consists of two resistances shown in figure 8.4, the electrode resistance R_e, and the oxide resistance R_{ox}, both of which are temperature dependent, with the electrode resistance being negligible at low temperatures, hence the assumption to be made that the cool electrode is at the potential of the negative terminal of the power supply. The absolute values of these resistances depend on the dimensions of the cathode emission spot and the temperature, and it is therefore necessary to use the appropriate temperature dependence of the resistivity to model both the oxide layer and copper layers. For a metal the resistivity is dependent on the mobility of the carriers, as the number of carriers does not vary with temperature. The mobility of the carriers, μ, at low temperatures is proportional to T^{-5}. At higher temperatures, above the Deybe temperature, the mobility is inversely proportional to temperature [8.13.] The resistivity is therefore proportional to the temperature and can be represented by the equation

$$\rho = \rho_{r.t.} + A_o T$$

Equation 8.3

where A_o is a constant and $\rho_{r.t.}$ is the room temperature value of resistivity. For the oxide the dependence of resistivity on temperature is more complex for copper II oxide which is a semiconductor and the carrier concentration will be strongly temperature dependent. The resistivity temperature function would be determined by the type of carriers that were dominant at the temperature range used. However in the higher temperatures of concern here the oxide becomes essentially degenerate and hence behaves more like a metal. A sequence of trial experiments showed that the oxide follows a similar relationship to equation 8.3, but A_o has the value $3.1 \times 10^{-3}\ \Omega^{-1}\ cm^{-1}\ {}^{o}C^{-1}$ [8.14.]

The resistivity function of the total crater area is approximated by combining the resistivity of the copper layer with that of the oxide layer. In graph 8.5 the thickness of the oxide layer was assumed to be 10 nm compared to the crater diameter of 1 μm. Even though the oxide layer was only one hundredth of the total thickness the very high resistivity, 1×10^{12} larger, than that of copper, meaning that resistance of the copper was negligible compared to that of the oxide layer. The net resistivity for the dimensions of the crater can be calculated by adding the combined resistances and dividing by the cross sectional area of the crater.

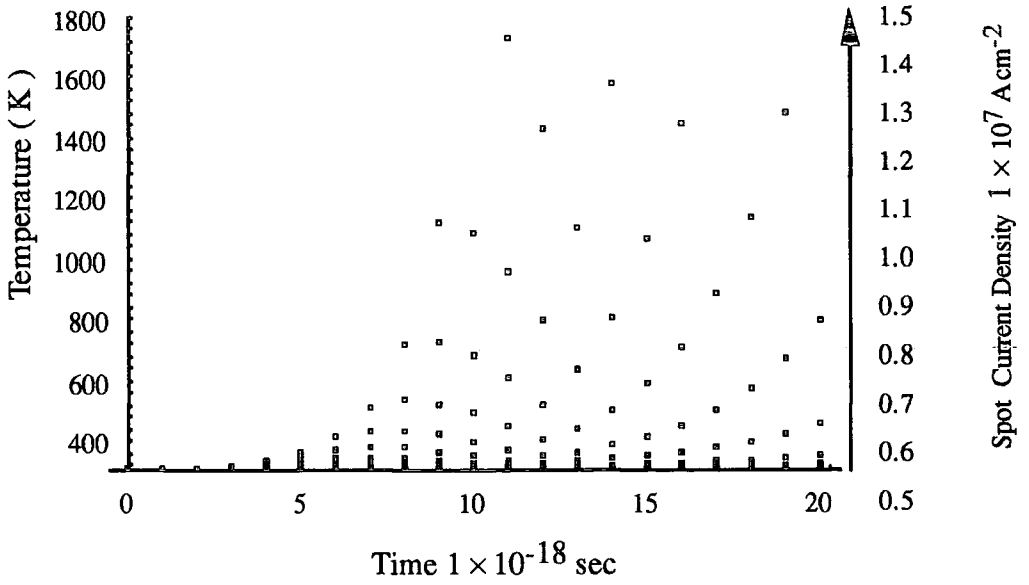

Figure 8.5 The temperature of the cathode spot as a function of time and cathode spot current.

This equivalent circuit of the copper / copper oxide interface is pivotal in these calculations,as it enables resistivity calculations and the effects on the cathode voltage fall to be modelled. Using equations 8.1 and 8.2 to assess the Joule heating of the cathode, together with the oxide layer increasing the resistivity, gave the results in figure 8.5.

Figure 8.5 shows clearly the effect a 10 nm layer has on heat that is dissipated in a cathode spot. If the current density was 1×10^7 A cm^{-2} the cathode spot would reach the melting point in approximately 1.5×10^{-18} sec. The emission spot then reaches the emission temperature in a much shorter time than the lifetime of the emission site, which would have implications on the mechanism of the emission process of the cathode when an oxide is present. The purpose of these calculation is to show how a thin oxide layer can have a dramatic effect on the Joule heating component of the arc and increase the energy dissipated in the emission spot. The extra thermal energy that is dissipated in the cathode spot implies that energy which will be reflected in the electric potential will be lost to the remainder of the arc. This redistribution of energy in the cathode spot can be modelled if a representation of the interaction between oxide layer and the electrode is assumed.

8-5 THERMALLY ENHANCED FIELD EMISSION

To utilize this model requires the use of the theories of emission mechanisms that include both temperature and electric field strength parameters as the equivalent circuit model will allow estimates of both of these to be made. The emission process mechanism involved is discussed in Chapter 3 and is given by

$$j_e = \frac{em}{2\pi^2\hbar^3}(kT)^2\left[\frac{F^{3/4}}{kT\sin[F^{3/4}/kT]}\right]\mathrm{Exp}\left[-\frac{\phi - \sqrt{F}}{kT}\right]$$

equation 8.4

where j_e is in A cm^{-2}, T is the temperature, Kelvin, $\mathbb{F}$ is the electric field strength, V cm^{-1}, ϕ is the work function, eV, k is Boltzmann's constant, e is the charge on an electron, $\hbar$ is Planck's constant divided by 2π and m is the mass of an electron. The relationship between the current density, the temperature and the electric field strength is illustrated in a general way in section 3.3. In the present section the effect of an oxide layer on these parameters can be examined, using the electrical equivalent circuit.

In section 4.7 of Chapter 4 the electric field strength and the temperature of the emission region of the cathode were discussed. The electric field is produced by the cathode voltage fall applied across the cathode fall region, and the changes in the cathode voltage fall resulting from the addition of an oxide layer can be predicted by calculating the voltage that would be dropped across the oxide layer and then removing this from the cathode voltage fall. The current density is also dependent on the emission spot temperature, but as the calculations in chapter 4 illustrate if a minimum current density of 1×10^7 A cm^{-2} is assumed then the energy available from positive ion bombardment is sufficient to raise the temperature to the boiling point of the electrode, assuming the electrode is made from a non refractory material. The upper limit on the temperature of the material is more likely to be caused by the properties of the material rather than the available energy in the cathode spot. The extra energy that is dissipated in the cathode region would enable the emission site to emit a lower current density, and still become molten within the observed lifetime of the site, enabling more craters to coexist, or for the emission site to have a shorter lifetime.

Figure 8.6 shows the current density as the oxide is varied from 2.5 nm to 1 μm thickness over the melting point to the boiling point of copper. The decrease in the electric field in the cathode region reduces the emission current. This is more clearly demonstrated in figure 8.6, where a constant emission site temperature of 2500 K is assumed and the theoretical oxide thickness is decreased from 1 μm to zero. The emission current density is approximately trebled by the removal of the oxide layer, with the electric field strength being calculated using the equivalent circuit model.

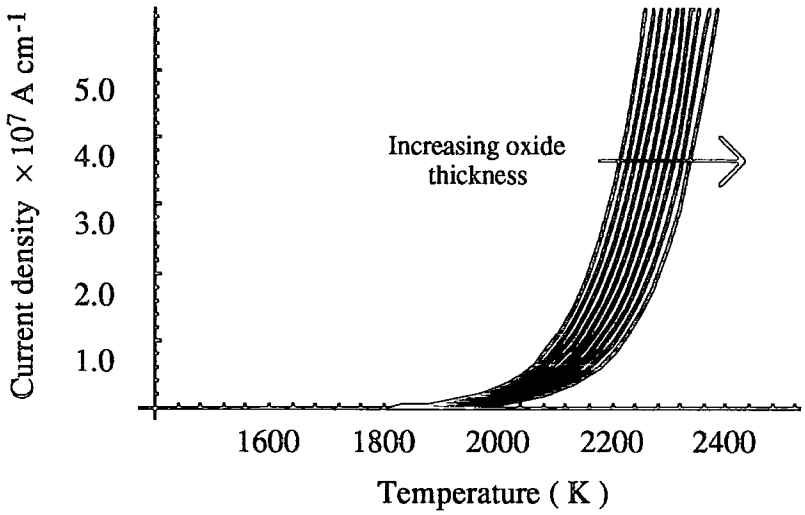

Figure 8.6. The predicted fall in the current density as a function of the emission site temperature as the electric field decreases as the oxide layer is increased from 0 to 1 μm thickness.

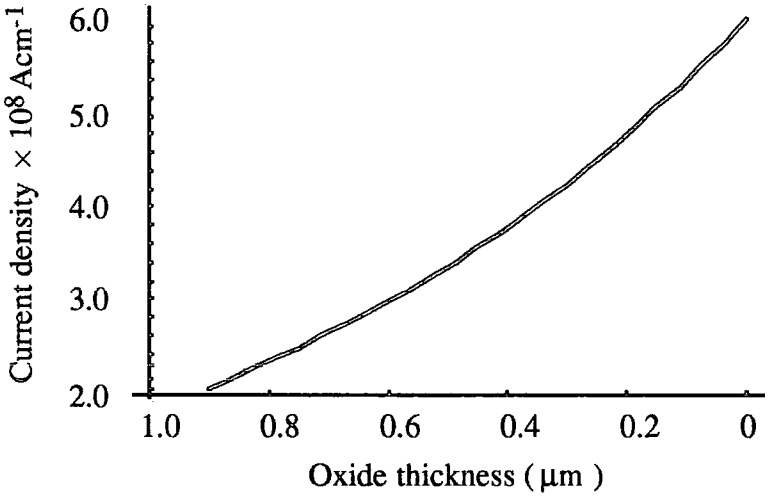

Figure 8.7. The current density increase as a function of the oxide thickness.

8-6 DISCUSSION

This approach to the analysis of the role of an oxide layer enables some of the properties of a non refractory cathode electrode to be predicted when it is coated in an oxide layer. When the oxide layer is thick the high resistivity causes the cathode voltage fall to decrease and releases a large amount of thermal energy in the cathode region. The excess oxide is vaporized by the high temperatures and the cathode voltage fall is

restored. It is shown that the increase in temperature that could result from a thin oxide layer may be significant as the emission mechanism of the cathode is more sensitive to temperature than the electric field strength. The model predicts a much higher oxide thickness being beneficial than is indicated by experimentation, but this could be accounted for by the enormous currents that are flowing in the electrode. The power dissipated by even a 50 nm oxide layer is sufficient to raise the theoretical temperature to a level that is not physically sustainable in a non-refractory cathode.

The model can be used to predict the properties of electrode materials that would enhance the performance of the cathode. The cathode should be able to withstand as high a temperature as possible, but if the conditions of the arc are such that oxidation of the electrode material occurs, then the oxidized layer should be as thin as possible as oxides thicker than 10 nm will be vaporized by the subsequent increase in temperature. The increase in dispersed energy on the cathode surface caused by a thin oxide layer would increase the number of crater sites on the surface, either decreasing the emission site lifetime, t_s, or the current density, J_s.

While it is not assumed that this model is absolutely correct it does illustrate the usefulness in taking this approach to electron emission from an electrode within the unusual confines of a thermal arc. It describes some of the properties of a thermal arc and enables the prediction of some properties that might enhance the performance of such a cathode. It shows that the performance of the cathode, in terms of erosion rate, will depend on the operating conditions the thickness of the oxidized.

8-7 REFERENCES

8.1. Hitchcock A.H, Guile A.E. *A scanning electron microscope study of the role of copper oxide layers on arc cathode erosion rates.* 1977 Journal of Material science Vol. 12 p. 1095 to 1104.

8.2. Guile A.E. Jüttner B. *Basic erosion processes of oxidized and clean metal cathodes by electric arcs.* 1980 I.E.E.E. Trans. on Plasma Science Vol. PS-8 No.3 p. 259 to 268.

8.3. Pfender E, Boulos M. and Fauchais P. 1987 *Plasma Technology in Metallurgical Processing.* ed Feinman J. (Iron and Steel Society ISBN 0-932897-12-6.) p. 37.

8.4. Anders S. Jüttner B. *Influence of residual gases on cathode spot behaviour.* 1991 I.E.E.E. Trans. on Plasma Science Vol. PS-19 No.5 p. 705 to 712.

8.5. Wagner S. Herrmann G. *The oxide-coated cathode.* 1951 London: Chapman and Hall.

8.6 Kittel C *Introduction to Solid State Physics.* 1986 (New York: Wiley sixth Edition)

8.7. Hare A. L. Guile A.E. Hitchcock A.H. *Joule heating as the cause of erosion on copper cathodes in atmospheric air.* 1975 Proc. I.E.E. Vol 122 No.9 p.950

8.8. Rich J.A. *Resistance heating in the arc cathode spot zone.* 1961 Journal of Applied Physics. Vol. 32 No. 6 p. 1023 to 1031.

8.9 Chapter 2, section 2.5

8.10. Dickson D.J. Engel A. von *Resolving the electrode fall spaces of electric arcs.* 1967 Proc. of the Roy. Soc. Series A Vol. 300 p. 316 to 325.

8.11.Daalder E. 1977 J.Phys. D: appl. Phys. Vol. 10 p.2225 to 2234

8.12. Nemirovskii A.Z. Puchkarev V.F. *Arc voltage as a function of cathode thermophysical properties.* 1992 J. Phys. D: Appl. Phys. Vol 25 p. 798 to 802.

8.13. Bube R. H. *Electrons in Solids: An Introductory Survey* 1980 (Academic Press INC 0-12-138552-3)

8.14. Thorp J.S. Mollart T.P. *Copper oxide conductivity.* internal report 1991.

8.15 Rageh M.S.I. Guile A.E. Morgan D.V. Hitchcock A.H. *Initiation of arc cathode emission in Cu_2O films*. 1978 Proc. I.E.E. Vol. 125, No. 1 p. 81 to 84.

CHAPTER 9 CONCLUSION AND FURTHER WORK

9-1 INTRODUCTION

This chapter attempts to draw together the conclusions from the experimental work and theoretical calculations. Wider, more general, conclusions from the observations of heavy current overload emitters will be made noting what would be the behaviour of an ideal cathode electrode under these conditions. A section is also included that suggests some further experimental work, both continuing with the same apparatus used in this research and some ideas for other experiments that would forward the investigations into the operation of the cathode of an electric arc.

9-2 EXPERIMENTAL AND THEORETICAL WORK CONCLUSIONS

The derivation of the general emission equation and the subsequent specific solutions for different combinations of electric field and temperature, in Chapter 3, shows the need to define these conditions clearly to enable theoretical predictions to be made of the performance of the cathode. The electric field and temperature of the cathode, identified in Chapter 4, indicate that the form of emission from a cathode spot is most likely to be electric field enhanced thermionic emission as defined by equation 3.21. The electric field is crucial, because it allows the narrowing of the work function potential barrier to a level low enough for the hot electrons, created by the high temperature, to escape in sufficient numbers to sustain the high current densities required for a thermal arc. The magnitude of the currents imply that the arc has to be attached by a series of points onto the surface, to achieve the required emission current. The size of the attachment points and the pressure of incoming positive ions enable the emission spot to reach temperatures much higher than can normally be sustained by the electrode material, in turn supplying enough electrons with the thermal energy needed to overcome the workfunction. Crater mode emission also controls the melting of the cathode enabling the thermionically emitted electrons to be supplemented by electrons liberated into the arc be means of vaporized material.

D.C. thermal arcs were readily generated by the apparatus described in Chapter 5 and this was a suitable apparatus to use for single shot thermal arc experiments. The apparatus was built for continuous operation and at full current capacity it was possible to run the supply for up to one hour. Ignition of a thermal arc by using a thin strand of copper wire to pre-ionize the arc gap was a successful method, suitable for single shot arc experiments. Studies of crater formation on polished electrodes were best performed when the operating conditions of the arc, in terms of arc current and arc velocity, caused the electrode to operate as close to the melt mode emission threshold as possible. This produces the maximum crater formation on the electrode which makes experimental measurements more accurate.

Crater formation on copper electrodes with 2.5 nm natural oxide layers were found to be caused by a thermal arc, with single emission site lifetimes and current densities ranging from 8×10^{-9} to 1×10^{-9} seconds and 5×10^{10} to 1×10^{9} A cm^{-2}, respectively over the arc velocity range of 3 to 80 ms^{-1}. The lifetime of the craters formed on the electrode was found to be a function of the reciprocal of the arc velocity over this velocity range with an arc current of 90 amps. The formation of these craters was found to be independent of the external applied magnetic field. The subsequent values of the lifetimes and current density of aerodynamically driven arcs were found to be in close agreement with those driven magnetically.

When an oxide layer, Cu_2O, was present on the surface of the copper electrode the attachment of the arc to the electrode is more diffuse. On a macroscopic scale the burn marks left by the arc covered a larger area of the electrode and were less uniform in their distribution. On a microscopic scale there are changes to the characteristics of the emission sites, with a higher number of emission spots being found on the electrodes compared with non oxidized electrodes. As a consequence they were thought to exist for a shorter period of time and more coexisted to support the arc. The absolute values depended on the actual numbers placed on the parameters of J_s and τ_s for oxide coated electrodes. In the arc velocity range 30 to 75 ms^{-1} the average values of the

single emission site lifetime and current density were found to be 0.5×10^{-10} seconds and 14.0×10^{10} A cm^{-2}, respectively.

Experiments to measure the conductivity of thin oxide layers as a function of an applied external magnetic field found no evidence of magneto-resistance effects. Equally aerodynamically driven arcs resulted in no observable difference in the macroscopic burn marks on the electrodes, suggesting that the external applied magnetic field did not alter the mechanism of crater formation on oxide coated electrodes in single shot arc experiments.

The addition of an oxide layer to the cathode electrode did not appear to increase the overall resistance of the arc, when measured over the duration of the arc. A model where the oxide layer was represented as an ohmic conductor with a high resistance was used to predict the effect of the oxide layer on the crater formation. The large amount of energy that would be dissipated in this layer would result in rapid stripping of the oxide from the electrode, preventing the extra resistance of the oxide being detected in the experiment. Using this representation of an oxide layer it was possible to predict the excess energy dissipated in the cathode region of the electrode providing an explanation of the increase in the number of emission sites on the electrode.

9-3 ELECTRON EMITTERS FOR THERMAL ARC APPLICATIONS

Emission spot formation is vital for the longevity of cathodes supporting thermal arcs. The formation of a crater approximately 1 μm in diameter enables the localized high temperatures to be reached that are needed to extract a sufficient fraction of the current density, by thermionic emission, from the electrode to sustain the arc, without excessive vaporization of the electrode.

Oxidation of the electrode produces a relatively high resistivity layer on the surface of the electrode, that is removed by thermal vaporization and which increases the erosion rate of the electrode. Ideally, oxidation of the electrode surface should be avoided, but it is obvious where thermal arcs are used in air or oxidising ambients,

oxidation of the electrode is unavoidable. Ideally the electrode material should oxidize at a slow rate to form as thin an oxidized surface as possible. It is possible that if the oxide layer is kept thin enough and has a low resistance, erosion of the electrode will be kept to a minimum.

The use of material with a high melting point will aid the thermionic emission process from the cathode, as the localized temperature of the cathode spot can be made higher. However the melting point of the electrode is less important than the rate at which an oxide is formed as cathode spot attachment makes it possible to achieve high temperatures on non refractory materials.

9-4 FUTURE WORK

It would be possible to extend this existing experimental programme to confirm the results and conclusions that have been drawn in these experiments. Work on extending the arc velocity range to include the range 20 to 30 ms^{-1} and examine crater formation in the experiments completed in Chapters 6 and 7 should be included. The experiments in Chapter 6 could be extended to include a wider range of arc currents, to investigate the variation in crater formation. This experiment would help to establish the connection made with crater formation and the charge flowing through the arc. The aerodynamically driven arc experiments should be extended to sample electrodes with oxide layers, but the magnetically driven experiments with oxidized electrodes would have to be extended to the 3 to 20 ms^{-1} range, to enable direct comparison of results. An experiment to examine the onset of oxide stripping on the electrodes by using a constant current and velocity arc to damage sample electrodes with progressively thicker oxide layer on the surface may reveal further information on the role played by oxide layers on the formation of craters. The experiment would not reveal the thickness of oxide left on the electrode since oxide stripping occurs when a 2.5 nm oxide layer is present. It will probably not be possible to detect the minimum thickness of oxide by macroscopic observations. However useful information may be

gained by finding the threshold thickness transition from the crater formation of the type found in Chapter 6 to the type illustrated in Chapter 7.

The difficulty that has held back all the crater formation experiments is the fact that there is no way of avoiding the uncertainty in the measurements. The lifetime and current density will depend on the number of emission sites that coexist to sustain the arc. The problems of not being able to make precise measurements of these basic parameters is one that is common to all experimentation with high power plasmas and remains a barrier to the wider adoption of plasma processing. It is felt that future experimentation should look at ways to improve the diagnostic techniques used to measure the performance of non refractory cathodes in these plasma devices. Experiments have to be designed to achieved this. The approaches of Drouet [9.1] and Jüttner [9.2] whose experiments overcame the problems of measuring one of the parameters are admirable attempts to overcome the problems. An alternative approach is to measure the emission current of electrodes in specially designed apparatus where the electrode can be heated to high temperatures and the emission current measured, when a voltage probe is placed near the surface. This apparatus would resemble a field effect microscope, but with adaptations to prevent the inadvertent formation of an arc.

The investigation of oxide layers could be furthered by following a similar approach to the one attempted in Chapter 8, measuring an external parameter, the resistance, as the surface of the electrode is changed. The failure of this experiment was probably due to the time resolution of the measurements. If the experiment were repeated with an increased time resolution, Eg with a 100 MHz sample rate taken within the duration of the arc, it may be possible to record the stripping of the oxide from the surface of the electrode, in terms of a momentary increase in the resistance of the arc. A high time resolution measurement of the current and voltage characteristics of the arc would reveal the characteristic of the cathode spot motion on oxide coated electrodes. Extensive modification of the existing apparatus would have to be made as the frequency response of the voltage and particularly the current instrumentation are not sufficient to make these measurements.

There are a number of experiments that are outside the approach of this programme that would yield useful information to aid the understanding of non refractory cathodes. The first would be to compare the erosion rate, (kg sec^{-1},) in an oxidizing environment with an identical arc, of a known efficient emitter, (such as the Tioxide UK Ltd. electrode material,) with copper, in the non oxidizing environment of a vacuum. This could be done using a rotating arc apparatus on cylindrical electrodes placed in an appropriate vacuum vessel. The temperature of the arc makes many other, normally inert environments reactive, causing compound layers such as nitrides to form on the surface. The proposed experiment would measure directly the performance of a cathode material, avoiding complex analysis techniques, enabling conclusions to be drawn concerning efficient mechanisms for electron emission. This experiment may prove that crater mode emission, of the type seen on electrodes with 2.5 nm oxide layer is the most efficient form and that an oxide increases the erosion rate.

9-5 REFERENCES

9.1 Drouet M.G. Gruber S. *Dynamic Measurements of cathodic emission in a moving arc*. 1976 I.E.E.E. trans. on Power apparatus and systems. Vol PAS-95 No. 1 p. 105 to 112.

9.2 Jüttner B. Pursh H. Anders S. *On the current density at the cathode of vacuum arcs*. 1984 J. Phys. D. Appl. Phys. Vol. 17 L. 111 to 114.